M 2015

U.PORTO

INSTITUTO DE CIÊNCIAS BIOMÉDICAS ABEL SALAZAR
UNIVERSIDADE DO PORTO

Role for CCL2 in Breast Cancer: A possible modulator of iron homeostasis in neoplastic context

ANA MARGARIDA ALVES OLIVEIRA DA ROSA
DISSERTAÇÃO DE MESTRADO APRESENTADA
AO INSTITUTO DE CIÊNCIAS BIOMÉDICAS ABEL SALAZAR
DA UNIVERSIDADE DO PORTO EM
ONCOLOGIA

ANA MARGARIDA ALVES OLIVEIRA DA ROSA

THE ROLE OF CCL2 IN BREAST CANCER: A POSSIBLE MODULATOR OF IRON HOMEOSTASIS IN NEOPLASTIC CONTEXT

Dissertação de Candidatura ao grau de Mestre em Oncologia submetida ao Instituto de Ciências Biomédicas de Abel Salazar da Universidade do Porto.

Orientadora: **Maria da Graça Beça Gonçalves Porto, MD, PhD**
Categoria – Professora catedrática convidada
Afiliação – Instituto de Ciências Biomédicas Abel Salazar da Universidade do Porto;

Categoria – Diretora de grupo
Afiliação - Basic & Clinical Research on Iron Biology group, IBMC/i3s

Categoria – Chefe de serviço
Afiliação – Serviço de Hematologia Clínica, Centro Hospitalar do Porto, Hospital de Santo António, Porto

Co-orientadora: **Oriana Alexandra de Paixão Praças Marques, MSc**
Categoria – Mestre em Genética Molecular, Comparativa e Tecnológica
Afiliação – Universidade de Trás-os-Montes e Alto Douro

Categoria – Aluna de Doutoramento em Patologia e Genética Molecular
Afiliação – Instituto de Ciências Biomédicas Abel Salazar da Universidade do Porto.

Parte dos resultados obtidos neste trabalho foram apresentados sob a forma de *poster* no *XXIII Porto Cancer Meeting*, no *1st Symposium on Immunomodulation in Cancer & Regeneration* e no *27th European Congress of Pathology*.

Parte dos resultados obtidos neste trabalho foram publicados com a seguinte referência: Lopes, C, **A Rosa**, O Marques, L Leite, A Rema, F Faria, A Canadas, BM Martins da Silva, and G Porto. 2015. "A New Role for CCL2 in Breast Cancer: A Modulator of Local Iron Homeostasis." Pp. S59-S59 (1) 1, vol. 467. *J Virchows Archiv*.

Este trabalho está inserido no projeto de Doutoramento em Patologia e Genética Molecular

"*Iron Homeostasis in Breast Carcinogenesis*"

da Mestre Oriana Alexandra de Paixão Praças Marques

AGRADECIMENTOS

No culminar desta etapa, gostaria de deixar o meu agradecimento a todos aqueles que, direta ou indiretamente, deram a sua contribuição para a concretização deste projeto.

Gostaria de agradecer à Professora Berta Martins da Silva, diretora do Mestrado em Oncologia, pela oportunidade de ingressar neste mestrado e por todo o apoio institucional fornecido durante estes dois anos. Um agradecimento especial pela oportunidade de desenvolver este projeto no Laboratório de Imunogenética do Instituto de Ciências Biomédicas de Abel Salazar, do qual é responsável.

À Professora Graça Porto, minha orientadora, pela incansável disponibilidade, pelas trocas de ideias, críticas construtivas e pelo conhecimento partilhado durante este ano. É com muita gratidão que agradeço todas as oportunidades que me proporcionou para que pudesse aprender mais e adquirir espírito crítico.

À Mestre Oriana Marques, minha co-orientadora, pela paciência e exigência para que eu fizesse sempre mais e melhor. Um muito obrigado pela disponibilidade demonstrada ao longo da realização deste trabalho.

Um agradecimento à Professora Fátima Gärtner, Diretora do Departamento de Patologia e Imunologia Molecular, por todas as facilidades proporcionadas para que a execução deste trabalho fosse possível.

Ao Professor Carlos Lopes, pelo interesse demonstrado neste projeto, pela incansável ajuda e por todos os conhecimentos transmitidos desde o meu estágio até ao culminar deste trabalho.

Ao Mestre Arnaud Paula, por toda a ajuda prestada durante a realização deste projeto e pela constante lembrança de “fazer boa ciência”.

Um agradecimento à Dra Ana Canadas pela ajuda na avaliação das lâminas e às Dras Alexandra Rêma e Fátima Faria pela simpatia, disponibilidade e apoio técnico.

A todo o laboratório de Imunogenética – Cláudia Carvalho, Bárbara Guerra Leal, Daniela Boleixa, Andreia Bettencourt, Dina Lopes, Sandra Brás e Maria Rebelo – por me terem recebido e pelo constante espírito positivo.

À Doutora Paula Faustino, do Instituto Nacional de Saúde Dr. Ricardo Jorge, pelo apoio prestado na genotipagem do gene HFE.

Aos meus colegas de laboratório e amigos – Luciana Leite, Hildeberto Moreira e Rita Ferreira – por terem estado sempre presentes nos momentos menos bons e os terem tornado em momentos inesquecíveis. Um agradecimento especial à Diana Pinto e à Joana Guerra, por todo o companheirismo e amizade demonstrados durante estes dois anos. Boa sorte para todos!

À Sónia, minha amiga de sempre, por todo o incentivo e paciência nos momentos mais difíceis e pela alegria contagiante.

Um agradecimento aos meus pais e à minha irmã, a quem devo tudo o que sou, este trabalho é dedicado a vocês, sem o vosso apoio incondicional a concretização deste projeto não teria sido possível.

ABSTRACT

Breast carcinoma is the most common neoplasm affecting women worldwide, accounting for 25% of all malignancies diagnosed in 2012.

Iron is an essential microelement, vital for a variety of biological and cellular processes. However, iron is also considered to be potentially carcinogenic through several mechanisms, such as formation of mutagenic hydroxyl radicals, suppression of the host immune response and by acting as a limiting nutrient for proliferating tumor cells. Epidemiological, experimental and clinical evidences support the hypothesis that iron is strongly associated with breast cancer initiation, behavior and progression. Results from several studies provide evidence that cancer cells behave as iron deficient and are able to undermine the tightly physiological process of iron regulation.

Accumulating evidence provides now a new insight about the role of stromal inflammatory cells in cancer. A multitude of studies reported that epithelial malignant cells require an appropriate support structure from stromal cells to successfully acquire a full malignant potential. The recruitment of inflammatory leukocytes into the tumor microenvironment involves the role of chemotactic cytokines.

CCL2 (chemokine [(C-C motif)] ligand 2) is one of the most studied chemotactic cytokines in the context of tumor progression, particularly in breast cancer and its expression has been correlated with tumor progression and poor prognosis.

The aim of this work was to understand if the expression of CCL2, in the breast cancer model, could be related to tissue iron status. More specifically, it assesses tissue iron deposition and CCL2 expression in epithelial and stromal inflammatory cells in well characterized breast cancer samples. Associations between CCL2 expression, established iron profiles and HFE variants were evaluated and CCL2 expression was also correlated with clinico-pathological parameters.

To address those aims, hemosiderin deposits in control and carcinoma samples, in epithelial and in stromal inflammatory cells, were identified by DAB-enhanced Perls' staining technique. Immunohistochemistry was performed in order to assess the expression of CCL2 in epithelial cells and macrophages; CD68 immunostaining was performed to assess total macrophage infiltration. PCR-RFLP was performed for the detection of the C282Y and H63D HFE allele variants.

Comparing with normal samples, a higher proportion of carcinoma samples presented iron deposition in epithelial and stromal inflammatory cells. The presence of hemosiderin deposits in macrophages and/or lymphocytes was statistically associated with increased malignancy. Epithelial CCL2 expression was not associated with total macrophage infiltration, but was statistically associated with the infiltration of CCL2-positive

macrophages. Ferroportin 1 (FPN 1) expression in macrophages and lymphocytes was found to be increased in carcinoma samples, in comparison to normal cases. Furthermore, the median expression of CCL2 was higher in the presence of iron deposits in stromal inflammatory cells and its expression in epithelial cells was also associated with the FPN 1 expression in lymphocytes. Concerning clinico-pathological parameters, epithelial CCL2 expression was statistically associated with the estrogen-receptor negative status.

In conclusion, this study further supports the notion that stromal inflammatory cells display a deregulation of iron homeostasis, possibly favoring the supply of iron to actively proliferating breast tumor cells. Moreover, associations found between the epithelial expression of CCL2, infiltration of CCL2-positive macrophages and total macrophage infiltration suggest the existence of a paracrine signaling pathway where CCL2, whose expression may be putatively enhanced by increased iron deposition in stromal inflammatory cells, contributes not only to increased macrophage infiltration into the tumor microenvironment, but may also play an indirect role in regulating tumor iron nutrition and progression.

RESUMO

O carcinoma da mama é a neoplasia mais frequente na população feminina a nível mundial, sendo responsável por 25% de todas as neoplasias registadas no ano de 2012.

O ferro é um microelemento essencial e fundamental para uma variedade de processos biológicos e celulares. No entanto, este metal é considerado potencialmente carcinogénico, por participar em diversos processos, tais como a formação de radicais hidroxilo, supressão da resposta imunitária do hospedeiro ou por ser um nutriente limitante para as células tumorais em proliferação. Evidências epidemiológicas, experimentais e clínicas suportam a hipótese de que o ferro está associado à iniciação, comportamento e progressão do carcinoma da mama. Resultados de diversos estudos indicam que as células neoplásicas se apresentam como deficientes em ferro e são capazes de desregular os mecanismos de homeostasia deste metal.

Diversos estudos demonstraram que as células do microambiente tumoral têm uma função relevante na tumorigénese e que as interações recíprocas que se estabelecem entre as células neoplásicas e do estroma regulam e potenciam a progressão tumoral. O recrutamento de leucócitos para o microambiente tumoral envolve a participação de citoquinas quimiotáticas. O CCL2 (*chemokine [(C-C motif*)] *ligand* 2) é uma das quimiocinas mais estudadas no contexto da progressão tumoral, especialmente no carcinoma da mama, estando a sua expressão associada com progressão tumoral e mau prognóstico.

O principal objetivo deste trabalho foi perceber se a expressão de CCL2, no modelo de carcinoma da mama, está relacionada com o *status* de ferro no tecido. Mais especificamente, neste estudo foi avaliada a deposição de ferro no tecido mamário e a expressão de CCL2 nas células epiteliais e inflamatórias do estroma. Foram testadas associações entre a expressão de CCL2, perfis estabelecidos de (des)regulação de ferro e a presença de variantes do gene HFE e a expressão de CCL2 foi correlacionada com variáveis clínico-patológicas.

Para estudar estas questões, várias técnicas foram realizadas. Os depósitos de hemosiderina em amostras normais e de carcinomas, em células epiteliais e inflamatórias do estroma, foram identificados usando a técnica de *DAB-enhanced Perls*'. A expressão de CCL2 nas células epiteliais e nos macrófagos foi avaliada através de técnicas de imunohistoquímica; a mesma técnica foi utilizada para a determinação da infiltração total de macrófagos, recorrendo a um anticorpo anti-CD68. A técnica de PCR-RFLP foi executada para a deteção das variantes C282Y e H63D do gene HFE.

Comparando com amostras controlo, uma maior proporção de amostras de carcinoma da mama apresentava deposição de ferro nas células epiteliais e inflamatórias

do estroma. A presença de depósitos de hemosiderina nos macrófagos e/ou linfócitos estava significativamente associada com o grau de malignidade. Não foi encontrada uma associação estatisticamente significativa entre a expressão de CCL2 nas células epiteliais e infiltração total de macrófagos, mas esta estava significativamente associada à infiltração de macrófagos CCL2-positivos. Os resultados obtidos indicam ainda que a expressão de ferroportina 1 (FPN 1) em macrófagos e linfócitos era superior em amostras de carcinoma, comparando com amostras normais. Mais ainda, a expressão mediana de CCL2 era superior na presença de depósitos de ferro nas células inflamatórias do estroma, e a sua expressão nas células epiteliais estava também associada com a expressão de FPN 1 nos linfócitos. No que diz respeito às variáveis clínico-patológicas, a expressão de CCL2 nas células epiteliais estava associada à negatividade do recetor de estrogénios.

Concluindo, este estudo demonstra que as células inflamatórias do estroma também apresentam desregulação dos mecanismos de controlo homeostático do ferro, possivelmente favorecendo o fornecimento deste metal a células neoplásicas em constante proliferação. Este estudo reporta associações entre a expressão de CCL2 em células epiteliais, a infiltração de macrófagos CCL2-positivos e a infiltração total de macrófagos, sugerindo a existência de uma via de sinalização parácrina onde a quimiocina CCL2, cuja expressão pode ser possivelmente aumentada pela presença de depósitos de hemosiderina em células inflamatórias do estroma, não só contribui para o aumento da infiltração de macrófagos no microambiente tumoral, mas poderá também ter uma função indireta na nutrição tumoral, através da regulação do fornecimento de ferro no tecido.

TABLE OF CONTENTS

FIGURE INDEX

TABLE INDEX

ABBREVIATIONS LIST

µL – Microliter

µM – Micromolar

ABC – Avidin-Biotin Complex

APES - 3-aminopropyltriethoxysilane

BCa – Breast cancer

CCL2 - Chemokine (C-C motif) ligand 2

CCR2 – C-C chemokine receptor type 2

CD – Cluster of differentiation

CD1 – Cyclin D1

cf. - confer

CI – Confidence Interval

CSF-1 – Colony stimulating factor 1

DAB - Diaminobenzidine

DCIS – Ductal carcinoma *in situ*

DcytB - Duodenal cytochrome b

DFO - Deferoxamine

DMBA - 7,12-Dimethylbenz[a]anthracene

DMT1 - Divalent metal transporter 1

DNA – Deoxyribonucleic Acid

EC – Epithelial cells

EDTA - Ethylenediaminetetraacetic acid

EGF – Endothelial growth factor

ER – Estrogen receptor

FAC – Ammonium ferric citrate

Fe/S – Iron-sulfur

FFPE – Formalin fixed paraffin-embedded

FPN1 – Ferroportin 1

H&E - Heamotoxylin-eosin

H_2O_2 – Hydrogen Peroxide

HCC - Haemofiltrate CC chemokine

HCP-1 - Heme-carrier protein 1

HER-2 – Human epidermal growth factor 2

HH - Hereditary hemochromatosis

HIF – Hypoxia inducible factor

HPF – High power field

HRE – Hypoxia responsive element

IDC – Invasive ductal carcinoma

IFN-γ – Interferon-gamma

IL - Interleukin

IRE – Iron-regulatory element

IRP – Iron-regulatory protein

LIP – Labile iron pool

LPS - Lipopolysaccharide

Ly – Lymphocyte

M0 – Macrophage

MCP-1 – Monocyte chemoattractant chemokine 1

MHC – Major histocompatibility complex

MMP – Metalloproteinase

mRNA – Messenger RNA

NaCl – Sodium chloride

ng – Nanogram

NK – Natural killer

ºC – Celsius degree

PCR – Polymerase chain reaction

PCR-RFLP – PCR – Restriction Fragment length polymorphism

PR – Progesterone receptor

RCLB – Red cell lysis buffer

RES - Reticuloendothelial system

RNA – Ribonucleic acid

ROS – Reactive oxygen species

rpm – Rotations per minute

RR - Ribonucleotide reductase

SDS – Sodium dodecyl sulfate

SEM – Standard error of mean

SIC – Stromal inflammatory cells

SNP – Single nucleotide polymorphism

STEAP3 –Six-transmembrane epithelial antigen of the prostate 3

TAE - Tris-acetate-EDTA

TAM – Tumor-associated macrophage

TBS - Tris-buffered saline

TDLU – Terminal ductal lobular unit

TE – Tris-EDTA

TE-2 – Tris-EDTA 2X

Tf – Transferrin

TfR1 – Transferrin receptor 1

TMA – Tissue microarray

TME – Tumor microenvironment

UTR – Untranslated region

V - Volt

VEGF – Vascular endothelial growth factor

VEGFR – Vascular endothelial growth factor receptor

VHL – Von Hippel Lindau

WHO – World health organization

INTRODUCTION

1.1 Breast anatomy and histology

The breast is an apocrine modified gland, responsible for the production of milk, essential for the nutrition of the newborn. This gland is permanently under hormonal control, which regulates its development during puberty and secretory activity during the latter half of pregnancy (1).

The mammary gland is localized between the second and sixth ribs in the vertical axis and between the sternal border and the mid-axillary line in the horizontal axis. The mammary gland develops within the superficial fascia and is maintained in place by the Cooper suspensory ligaments (2).

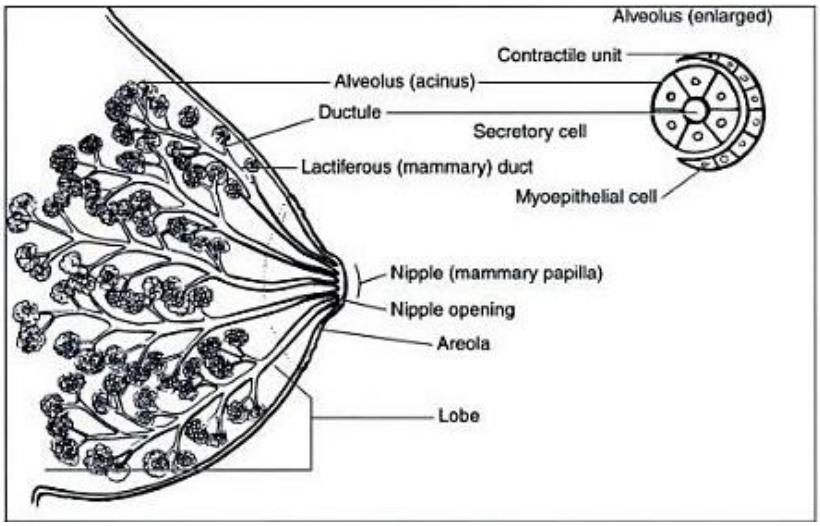

Figure 1: Schematic diagram of the breast. Adapted from (3).

The adult breast is formed by skin, subcutaneous tissue and breast tissue, which comprises the parenchyma and stroma (2). The parenchyma is divided into 15 to 20 irregular lobes that converge at the nipple in a radial manner, to the lactiferous ducts, which are the excretory canals (4). Lobes diverge into a progressive branching system of ducts that end in terminal ductal lobular units (TDLU), the smallest functional units of the breast (5). These structures are responsible for the production of milk and are also the primary origin of most mammary carcinomas (6).

Stromal and subcutaneous components contain adipose and connective tissue, blood and lymphatic vessels and nerves (2).

The mammary papilla or nipple is a cylindrical or conical projection from just below the center of the anterior surface of the breast (7).

2.1 Epidemiology

2.1.1 Cancer

The global burden of neoplastic diseases keeps increasing worldwide, reinforcing its status as a major health problem. This is mainly due to population growth, together with aging, but also improvement of screening and early detection techniques (8). Also associated with this increase is the maintenance of cancer-promoting habits, such as smoking, alcohol consumption and sedentary lifestyle, particularly in economically developing countries (9).

Cancer is the leading cause of death in economically developed countries and is the second cause of death in developing countries, following cardiovascular conditions (10).

The most frequent cancers worldwide, considering both sexes, are lung, breast and colorectal cancer In females, breast cancer is the most frequent (23%), followed by colorectal (9.2%) and corpus uteri cancer (9%) (9).

In Europe, and in Portugal, amongst females, breast cancer is the most frequent malignancy (11).

2.1.2 Breast Cancer

Breast carcinoma is the most common neoplasm affecting women worldwide, accounting for 25% of all malignancies diagnosed in 2012 (12). Moreover, it is the fifth cause of death from cancer worldwide, taken both sexes into account, comprising 6.4% of the total cancer deaths (9).

In more developed countries, among women, breast cancer is the second cause of death (15.4% of total), following lung cancer (19.4%), while in developing countries it is the leading cause of death (14.3%) (12).

In Europe, breast cancer is the most common neoplastic disease, accounting for 464000 cases (14% of all cancer cases). This malignancy was also the fourth leading cause of cancer-related death, with an estimated of 131000 deaths (11).

In Portugal, is the fifth cause of cancer-related death (6.5%), considering both sexes. Among females, is the leading cause of cancer death, comprising 16% of total cancer registered in 2012 (13).

2.2 Histological classification

The natural history of mammary carcinomas starts with abnormal benign proliferation, which may result in *in situ* and invasive carcinomas and culminating in metastatic disease (14). The “linear” multistep model is universally accepted, which suggests a transition from normal epithelial to invasive breast carcinoma via typical and atypical hyperplasia and *in situ* carcinoma, through accumulation of genetic mutations, as illustrated in figure 2 (5).

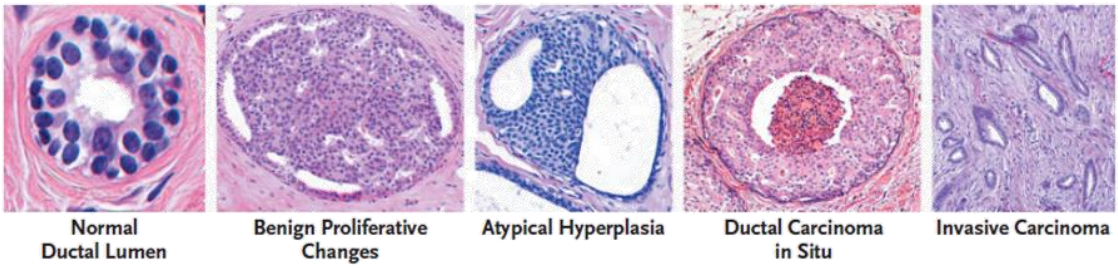

Figure 2: Histopathological-based model of human ductal breast cancer progression, demonstrating the transition from benign proliferative changes, which may evolve to atypical or typical hyperplasia and *in situ* carcinoma, culminating in an invasive lesion. Adapted from (14).

Pre-invasive and invasive lesions are divided into 2 general histological categories: ductal or lobular subtypes. Data regarding histogenesis of mammary carcinoma has demonstrated that most breast cancers, ductal or lobular subtype, arise from TDLUs (15). Nowadays, distinction between the 2 subtypes is based upon differences in cell morphology (5).

Malignant tumors may arise from any of the tissues composing the breast. Ductal carcinomas are the most frequent, followed by lobular malignancies, both arising from the epithelial compartment of the breast. Another histological subtypes, more rare, are listed and classified by WHO and can be found in reference (16).

2.2.1 Benign tumors

The designation of benign tumors comprehends a heterogeneous group of lesions, which are normally detected as a palpable mass, a non-palpable abnormality detected on breast imaging examination or an incidental microscopic finding (2). Histologically, these lesions remain constricted and display no cellular heterogeneity (4).

Dupont and colleagues performed a retrospective study evaluating benign breast disease and cancer risk. For this, more than 10000 slides from women diagnosed with benign breast lesions were analyzed and, accordingly to stipulated criteria, grouped into one of 3 groups: non-proliferative lesions, proliferative lesions without atypia or atypical hyperplasias. Women diagnosed with non-proliferative lesions did not have an increased risk for subsequent cancer. On the other hand, women diagnosed with proliferative lesions without atypia or atypical hyperplasias had an increased risk of subsequent breast cancer, compared with non-proliferative diseases (1.9 and 5.3 times, respectively). According to this study, the majority of women (70%) who underwent breast biopsy for benign disease were not at increased risk for breast cancer (17).

2.2.2 Ductal carcinomas in situ

Ductal carcinomas *in situ* (DCIS) are the most common type of non-invasive breast cancer in women (18). In the past 20 years, incidence of this lesion has increased, mostly due to increased detection, through the widespread implementation of radiographic screening for invasive carcinoma (19, 20).

DCIS is defined as the clonal proliferation of neoplastic cells, which remain confined to the lumens of the mammary ducts (16). Ducts are surrounded by myoepithelial cells, which form an intact basement membrane (20). It is considered to be a precursor lesion, associated with an increased risk of subsequent invasive carcinoma (5).

DCIS is considered to be a spectrum of disease, ranging from small, low-grade lesions, treatable by surgical excision to extensive, high-grade lesions, which require a mastectomy for complete eradication (21). At present, there is no universally accepted classification system for *in situ* lesions. To correctly differentiate lesions and consequently stratify patients that will most benefit from each treatment, the pathological report must refer information regarding tumor size, nuclear grade, architectural patterns, presence of necrosis, margin assessment and existence of microcalcifications (22).

2.2.3 Invasive ductal carcinomas

Invasive ductal carcinoma (IDC) is the most frequent malignant mammary tumor, comprising approximately 75% of mammary carcinomas (4). Classification used is that of WHO, which is based particularly on growth patterns and cytologic features of invasive tumor cells (16). The principal diagnostic criterion that allows the differentiation of invasive from *in situ* carcinomas is the disruption of the myoepithelial cell layer and basement membrane (23).

A vast majority of invasive tumors are associated with an *in situ* carcinoma (2). The prevailing view is that invasive carcinomas derive from the *in situ* component, based on the frequent coexistence of the 2 lesions, but also on the histological resemblances between both components within the same lesion (24). Moreover, coexisting *in situ* and invasive carcinomas often share the same genetic alterations and immunophenotypes (25).

3.1 Role of iron

Iron is an essential microelement, vital for a variety of biological and cellular processes, such as DNA synthesis, oxygen transport and cell cycle regulation (26, 27). Iron is pivotal for the functioning of numerous enzymes and proteins, such as ribonucleotide reductase (28), hemoglobin (29), cyclins (30) and p53 (31). Iron depletion leads to inhibition of cell proliferation, cell cycle arrest at G1/S phase transition and apoptosis (26).

3.1.1 Iron and DNA synthesis

Ribonucleotide reductase (RR) is a rate-limiting enzyme, formed by two dimers, responsible for the conversion of ribonucleotides into deoxyribonucleotides (26). Protein R1, or $\alpha 2$ dimer, contains the active and binding site for the allosteric effectors, and protein R2, also called $\beta 2$ dimer, is composed by a binuclear ferric iron center, responsible for the generation and maintenance of a tyrosyl radical, necessary for catalysis (28, 32, 33). Iron is fundamental for the enzyme activity, because the free radical needs its constant supply to regenerate (28).

Studies performed by Lederman and colleagues, in which they supplied deferoxamine (DFO), an iron chelator, to human B lymphocyte and T lymphocyte cell lines, led to a loss of function of RR, resulting in cell cycle arrest and inhibition of proliferation (34). Subsequent studies performed by Nyholm and his group led to the conclusion that some iron chelators inhibited RR activity, in a mammary cell line, by removing all soluble iron from the medium and preventing the regeneration of the iron center in the apo-R2 subunit (35). Further studies confirmed these reports (36).

3.1.2 Iron in the cell cycle

Highest demands for iron occur during late G1 phase and throughout S phase of the cell cycle (37). Although this happens mostly because of the increasing activity of RR, iron also plays a role in regulating cyclins (30).

Iron depletion decreases the protein levels of cyclin A, B and D, and increases the levels of cyclin E (38).

Cyclin D1 (CD1) is the most important regulator of cell progression to replication phase and is also considered an oncogene, because its overexpression releases cells from tight regulation (39).

CD1 is decreased by iron depletion, leading to G1/S arrest and impaired cellular proliferation. Thereby targeting its degradation may represent a new chemotherapeutic approach (40).

3.1.3 Iron in oxygen transport

Hemoglobin is an oxygen-carrier metalloprotein present in erythrocytes (41). This protein is formed by two polypeptide chains, *α* and *β*, each bound to a heme group. Each heme group is composed by a ferrous atom and a porphyrin ring and functions as a reversible carrier, supplying oxygen into tissues and transporting carbon dioxide back to the lungs (29, 41, 42).

In erythroid cells, heme biosynthesis is dependent on the availability of iron in the form of iron-sulfer (Fe/S) clusters. Plus, the enzyme ferrochelatase, which catalyzes the insertion of iron into protoporphyrin IX, needs iron for the efficient formation of heme (29). Iron deficiency anemia leads to impaired heme biosynthesis and reduced hemoglobin synthesis, resulting in abnormally small and fragile red blood cells. The outcome is the reduction in the capacity of the erythrocytes to transport oxygen into the body cells and tissues (43).

As described above iron is fundamental for the correct function of a variety of cellular processes. However, iron is also associated with toxicity. Through the Fenton and Haber-Weiss reactions, ferrous iron, in the presence of hydrogen peroxidase, is able to donate an electron to produce hydroxyl radicals, a type of reactive oxygen species (ROS). This is causative of DNA base modifications and strand breaks, causing oxidative stress. Moreover, iron deficiency or overload is responsible for a multitude of diseases (44).

Due to its potential toxicity and pathogenicity, iron is tightly regulated at the systemic and cellular level and this is accomplished by a synchronized control of iron uptake, storage and export (45).

3.2 Systemic iron regulation

In mammals a controlled physiological mechanism for iron excretion is absent, so absorption by enterocytes is highly regulated in order to maintain iron homeostasis (46).

About 1-2 mg of iron is absorbed per day from diet and it can be obtained in an inorganic non-heme or organic heme formulation. Non-heme iron, mostly present in vegetables, accounts for 90% of dietary iron, but only approximately 10% of it is absorbed in the intestine; on the other hand, heme iron, present in meat, is more efficiently absorbed (47).

Iron is absorbed accordingly to the organism demands, in order to replace losses in urine, sweat and from desquamation of intestinal cells (45). In healthy individuals, intestinal iron absorption is regulated by body iron stores, hypoxia, inflammation and erythropoietic activity (48).

3.2.1 Intestinal Iron Absorption

Enterocytes lining the absorptive villi, close to the gastroduodenal junction, are responsible for iron absorption. Mechanisms by which heme iron is absorbed are dependent on the heme-carrier protein 1 (HCP-1), which also transports folate (49). Dietary non-heme iron is absorbed at the apical border, through DMT1 (divalent metal transporter 1) and after reduction by membrane ferrireductases, such as DcytB (duodenal cytochrome B), it enters a common pathway with dietary heme iron (44, 50)**.**

Iron inside the enterocyte may remain in the form of ferritin, until these cells reach senescence and slough off (44). Iron can also be exported into blood circulation via the only known exporter identified to date, ferroportin 1 (FPN1), localized on the basolateral membrane (51). The egress of iron from the enterocyte is dependent on its oxidation, by the membrane bound multicopper oxidase hephaestin, which enables iron binding to plasm transferrin (Tf) (52).

3.2.2 Iron distribution and utilization

The major depots of iron are circulating hemoglobin and myoglobin, which contain about 85% of the total body iron content (53, 54). About 20% of the remaining body iron is stored in hepatocytes and in reticuloendothelial macrophages (44). Although only 1% of body iron is stored in transferrin, it is the most important dynamic iron pool, with the highest

turnover rate (55). About 80% of iron bound to transferrin is delivered to the bone marrow for the development of new erythrocytes (56).

In order to encounter large iron needs for erythropoiesis, the Reticuloendothelial System (RES), composed of monocytes and macrophages, recycles iron from senescent red cells by a process named erythrophagocytosis (57). Iron can be stored within the macrophage or loaded onto transferrin for reuse, depending on systemic iron requirements (58).

3.2.3 Regulation of systemic iron balance

Systemic iron homeostasis is regulated by hepcidin, a hormone secreted mainly by hepatocytes (59). Hepcidin production is regulated by iron levels: when iron is abundant, more hepcidin is produced, therefore limiting iron absorption and release from body stores; when iron is deficient, hepatocytes produce less or no hepcidin, allowing iron to be absorbed and enter the plasma. So, hepcidin is a negative key regulator of iron metabolism at the systemic level, controlling absorption, release from macrophages or mobilization from depots (60).

Hepcidin is also regulated by erythropoietic demands. Through a not completely clarified mechanism, hepcidin production is suppressed in times of active erythropoiesis, increasing iron availability for hemoglobin synthesis (60). Erythroferrone was recently identified as the putatively mediator of hepcidin suppression during active erythropoiesis (61).

Hepcidin regulates iron efflux through binding to ferroportin 1, which leads to its internalization and degradation, resulting in cellular iron retention in hepatocytes, enterocytes and macrophages (62).

Schematic representation of iron regulation via hepcidin is illustrated in figure 3.

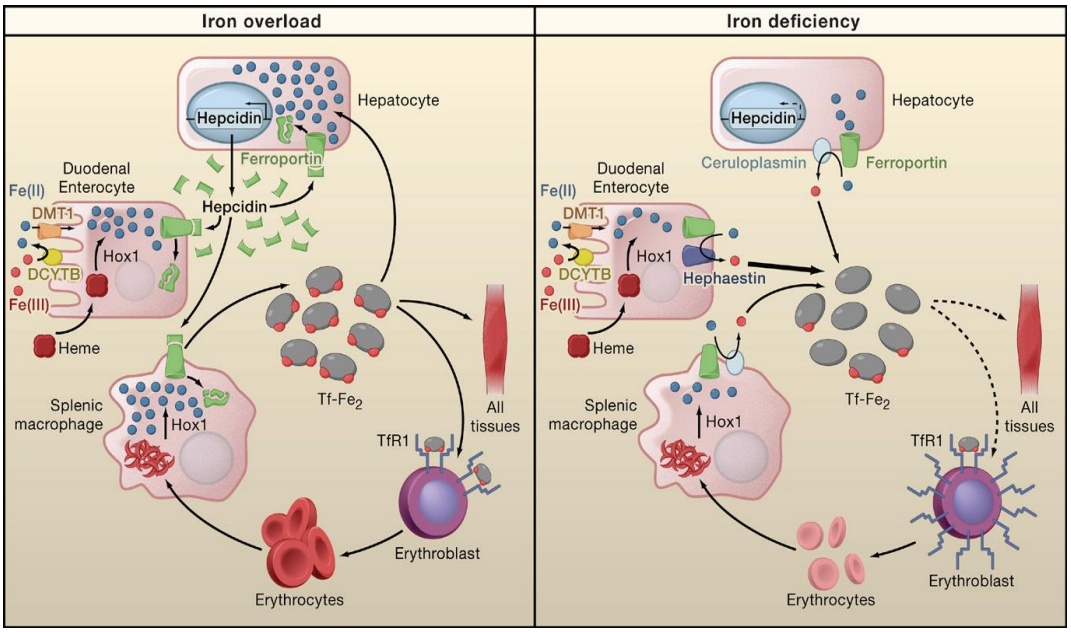

Figure 3: Regulation of Systemic Iron Homeostasis through hepcidin. Iron overload leads to hepcidin secretion by hepatocytes with consequent iron retention in enterocytes, hepatocytes and macrophages of the RES. Conversely, in situations of iron deficiency, hepcidin production is suppressed and iron actively exported. Adapted from (63).

3.3 Cellular iron regulation

In order to prevent cellular toxicity and ensure iron availability for essential molecular processes, coordination of iron uptake, utilization and storage at the cell level are also tightly regulated (63).

Iron in the ferric form (Fe(III)), bound to transferrin, binds to the transferrin receptor 1 (TfR1) and this complex is internalized by clathrin-dependent endocytosis. Acidification of the endosome leads to iron release from the complex, and transferrin plus TfR1 are recycled back into the cell surface. In the endosome, the ferrireductase STEAP3 reduces iron into a Fe(II) form, which allows its transport into the cytosol by DMT1. Iron can then be stored into ferritin or enter the intracellular labile iron pool (LIP) (63). LIP is considered to be the transitional step between iron released from the endosomal compartment and storage in ferritin or for use in cellular processes. In physiological conditions, this iron pool is maintained in small amounts, because of iron's cytotoxicity (64).

3.3.1 Regulation of cellular iron metabolism

Cellular iron homeostasis is regulated at the post-transcriptional level by the iron regulatory proteins 1 and 2 (IRP1 and IRP2). Target mRNAs that codify proteins involved

in iron regulation have iron responsive elements (IRE), which are *cis*-regulatory hairpin structures (63). Binding of IRP1 and IRP2 to the IREs is regulated by intracellular iron levels (65).

In iron-depleted cells, IRPs bind to the IREs present in the 5'-untranslated region (UTR) of the ferritin and ferroportin 1 genes, repressing their translation by preventing the binding of the small ribosomal subunit to the mRNA. Moreover, IRPs bind to the 5 IREs in the 3'-UTR of the TfR1 mRNA, leading to its stabilization and translation. This results in increased cellular iron uptake and decreased iron storage and export from the cells.

When cells are iron replete, IRP1 and IRP2 are inactivated, resulting in inhibition of TfR1 mRNA translation and translational de-repression of the ferritin and ferroportin 1 genes. This leads to decreased iron absorption and increased iron storage and egress from the cells (66).

3.4 Iron (de)regulation in neoplastic cells

In the past several years, the role of iron in neoplastic disease has been extensively studied (67). Results from several studies give evidence that cancer cells behave as "iron-deficient" and are able to undermine the tightly physiological process of iron regulation in order to accumulate iron (67). Alterations in the expression of proteins related to iron metabolism, in neoplastic context, have been extensively reported and some are presented next.

One of the first findings that demonstrated the high requirements for iron was the upregulation of TfR1 in many tumors. This evidence of increased expression of TfR1, together with studies using anti-TfR1 monoclonal antibodies in different cells lines, suggest the fundamental role of iron in cancer cell proliferation (68-70).

Normal cells predominantly take up iron through binding of Tf to TfR1, which is then internalized via receptor-mediated endocytosis (71). A different mechanism of iron uptake has also been reported in cancer cells. In this process iron potentially enters the cells through a membrane-bound oxidoreductase, not involving the endocytosis of transferrin (65). This non-saturable, non-receptor-mediated process was first described in fetal rat hepatocytes by Trinder and colleagues (72). Subsequent studies demonstrated that this advantageous mechanism is also present in several cancer lines and after saturation of the TfR binding sites, there was still a marked increase in iron uptake (73-75).

Serum ferritin is also increased in a number of neoplasias, such as liver cancer, neuroblastoma, colon cancer and breast cancer (76-79). Tumor cells typically have lower ferritin levels than cells from normal counterparts. Neoplastic cells from neuroblastomas are an exception, because they show higher intracellular ferritin content than normal cells (80). Ferritin, namely the heavy subunit (H-ferritin) sequesters excess iron, so its downregulation presumably increases iron accessibility (81). Furthermore, H-type ferritins may be involved in immunological antitumor responses, so its decrease potentially benefits cancer cell proliferation (82, 83). Additionally, genes associated with neoplastic transformation can also result in altered ferritin expression (84). Tsuji and colleagues have found that transfection with the adenovirus E1A repressed H-ferritin expression (85). The proto-oncogene *c-myc* seems to have the same effect of H-ferritin, besides increasing IRP2 expression (86).

Production of siderophore-like molecules by tumor cells has also been reported. Siderophores are organic molecules produced by microorganisms to acquire iron from the environment. When its acquisition is necessary, lipocalin 2, an innate immune protein, binds to sidephores to capture iron (87). Studies in breast cancer and leukemia cell lines report that lipocalin 2 is upregulated in these neoplasias, suggesting that cancer cells can pro-actively increase cellular iron uptake by this mechanism (88, 89).

In a recent study, Torti's group reported that prostate and breast cancer cells are capable of hepcidin production, leading to decreased ferroportin 1 expression and increased intracellular iron retention. The outcome was the promotion of cancer cell survival (90).

3.5 Iron (de)regulation in breast cancer cells

Although studies are controversial, a large set of epidemiological, experimental and clinical evidences support the hypothesis that iron is strongly associated with breast cancer initiation and progression (91). This possibility is based primarily on the notion that cancer cells require iron for their nutrition and proliferation, and that iron may increase cancer risk through the formation of free radicals and production of oxidative damage (92).

3.5.1 Epidemiological studies

Epidemiologic studies regarding dietary iron intake have not shown consistent results. In a study by Stevens and colleagues, higher transferrin saturation and serum iron

were positively correlated with cancer risk, both in men and women (93). Mainous and colleagues reported that increased transferrin saturation was associated with increased cancer risk, but only when it was combined with high iron intake (94).

Although several studies revealed positive correlations, a significant number of studies report inverse (95, 96) or null correlations (96).

3.5.2 Genetic association studies

Another approach employed to study iron deregulation in breast cancer has been the study of its association with hereditary hemochromatosis (HH) major allelles (97). HH is an autosomal recessive disorder of iron metabolism, characterized by excessive dietary iron absorption and deposition in several tissues, resulting in cellular toxicity (98). Feder and colleagues identified a major-histocompatibility complex (MHC) class I-like molecule, designated as HFE, as being the candidate gene for HH (99).
The majority of HH patients carry a missense mutation, which results in the substitution of a cysteine for a tyrosine at aminoacid 282, which is termed the C282Y mutation. A second mutation in the HFE gene results in the substitution of histidine for aspartate at amino acid 63 and is termed the H63D mutation (100).

HFE has a role in iron regulation. Under normal condition, HFE forms a stable complex with TfR1, lowering its affinity to Tf (101). The C282Y mutation abolishes the ability of HFE to associate with β_2-microglobulin (β_2m) and prevents cell-surface expression, resulting in loss of function (102). H63D variants appear to form a salt bridge with a residue in the α2 loop of HFE that binds to TfR1, which possibly provides a molecular basis for its effect on iron homeostasis (98).

Both the C282Y and H63D HFE variants are highly prevalent in the general population and carriers of these polymorphisms frequently have higher transferrin saturation and ferritin levels than wild-type individuals (103). Given the fact that carriers are able to modulate body iron deposition, several studies were performed to analyze the relationship between HFE alleles and breast cancer.
Kallianpur and co-workers reported a high prevalence of HFE C282Y alleles in women with breast cancer (104). In a large study performed by Osborne and colleagues, with 24469 participants, C282Y homozygotes were at increased risk of developing breast cancer, but not C282Y/H63D heterozygotes (105). Moreover, Beckman reported that, in the context of multiple neoplasias, the interaction between the HFE and TfR alleles could be associated

with increased risk for cancer. Particularly, individuals with the HFE C282Y allele (homo- or heterozygotes), together with TfR Ser142/Ser142 genotype showed an increased frequency of breast cancer. This study found no association when each gene was analyzed in separate (106).

An explanation for the lack of association between HFE major alleles and breast cancer in some studies can be found in a study performed by Hunt and colleagues, where they report that most C282Y heterozygotes do not absorb dietary iron more efficiently and do not present increased body iron stores (107).

3.5.3 Animal Models

Using the 7,12 dimethylbenz[a]anthracene (DMBA)-induced mammary cancer model in rats, Hrabinski and colleagues studied the influence of iron-replete or iron-deplete diets on tumor progression. The authors demonstrated that severe iron deficiency significantly lowers the incidence of mammary tumors in DMBA-treated rats and that this protective effect is diminished by supplying an iron rich diet to the rats during the promotion phase of tumorigenesis (108).

3.5.4 Expression of iron-related proteins in cancer

Neoplastic cells have higher demands for iron, which is reflected in the gene expression profile manifested during tumor progression: through multiple pathways, breast cancer cells increase iron uptake and decrease iron efflux (97). These cells express higher levels of TfR1, compared to non-neoplastic breast tissue, which leads to increased iron intake, independently of intracellular iron levels (69). Studies in the MCF-7 mammary tumor cell line indicate that these cells produce Tf and TfR1, which confers selective advantage to these rapidly proliferating cells (109).

Serum ferritin expression levels were reported to be useful to stratify patients at higher risk of recurrence (110). Hypothesizing that the source of ferritin levels is the tumor mass and that this measure could reflect more directly the ferritin status of the tumor, Guner and associates studied tissue ferritin levels instead of serum levels. Besides reporting that there was no significant differences in the serum ferritin values between the cases of breast carcinoma and those with benign tumors, the authors showed higher tissue ferritin levels in breast cancer tissue, compared with benign or normal tissue (111). Studies by Rossielo revealed that ferritin staining was found mainly in the stroma and in macrophages surrounding neoplastic cells, which could explain contradictory results (112).

Ferroportin 1 is downregulated in breast cancer cell lines and human breast tumors. This evidence, together with the upregulation of hepcidin, indicates that these cells acquire a “high intracellular iron” phenotype, which is associated with worse prognosis (113). In the same study, transfection of a mammary carcinoma cell line with an expression vector for ferroportin 1, resulted in decreased final tumor weight and rate of tumor growth in mice (113).

Using a bioinformatics approach, the same group reported that the anti-export phenotype, characterized by low ferroportin 1 expression and high hepcidin expression, and pro-import phenotype, assigned to tumors showing high TfR1 expression and low HFE expression, were associated with increased metastasis rate in breast tumors (114).

4. TUMOR MICROENVIRONMENT

4.1 Importance of the tumor microenvironment

Current knowledge in breast cancer has been leading to a shift in perspective, providing a bigger body of evidence to support the idea that not only epithelial tumoral cells are relevant for tumor progression, but also their dynamic interactions with stromal cells (115-117).

Tumor microenvironment (TME) is the designation attributed to the set of cells, soluble factors, cytokines, extracellular matrix and cell-cell interactions that support neoplastic transformation, tumoral progression and invasion (118).

As cells undergo neoplastic transformation, the expression of particular genes, which cannot be classified as oncogenes or tumor suppressor genes, changes and helps to promote high malignancy and metastasis (119). Ma and collaborators performed a microarray analysis of genes expressed during the transition from normal to ductal carcinoma *in situ* and from DCIS to invasive ductal carcinoma. Numerous genetic alterations were detected between these stages of tumor progression, in the epithelial and stromal compartments, which demonstrates that tumor-adjacent tissue co-evolves with epithelial cells (120). These data suggest that epithelial malignant cells require an appropriate support structure from the stromal cells to successfully acquire a full malignant potential (121).

The microenvironment of a breast carcinoma is occupied by a huge variety of resident cells, including adipocytes, fibroblasts, endothelial cells and newly formed blood vessels and migratory cells, such as leukocytes (122, 123). This stromal compartment plays an active role in tumorigenesis, through a wide range of pathways: immunosuppressing anti-tumoral responses, promoting resistance against therapy, stimulating angiogenesis through the release of pro-angiogenic factors, providing niches for metastatic cells or endorsing neoplastic growth through the release of growth factors (118, 124).

4.2 The role of macrophages

One of the major components of the tumor milieu are the macrophages (125). These are tissue-resident innate immune effector cells, with important functions such as tissue homeostatic regulation and immunological clearance (126). Locally, these cells are responsible for the resolution of inflammation, clearance of apoptotic cells, production of cytokines and growth factors and antitumor immunity (127, 128). Van Furth in 1968 (129) proposed that the homeostasis of tissue-resident macrophages relies on the constant

recruitment of monocytes. Macrophage precursor's monocytes circulate in the bloodstream, bone marrow and spleen and do not proliferate in a steady state. Inflammation, pathogen-associated pattern recognition receptors or cytokines lead to the migration of monocytes to tissues and differentiation into inflammatory dendritic cells or macrophages (127). More recent evidences, however, contradict that concept and suggest that tissue macrophages do not derive from monocytes, but are derived from embryonic precursors that seed the tissues before birth and can maintain themselves in adulthood by self-renewal (128).

Macrophages show a high level of plasticity, because they are able to assume diverse activation states depending on specific stimulation (130). The M1/M2 dicotomy is frequently used, in which macrophages are classified as M1, or classically activated, or M2, alternatively activated, depending on phenotypic characteristics, effector function, chemokine secretion and by the expression of specific receptors (131).

In response to "classic" stimulants, such as interferon-gamma (IFN-γ) or lipopolysaccharide (LPS) macrophages become "classically activated" and acquire a M1 phenotype. These cells promote a Th1 response, killing of intracellular pathogens, efficient antigen presentation capacity and tumor destruction (132).

Anti-inflammatory molecules, like glucocorticoid hormones, IL-4, IL-10 and IL-13 induce an "alternatively activated" M2 phenotype. M2 macrophages show more a phagocytic activity, participate in Th2 responses, help with parasite clearance, attenuate inflammation, promote tumor progression and have immunoregulatory functions (132).

Recalcati and colleagues investigated the differential expression of the genes involved in iron homeostasis and M1/M2 polarization. The authors reported that M1 macrophages show a gene profile that favors iron sequestration, with ferroportin 1 downregulation and ferritin upregulation (133). This strategy can be employed during infection and inflammation, in which pro-inflammatory macrophages sequester iron into ferritin to reduce iron availability to pathogens (134). On the other hand, M2 macrophages present enhanced iron release, because they upregulate ferroportin 1 expression and decrease ferritin induction (135).

Macrophages can also be polarized into a "M2-like" phenotype. These cells share characteristic of both M1 and M2 sub-populations and have been named tumor-associated macrophages (TAM) (132).

4.3 The tumor-associated macrophages' functions

4.3.1 Tumor progression

Tumor-associated macrophages abundantly populate solid tumor microenvironments and several studies have demonstrated that they are able to shift clinical outcomes (123).

A large set of data supports the concept that macrophages help promoting tumor progression (121). Lin and colleagues reported that depletion of macrophages – through a homozygous null mutation of colony-stimulating factor 1 (CSF-1), which resulted in impairment of myeloid lineage development – decreased the recruitment of these immune cells, which was associated with delayed progression to malignancy and metastasis. Moreover, overexpression of CSF-1 accelerated tumor progression and metastatic seeding (136). Other studies reported that in macrophage-deficient mice, result of previous treatment with antisense oligonucleotides directed against Csf-1, there was a complete suppression of tumor growth (137).

These data implicate a causal relationship between macrophage recruitment and worse outcome in neoplastic disease. In fact, increased TAM density correlates with advanced tumor progression and metastasis in over 80% of the clinical studies published on the subject (122), including human breast cancer (138).

4.3.2 Tumor inflammation

The inflammatory process is responsible for leukocyte recruitment into the damaged tissue. In chronic inflammation, recruitment is persistent and these immune cells produce reactive oxygen and nitrogen species, which react with DNA, resulting in oxidative DNA damage and consequently, mutagenic events in epithelial cells (139). Furthermore, cells in the immunomicroenvironment produce growth factors and cytokines that can stimulate proliferation and survival of premalignant cells that suffered previous genetic alterations (121).

4.3.3 Tumor cells invasion and extravasation

Macrophages are abundant in the invasive front of breast carcinoma and overlap with areas of basement-membrane breakdown and tumor cell egress (122). These cells produce metalloproteinases, especially MMP-7 and MMP-9 that have the ability to destroy the extracellular matrix (140). Moreover, tumor cells produce CSF-1, which promotes

macrophage differentiation and survival (141). This cytokine induces macrophages to produce epidermal growth factor (EGF), which promotes the formation of elongated protrusions in carcinoma cells. CSF-1 released by tumor cells promote EGF expression by macrophages, which in turn promotes CSF-1 secretion by carcinoma cells, leading to a positive feedback in the paracrine loop, resulting in increased tumor cell invasion (142).

4.3.4 Angiogenesis

Restrictions in nutrient bioavailability and oxygen, due to excessive proliferation, impair tumor growth beyond a certain size. Angiogenesis, which is the formation of new blood vessels, can lead to increased nutrient supply and also provides an essential exit path for potential metastasizing tumor cells into the bloodstream (143, 144). This process requires degradation of the extracellular matrix, proliferation and migration of capillary endothelial cells and their differentiation into functioning capillaries. Clinical evidence shows a correlation between local macrophage density and areas of intense angiogenesis, suggesting a role for immune cells in neovascularization (145).

The hypoxia inducible factor (HIF) is the major regulator of oxygen homeostasis. In oxygen-replete cells, HIF-1α is bound to the Von Hippel-Lindau protein (VHL), which causes HIF-1α to become ubiquitylated and targeted for proteasomal degradation. On the other hand, reduced oxygen availability results in HIF-1α accumulation, by inhibiting its ubiquitin-proteasome degradation (146). HIF-1α is translocated into the nucleus and binds to the hypoxia-responsive elements (HREs), leading to the activation of hypoxia-response genes, such as the vascular endothelial growth factor (VEGF) and one of its receptors, VEGF-receptor 1 (VEGFR1) (147). VEGF is the key mediator of angiogenesis (148) and exerts a chemotactic effect on TAMs (149). This cytokine is expressed by macrophages and tumor cells, in multiple types of human tumors (150). Circulating VEGF binds to VEGFR1 present of the surface of endothelial cells, inducing these cells to invade the underlying matrix and form new blood vessels (151).

In summary, as extensively demonstrated by several authors, tumor growth and metastasis are influenced by the dynamic interplay between epithelial tumoral cells and cells from the tumor microenvironment (152). One prevailing vision is that tumoral cells secrete and release growth factors and cytokines that act like chemoattractrants and educative signals, which recruit certain cell types, leading to tumor progression. These stromal cells then produce growth factors and chemokines that support tumor cell nutrition, proliferation, escape from immunosurveillance and extravasation into metastatic niches (120, 123).

5. CCL2

Chemokines are a group of small soluble proteins that mediate immune cell trafficking through the formation of concentration gradients (153). In their physiological context, chemokines are produced during an inflammatory process, resulting in the recruitment of leukocyte populations during a variety of processes, such as embryonic development, tissue injury, infection or tumor growth (154).

These chemotactic cytokines can be subdivided into 4 classes: C–C, C–X–C, C and C–X3–C chemokines, depending on the location of the first two cysteines in their protein sequence (155).

Focusing on CC chemokines, these can be divided into various groups: allergenic, pro-inflammatory, haemofiltrate (HCC), developmental and homeostatic. Allergenic, pro-inflammatory and HCC proteins are inducible chemokines, while those in the developmental and homeostasis subgroups are constitutively expressed (153).

The role of chemokines in tumors has been extensively studied. Transcriptional profiling has shown that chemokines are not just leukocyte attractants, but they activate a restricted and distinct program in monocytes, including matrix metalloproteases and cytochrome CYP1B1, involved in carcinogenesis (131).

CCL2 (chemokine [(C-C motif)] ligand 2), also referred to as MCP-1 (monocyte chemoattractant protein-1), is an allergenic chemokine and one of the most studied in the context of tumor progression, especially in breast cancer (156).

5.1 CCL2 secretion

CCL2 is produced by a variety of stromal cells, such as T lymphocytes (157), natural killer (NK) cells (158), fibroblasts (159) and monocytes (160). When properly stimulated, bone, epithelial, endothelial, adipose and muscular tissues are also accountable for its production (161). The effects of this chemokine are mediated through the CCL2-CCR2 axis. CCR2 (chemokine (C-C motif) receptor type 2) is mainly expressed in non-malignant epithelial cells, endothelial cells and macrophages (162).

5.2 CCL2 expression in breast cancer

Valkovic and co-workers studied the expression of CCL2 in breast invasive ductal carcinomas by immunostaining. Of the 27 samples, CCL2 immunoreactivity in epithelial cells was found in 15 samples (56%). This chemokine was also found expressed on tumor-associated macrophages, in 23 of the 27 tumors (85%) (163). Latter studies by the same group reported that CCL2 expression was positively correlated with TAM infiltration, angiogenesis and poor survival (164). Another study by Fujimoto and colleagues revealed that CCL2 expression in the tumor stroma, but not in epithelial cells, was negatively associated with relapse-free survival (165). These data sustain the notion that CCL2 supports tumor progression (166).

Expression of CCL2 has been associated with poor prognosis in a multitude of studies. In a study performed by Qian and colleagues, expression of CCL2 was associated with the increase of inflammatory monocytes in the pulmonary metastatic niche, facilitating extravasation of tumor cells (160). In another study performed by Li and co-workers, in a CCL2 knockout mouse model, a significant reduction of tumor burden, but a surprising increase in pulmonary metastasis, was reported (167).

Due to this relationship between CCL2 and cancer, it seemed reasonable to hypothesize that this chemokine could be a promising target for the development of novel anticancer therapeutics (168).

In the same study by Li and colleagues described above, they also investigated whether the administration of an anti-CCL2 monoclonal antibody to a murine model of breast cancer could influence tumor progression. They demonstrated a decrease in the number of spontaneous metastasis and reduction of established neoplastic lesions (167). Loberg and associates demonstrated that systemic administration of anti-CCL2 neutralizing antibodies significantly retarded tumor growth (169). Moreover, Fujimoto and colleagues reported that treating immunodeficient mice bearing human breast cancer cells with a neutralizing CCL2 antibody resulted in significant decrease in macrophage infiltration, angiogenic activity and tumor growth. This reduction was observed when the anti-CCL2 antibody was administered in the setting of established lesions. Administration of the same antibody during tumor induction increased the frequency of neoplasms (165).

Collectively, these data support the idea that CCL2 is required for the immunosurveillance of developing tumors, but may play a tumor-promoting function under certain conditions (167).

On the contrary, cessation of the anti-CCL2 treatment resulted in an expected influx of monocytes into the metastatic site, enhancement of angiogenesis, metastatic disease and fatal outcome in a study performed by Bonapace and co-workers. The authors concluded that any tumor immunotherapy that only sequesters immune cells away from the tumor and does not reconfigure the surrounding cells or directly kill neoplastic cells, bear a risk of lethal rebound (170).

5.3 CCL2 and iron

In a recent study, published by Muckenthaler's group, a panel of 62 genes was selected with the purpose of identifying novel modifiers of iron homeostasis. The results showed that depletion of CCL2 increased TfR1 protein expression, an important player in cellular iron acquisition. Furthermore, CCL2-deficient mice displayed massive iron overload in the spleen, mild iron overload in the liver and high expression of TfR1 mRNA and protein (171). But the first study reporting an association between CCL2 expression and iron had been performed before by Lawless and colleagues. The aim of that study was to assess CCL2 serum levels in patients with HH and correlate the results with HFE genotypes and iron status. The authors reported that CCL2 serum levels were elevated in patients with the H63D variant but not in HH patients with the C282Y polymorphism (172).

Another evidence showing the relationship between CCL2 and iron is provided by Mitchell and colleagues who investigated the impact of HFE variants on CCL2 expression and iron accumulation in brain cells. They demonstrated that, regardless of cell type and HFE genotype, CCL2 secretion was increased by increasing intracellular iron levels and decreased by treatment with iron chelators, with the exception of cells carrying the C282Y variant (173). Thus, CCL2 seems to be influenced by cellular iron status, in the neuroinflammatory context.

AIMS

AIMS

The principal aim of this work was to understand if the tumor iron status, in the breast cancer model, was related with the expression of CCL2.

For that purpose, the specific aims were to:

- ✓ Assess tissue iron deposition in normal tissue and DCIS and IDC lesions, in epithelial and stromal inflammatory cells;

- ✓ Study CCL2 expression in epithelial cells and macrophages, in paraffin-embedded tissues of reduction mammoplasty samples, which account as controls, and neoplastic breast tissues (DCIS and IDC);

- ✓ Assess the total number of macrophages (total macrophage infiltration) in all samples and the number of CCL2-positive macrophages in breast tissue;

- ✓ Correlate CCL2 expression with established iron profiles in epithelial and stromal inflammatory cells, especially with proteins known to be deregulated during neoplastic progression;

- ✓ Analyze if the HFE variants could modulate CCL2 expression in the breast cancer model;

- ✓ Analyze if CCL2 expression could be correlated with clinical-pathological parameters of breast cancer behavior and prognosis.

MATERIALS AND METHODS

1. Breast Cancer Tissue Samples

A total of 54 invasive ductal carcinomas (IDC) and 34 ductal carcinomas *in situ* (DCIS), from formalin fixed, paraffin-embedded (FFPE) breast samples were used. These samples were previously collected from the archives of the Pathology Service, at Centro Hospitalar do Porto (Porto Hospital Centre, Porto, Portugal), for the PhD project in which this study is integrated and approved by the Ethics Committee. A total of 32 aesthetic reduction mammoplasty samples were also included, accounting as normal breast tissue.

These samples are representative of primary breast tumors, collected from women that were diagnosed between 2004 and 2009, not subjected to any neoadjuvant treatment.

Haematoxylin-eosin slides correspondent to the 88 samples of primary tumors and 32 reduction mammoplasty samples were also collected and analyzed by a pathologist, in order to select normal, *in situ* and invasive representative areas, whenever possible.

These FFPE blocks were used for all the techniques performed in these study: Tissue microarray (TMA) construction, Perls' staining, immunohistochemistry, DNA extraction and PCR-RFLP.

2. Tissue microarray construction

In 1998, Kononen and his colleagues developed the tissue microarray technology that enables researchers to sample up to 1000 tumors on one glass slide, which then can be analyzed by several histological and molecular procedures (174). This high-throughput technique facilitates the rapid analysis of hundreds of patient samples by a pathologist (175).

Staining of a few TMA sections in comparison to whole tissue sections offers a clear advantage with respect to the reduction of laboratory reagents, technician time and decrease of technical variability during the staining and interpretative process (175).

The most frequent disapproval to TMA use is the small size of each tissue core – there is apprehension that due to tumor heterogeneity, biomarker scores obtained from small TMA cores will not accurately reflect scores obtained from whole sections. Moreover, there is a technical problem with tissue loss during sectioning, transfer and staining. The combination of sampling error during core extraction, core loss during slide preparation, and non-reactive cores leads to missing biomarker data and underestimation of the true incidence of a molecular marker. These problems can be minimized by the extraction of multiples cores per source blocks (174, 175).

The TMA builder used in this project is a metallic structure with 24 orifices, which allows the molding of a paraffin block, where the previously selected spots were inserted.

Paraffin at 60ºC was poured into the TMA builder and a histology cassette was placed on top. Then it was left at -20ºC for the paraffin to solidify. Next, the paraffin block was carefully separated from the TMA builder, and an identification number was assigned to the block.

The next step was the inclusion of the areas of interest, previously selected by the pathologist, into the spots of the TMA block. This was performed using an extractor, which allows the selection of tissue areas with 2.0 mm. By applying force into the extractor, the area selected was removed from the donor block and then placed into the recipient block, following a previously designed map. More than 2 spots were obtained from the same block, in order to increase tissue representativity and TMA validation.

TMA recipient blocks were then left at 60ºC for 10 minutes, to facilitate the adherence of the cores to the recipient paraffin' walls. The final step was to place a heavy structure on top of the TMA block to facilitate the alignment of the spots.

Normal liver and lymph node tissue samples were also inserted, for correct slide orientation of cores and internal controls for stainings.

TMA blocks were kept in room temperature until further techniques were performed.

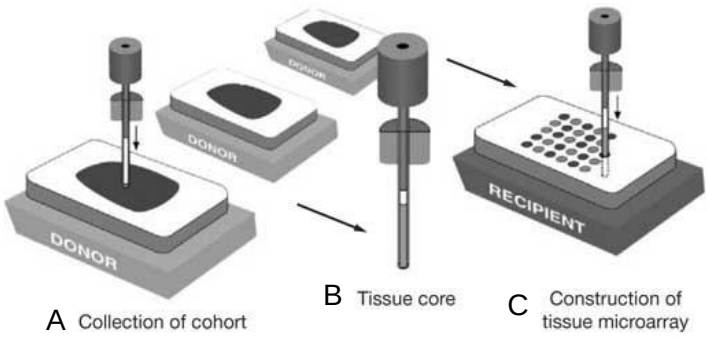

Figure 4: Representation of TMA construction. **(A)** Cores previously selected in the corresponding slide stained with H&E can be extracted from the original paraffin block with the help of an extractor. **(B)** Extractor allows the selection of regions with 2.0 mm and placing in the recipient block. **(C)** Tissue sample is placed in the paraffin block built in the TMA builder, according to a designed map. Image adapted from (176).

Apart from the controls, TMA blocks contained 452 spots from breast samples, of which 155 disappeared during alignment, sectioning or were lost during immunohistochemistry procedures.

3. *Heamatoxylin-eosin (H&E) staining*

TMA blocks were aligned, as previously described, and cut in a microtome in 2 µm sections. Slides were left for 5 minutes at 70ºC to increase tissue adherence to the glass surface and then placed at 37ºC until use.

After deparaffinization in 2 consecutive xylene baths, 5 minutes each, slides were rehydrated by immersion in absolute, 90% and 70% alcohol and then rinsed under running water. Slides were then submerged in Mayer's hemalum solution (Merck Millipore, Billerica, MA, USA) 5 times, rinsed under running water for 10 minutes and subsequently submerged in eosin for 1 minute. After this, slides were rinsed under running water and sequentially dehydrated in 70%, 90% and absolute alcohol and 2 changes of xylene. Slides were mounted with Entellan (Merck Millipore, Billerica, MA, USA).

H&E slides were evaluated under the light microscope by a pathologist in order to identify the type of lesion in each spot (normal, DCIS or IDC), blinded of diagnostic and clinical information regarding the original donor tissue.

Lesions were further classified and coded as following, for statistical evaluation proceedings:

0 –Normal (from the reduction mammoplasty samples);
1 - Normal, from a sample diagnosed as DCIS*;*
2 – Normal, from a sample diagnosed as IDC;
3 – Pure DCIS (from a sample diagnosed as DCIS)*;*
4 – DCIS*,* from a sample classified as in IDC;
5 – Pure IDC (from a sample diagnosed as IDC).

4. Perls' Prussian Blue staining

Perls's staining was performed to assess hemosiderin deposits in breast samples. Hemosiderin is a degradation product of ferritin, an iron storage complex (177) and this method provides a qualitative estimative, based on color intensity, of the amount of iron present in the tissue.

TMA blocks were cut in a microtome in 2 µm sections. Slides were left for 5 minutes at 70ºC to increase tissue adherence to the glass surface and then placed at 37ºC until the technique was performed.

After deparaffinization and rehydration, as previously described, slides were stained with Butting solution (mixture of equal parts of chloridric acid 2% and potassium ferrocyanide 2% solutions), for 20 minutes at 60ºC and then rinsed in distilled water. Chloridric acid denatures the binding proteins of the hemosiderin molecule, leading to the release of ferric (3+) ions, which then bind to potassium ferrocyanide, resulting in the formation of the blue pigment, known as Prussian Blue.

Tissues were counterstained with nuclear red for 4 minutes. Slides were then differentiated in absolute alcohol until a pink contrasting color was achieved. The slides with the stained samples were mounted with Entellan (Merck Millipore, Billerica, MA, USA).

When performing Perls' staining, a positive control tissue, such as an iron loaded liver tissue, was included in the experiment. Considering a situation of absence of hemosiderin deposits in the tissues, the positive control allows the researchers to understand if this absence is caused by lack of deposits or inaccuracy of the technique.

Slides with Perls' staining were evaluated under the light microscope for detection of hemosiderin deposits, in the epithelial and stromal compartment separately. Each compartment was evaluated as 1, if at least one cell had hemosiderin deposits or 0, if no deposits were visualized.

5. DAB-enhanced Perls' technique

Considering that iron concentration in most tissues is low and the threshold of detection using the Perls' method is hardly reached in epithelial cells (178), intensification with DAB can be performed to increase sensitivity, as described by Meguro (64). Samples were stained as described by this author, with an increase in incubation times of 25%, as described by Van Duijn and colleagues (179).

TMA blocks were cut in a microtome in 4 µm sections and mounted in adhesive slides with 3-Aminopropyltriethoxysilane (APES). Slides were left for 5 minutes at 70ºC to increase tissue adherence to the glass surface and then placed at 37ºC until use.

After deparaffinization in xylol and rehydration, as previously described, slides were stained with "freshly" prepared 1% potassium cyanide in distilled water (pH inferior to 5.5), for 40 minutes. After this, slides were washed in distilled water. Samples were treated in methanol containing 0.01M NaN_3 and 0.3% H_2O_2 for 75 minutes and then washed with 0.1M

phosphate buffer. For the intensification reaction, slides were incubated with a solution containing 0.025% 3.3'-diaminobenzidine (DAB) and 0.005% hydrogen peroxide (H_2O_2) in a 0.1M phosphate buffer, for 40 minutes. The reaction was stopped by rinsing in distilled water.

Tissues were then counterstained with nuclear red for 4 minutes. Slides were differentiated in absolute alcohol until a pink contrasting color was achieved. The slides with the stained samples were mounted with Entellan (Merck Millipore, Billerica, MA, USA).

A negative control was used, as performed in Roschzttardz's work (178), by omitting the incubation with potassium ferrocyanide. No staining was observed in the negative controls, showing that the staining was hemosiderin dependent and not due to peroxidase-catalyzed degradation of H_2O_2, inducing the polymerization of DAB.

As performed in routine Perls' staining, a positive control tissue was also added to the experiment.

6. Immunohistochemistry

6.1 CCL2 immunohistochemistry

Immunostaining for detection of CCL2 expression was first performed using an antibody by R&D systems (MAB2791, R&D systems, Minneapolis). Datasheet suggested using lymph node as a positive control and a dilution of 8-25µg/µL. After studying the literature, and in order to optimize the protocol, dilution of 1:10, 1:40 and 1:100 were also tested. As the negative control, omission of primary antibody was used.

Immunohistochemistry was conducted according to manufacturer's details using the Novocastra Novolink Detection System (Leica Biosystems). This detection system is systematically used in the Department and has been giving consistent results over a wide range of antibodies.

In the first tests performed in lymph node tissue, independently of the dilution used, non-previously described, strong unspecific staining in lymphocytes, background and a nuclear staining in leukocytes was visualized, as seen in Table 1.

Table 1: Representative images of CCL2 immunostaining performed on negative and positive controls for protocol optimization. Different dilutions were tested and antigen retrieval was performed using Dako Target Retrieval Solution.

	200X	400X
NEGATIVE (OMISSION OF ANTIBODY)	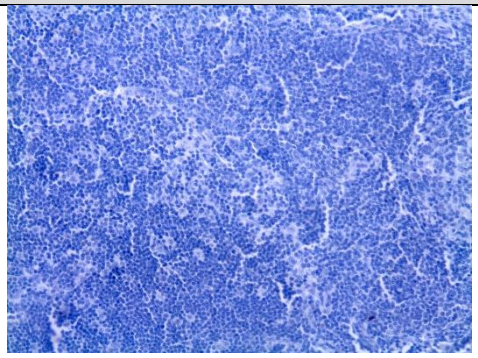	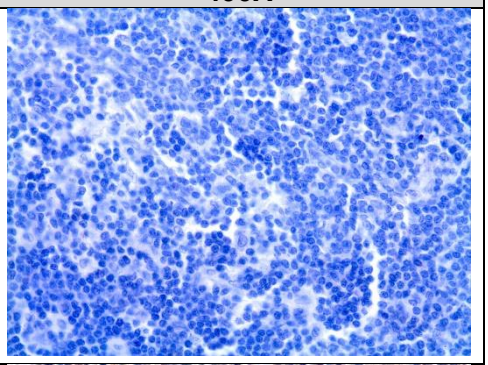
LYMPH NODE 1:10	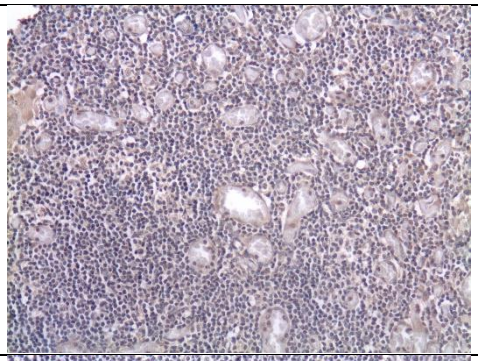	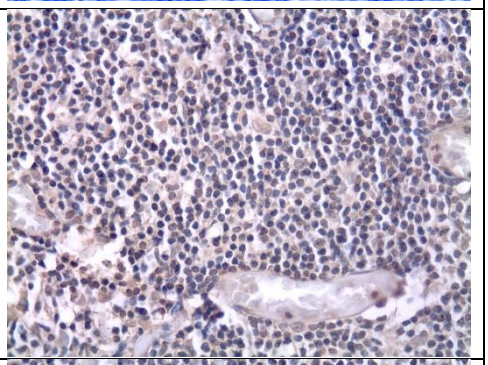
LYMPH NODE 1:20	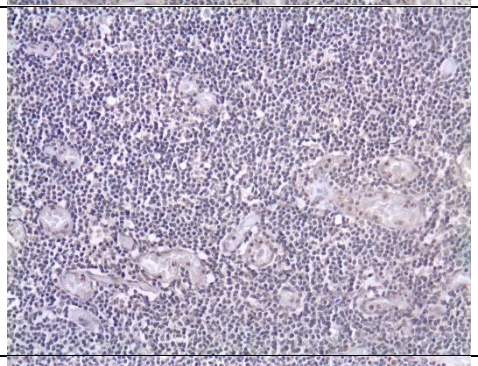	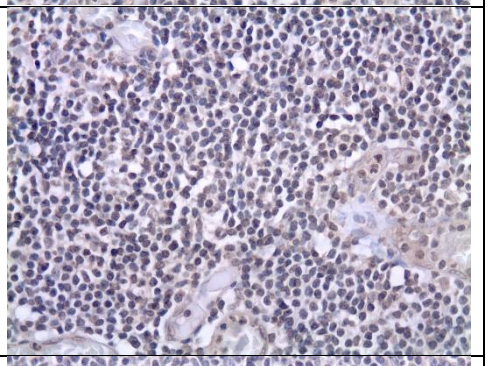
LYMPH NODE 1:40	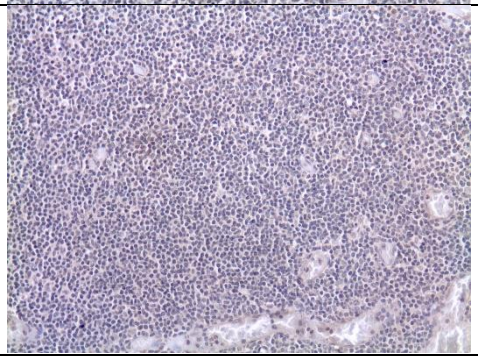	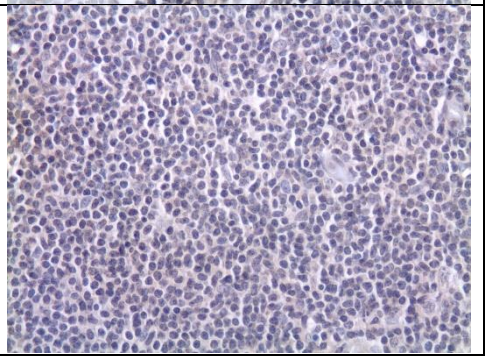

LYMPH NODE 1:60	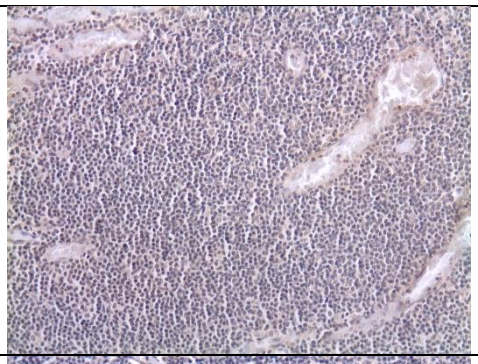	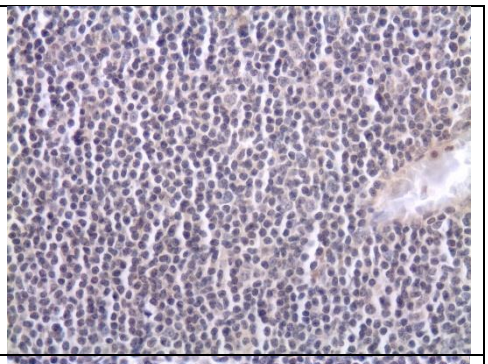
LYMPH NODE 1:100	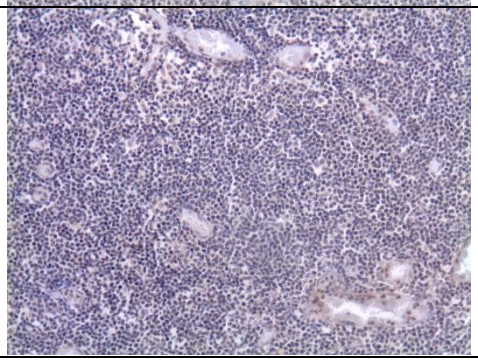	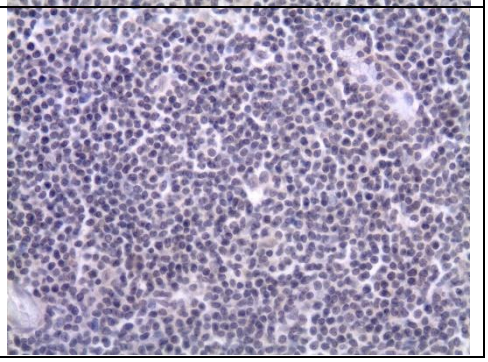

Considering that the lymph node is an immune-privileged site, overpopulated with immune cells, and CCL2 is a chemokine characterized by a mechanism of diffusion, this problem was disregarded and immunostaining using 1:60 and 1:100 dilutions was tested in breast tumor tissue.

Table 2: Representative images of CCL2 immunohistochemistry performed on breast cancer tissue. Different dilutions were tested and antigen retrieval was performed using Dako Target Retrieval Solution.

	200X	400X
1:60	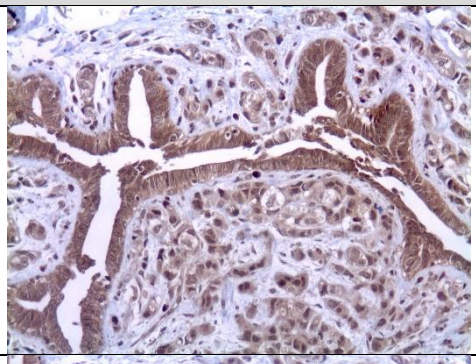	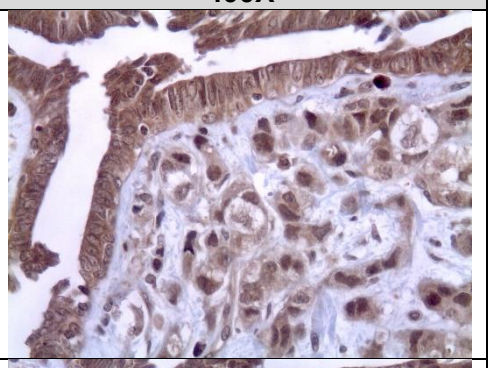
1:100	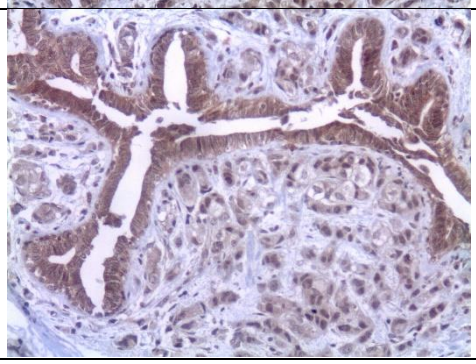	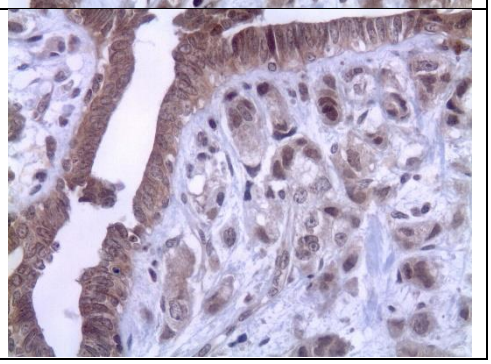

After visualization of slides, unspecific nuclear staining in epithelial cells was again detected (as seen in table 2). This staining was not previously reported in the literature analyzed. So, in order to solve this situation and optimize the immunohistochemistry protocol, different antigen retrieval methods were performed.

Immunohistochemistry, using lymph node tissue and a 1:100 dilution, was repeated, and the following antigen retrieval methods were performed:

- Extran, in a microwave, for 15 minutes;
- Pepsin (0.005%) based retrieval at 37ºC, in a heated chamber, for 45 minutes;
- EDTA 1X in boiling water (100ºC), for 30 minutes;
- Citraconic acid in boiling water (100ºC), for 45 minutes;
- Tris-EDTA 1X in boiling water (100ºC), for 1 hour.

The same antigen retrieval methods were tested, in breast tumor tissue, using 1:60 and 1:100 dilutions.

Despite the dilution or antigen retrieval method performed, predominant unspecific nuclear staining in lymphocytes (Table 3) and in epithelial cells (Table 4) was visualized.

Table 3: Representative images of CCL2 immunohistochemistry performed on positive controls. Same dilution was tested (1:100), with different antigen retrieval methods.

	200X	**400X**
Lymph Node, 1:100, Dako Retrieval Solution	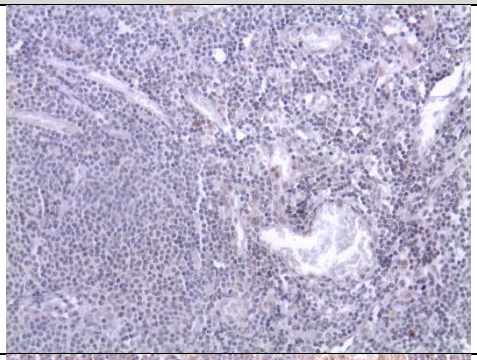	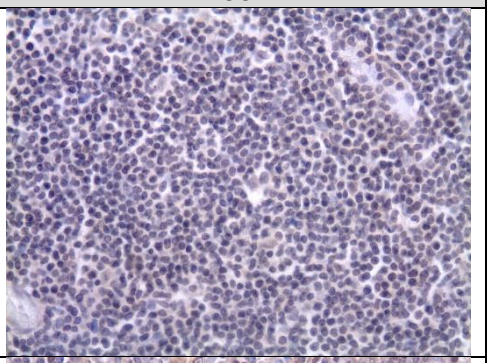
Lymph Node, 1:100, without antigen retrieval	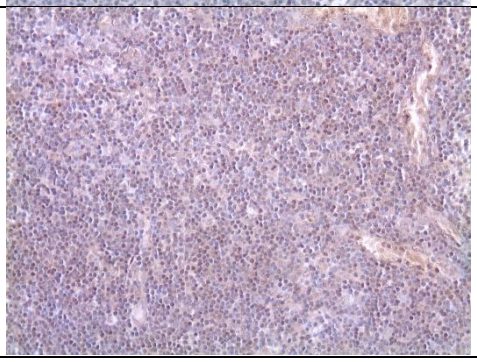	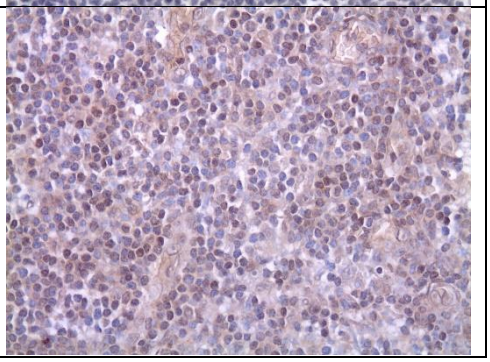

Lymph Node, 1:100, Extran	Lymph node, 1:100, EDTA	Lymph Node, 1:100, Tris-EDTA	Lymph node, 1:100,Pepsin	Lymph Node, 1:100, Citraconic anhydride
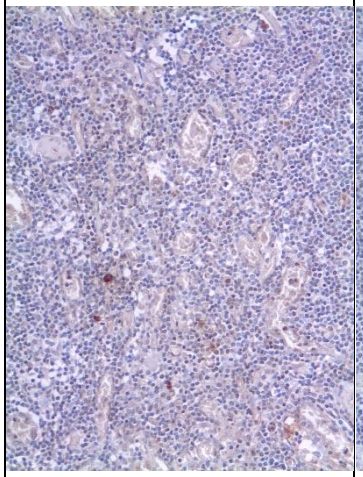	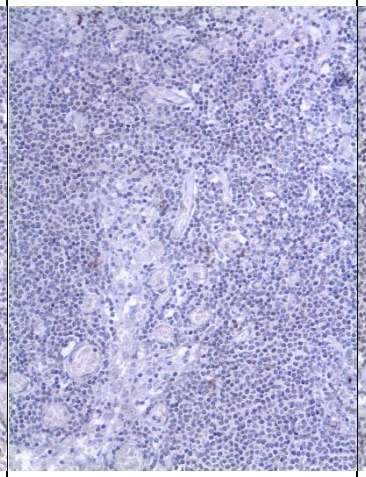	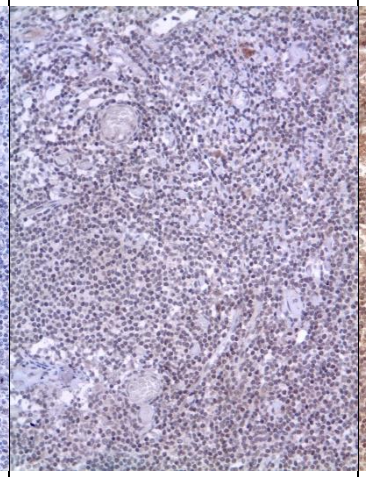	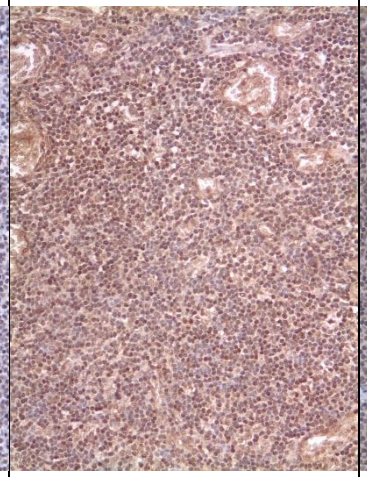	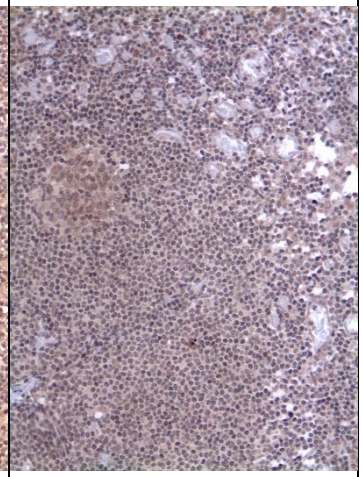
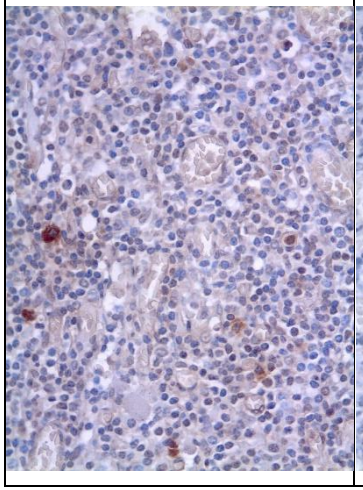	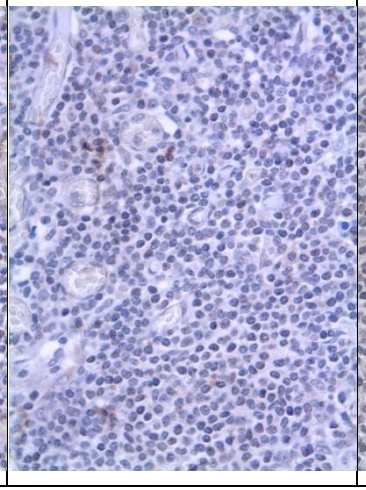	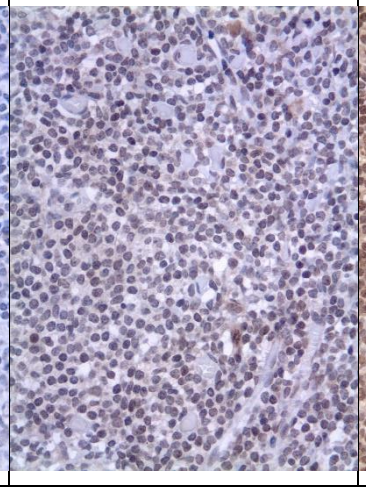	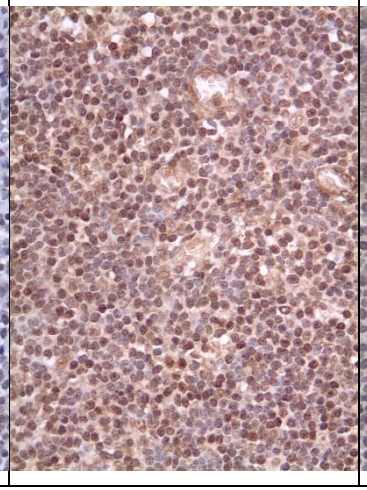	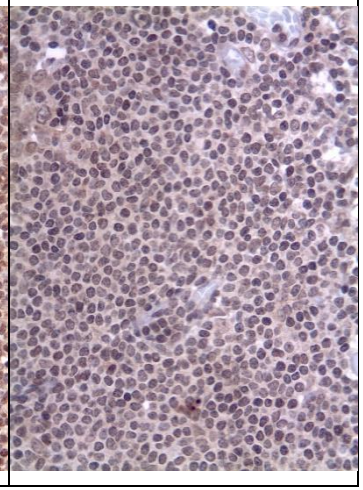

Table 4: Representative images of CCL2 immunohistochemistry performed on breast cancer tissue. Same dilution was tested (1:100), with different antigen retrieval methods.

	200X	400X
Breast tissue, 1:100, Without antigen retrieval	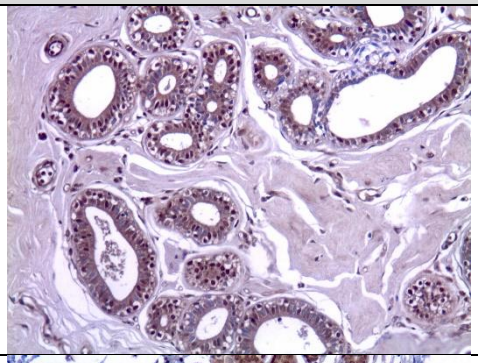	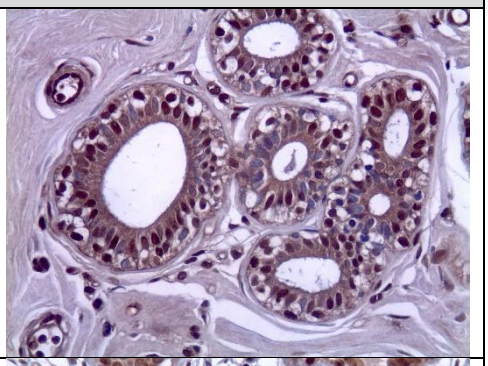
Breast tissue, 1:100, Citraconic anhydride	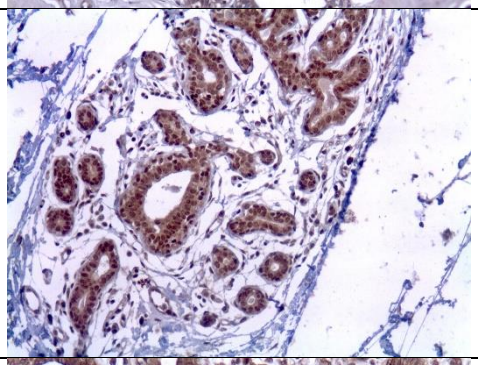	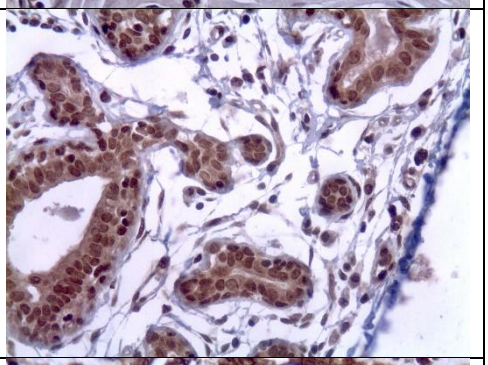
Breast Tissue, 1:100, Pepsin	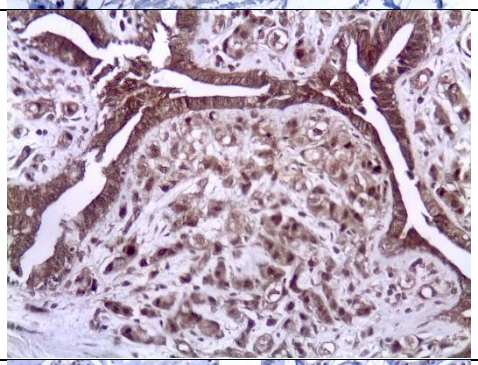	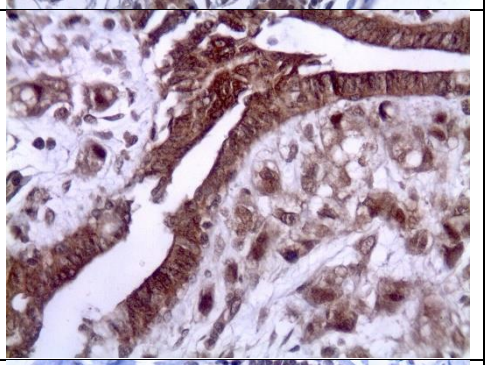
Breast Tissue, 1:100, Tris-EDTA	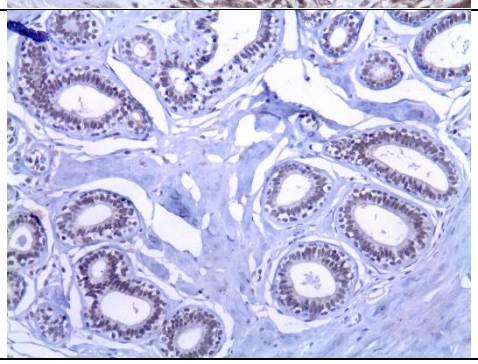	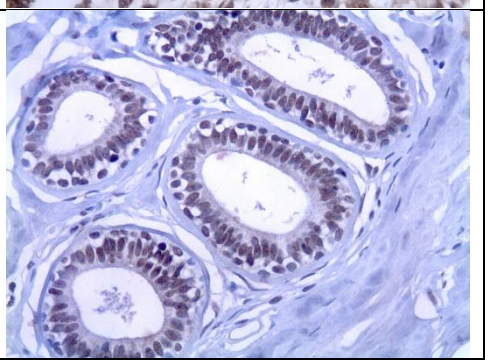

Breast tissue, 1:100 EDTA	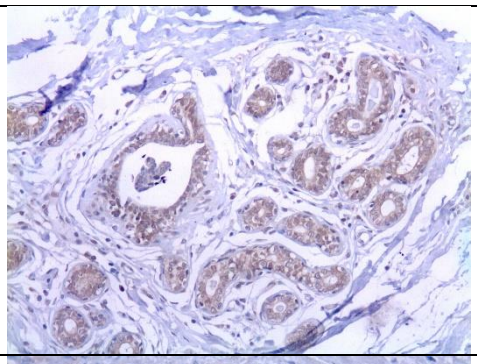	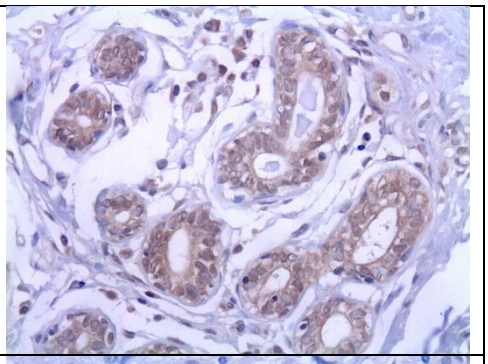
Breast tissue, 1:100 Extran	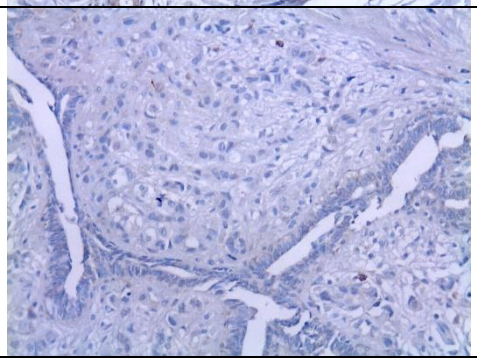	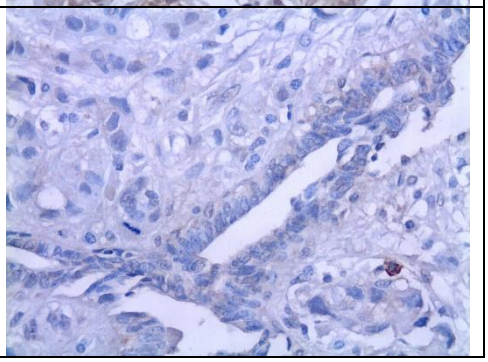

After these results, R&D systems was contacted, to provide technical support about the unspecific staining. The assistant suggest antibody revelation using the Avidin-Biotin Complex Method (ABC), instead of the Novocastra Novolink Detection System used previously.

As demonstrated in table 5, the problems previously detected persisted and R&D Systems was again contacted. Tests performed by R&D Systems revealed that this antibody was detecting non-specific protein and so, the anti-CCL2 antibody by R&D systems was replaced by another antibody by Abcam.

Table 5: Representative images of CCl2 immunohistochemistry performed on lymph node (positive control) and breast cancer tissue. Antigen retrieval with citrate buffer and revelation with the ABC method were performed.

	200X	**400X**
Lymph node, 1:40 ABC method, Sodium Citrate	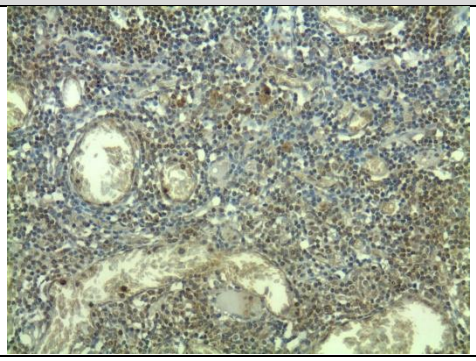	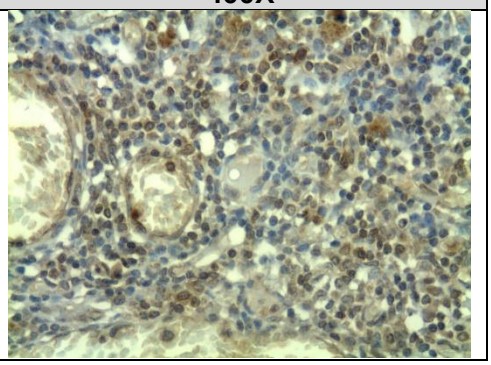

Breast Tissue, 1:40, ABC method, Sodium Citrate	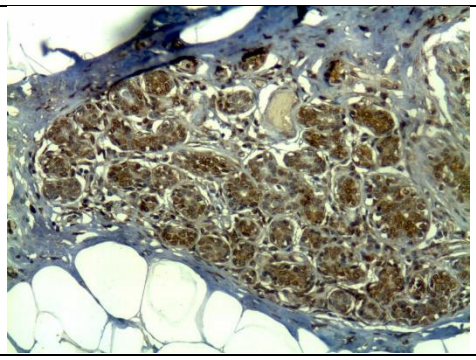	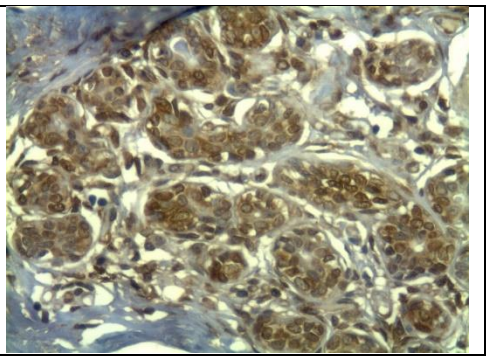

CCL2 immunohistochemistry protocol was optimized using the mouse anti-human monoclonal antibody CCL2, at a 1:25 dilution (ab9858, Abcam, Cambridge, United Kingdom) in TBS.BSA at 5%.

6.2 CD68 immunohistochemistry

CD68 immunohistochemistry was performed with the mouse anti-human monoclonal antibody, at a 1:2000 dilution (clone KP-1, Cell Marque Corporation, California, USA) in TBS.BSA at 5%, using the Novolink detection system.

6.3 Immunohistochemistry protocol

Immunostaining was performed using the same protocol for anti-CCL2 and anti-CD68 antibodies.

For both stainings, lymph node tissue was used as the positive control (internal control in each TMA slide), as advised by the supplier, and omission of the antibody was used as the negative control.

6.3.1 Sectioning

TMA blocks previously constructed were cut in 2 µm sections and mounted in adhesive slides, in order to increase adhesion and prevent separation during technical procedures (180). Slides were left for 5 minutes at 70ºC to increase tissue adherence to the glass surface and then placed at 37ºC until use.

6.3.2 Deparaffinization and hydration

Slides were deparaffinized in 2 baths of xylene, 5 minutes each, and sequentially rehydrated in absolute alcohol, 90% and 70% and washed in water.

6.3.3 Antigen retrieval

Antigen retrieval was then performed using Dako Target Retrieval Solution (Agilent Technologies, Denmark), at 10% in distilled water. Slides were placed in a staining jar, which was allocated in the water bath at approximately 100ºC, until retrieval solution turned blur (approximately 5 minutes) and 20 more minutes after that.

At the end of this time, the slides were taken out of the water bath and allowed to cool at room temperature.

During this time, the immunohistochemistry chamber was prepared. For this, absorbent paper was cut and placed in the bottom of the chamber and impregnated with TBS.

6.3.4 Endogenous Peroxidase Block

Slides were placed in the absorbent paper in order to eliminate the excess of antigen retrieval solution. Sections of interest in the slides were delineated with a hydrophobic pen (NovoPen, Novocastra, Leica Systems), which prevents waste of reagents by keeping liquids in tension. After this, slides were incubated with 3 drops of peroxidase block (Peroxidase Block, Novocastra Novolink Detection System, Leica Systems), in the immunohistochemistry chamber, for 5 minutes, at room temperature.

Slides were then rinsed twice in TBS, 5 minutes each.

6.3.5 Protein Block

Excess of TBS was eliminated from the slides by placing them in absorbent paper. Sections were again delineated with the hydrophobic pen and slides were incubated with 3 drops of protein block (Protein Block, Novocastra Novolink Detection System), for 5 minutes, at room temperature.

6.3.6 Primary antibody

The excess of protein block was drained from the slides and 150 µL of the primary antibody, at the correspondent dilutions, was poured in each glass slide. Slides were kept in the immunohistochemistry chamber, overnight, at 4ºC.

6.3.7 Secondary antibody

The following day, slides were rinsed twice in TBS, 5 minutes each.

Excess of TBS was eliminated from the slides by placing them in absorbent paper. Slides were then incubated with 3 drops of secondary antibody (Post-primary, Novocastra Novolink Detection System), for 30 minutes, in the immunohistochemistry chamber, at room temperature. Slides were then rinsed twice in TBS, 5 minutes each.

6.3.8 Polymer

Slides were placed in the absorbent paper in order to eliminate the excess of the secondary antibody. Slides were incubated with 3 drops of the polymer (Polymer, Novocastra Novolink Detection System) for 30 minutes. Then, slides were rinsed twice in TBS, 5 minutes each.

Right before use, chromogen was prepared, using 50µL of DAB to every 1000 µL of substrate.

6.3.9 Revelation

Revelation was performed with 3.3'-Diaminobenzidine (DAB). Slides were incubated with 150 µL of chromogen, until revelation occurred. Slides were then placed under running water for 10 minutes.

6.3.10 Counterstaining and slide mounting

Slides were immersed in Mayer's hemalum solution for 5 to 6 times, and then placed under running water for 10 minutes.

Slides were sequentially dehydrated in 70%, 90% and absolute alcohol and 2 changes of xylene. At last, they were mounted with Entellan (Merck Millipore, Billerica, MA, USA).

7. CCL2 scoring

TMA spots were then analyzed by a pathologist, in order to evaluate the area of expression and intensity of CCL2 staining.

For the analysis of CCL2 epithelial stained area, a semi-quantitative approach was used and the following cut-off values were considered:

- Score 0, which represents 0% of stained cells;
- Score 1, 1 to 10% stained cells;
- Score 2, 11 to 20% stained cells;
- Score 3, 21 to 35% stained cells,

- Score 4, 36 to 50% stained cells;
- Score 5, more than 50% cells presenting staining.

For the analysis of CCL2 epithelial staining intensity, the following criteria were used:

- Score 0: No staining;
- Score 1: Weak staining;
- Score 2: Moderate staining;
- Score 3: Strong staining.

The final score was obtained by multiplying the area score and the intensity score.

Macrophages with CCL2 positive staining were counted in each spot. For this, 5 HPFs (high power fields, 400X), per spot, were visualized under the light microscope and macrophages with CCL2 positive staining were counted. The values obtained from the 5 HPFs were added in order to obtain the total spot count of CCL2 positive macrophages.

8. Macrophage counting

CD68 staining was performed in TMA slides to help identify cells from the myeloid lineage and quantitatively evaluate its infiltration in the tumor nest and/or tumor stroma.

This antibody is a 110-kDa transmembrane glycoprotein highly expressed by monocytes and tissue macrophages (181).

Clone KP-1 was considered by Saito and colleagues to be an efficient antibody to identify tissue macrophages in a variety of tissues (182). CD68 recognized by this clone is resistant to conventional fixatives such as formalin, making it useful for diagnosis and routine analysis (183).

On the other hand, CD68 is also expressed in fibroblasts, plasmacytoid T cells and neutrophils. This makes CD68 a pan-marker of cells of the myeloid lineage and not specific of macrophages (183).

To perform macrophage count in each spot, CD68 positive cells were counted in 5 HFPs, taking into account CD68 immunoreactivity, cell and nuclear morphology, to distinguish between macrophages and other non-specifically stained cells. The values obtained from the 5 HPFs were added in order to obtain the total spot count of tissue macrophages.

9. DNA extraction

9.1 Biologic samples

One paraffin block from each patient was selected, in order to perform DNA genotyping. FFPE blocks used for DNA extraction were the same as previously selected from Centro Hospitalar do Porto.

In some cases extraction from FFPE blocks and PCR-RFLP was not possible to perform, due to extreme DNA degradation. In these cases, DNA extraction from peripheral blood was performed.

Peripheral blood was collected from women, diagnosed with Breast Cancer between 2004 and 2009, which were followed by the Oncology Service, Centro Hospitalar do Porto. Blood was collected, by venipuncture into tubes already containing EDTA, an anticoagulant, as routinely performed in the Service.

9.2 DNA extraction from FFPE blocks

9.2.1 Deparafinization and hydration

Genomic DNA was extracted from FFPE breast sections using the Ultraprep Tissue DNA kit (AHN Biotechnologie, Nordhausen, Germany). FFPE blocks were trimmed in the microtome and first cuts were rejected, to avoid potentially more degraded DNA, due to air exposure, and contamination. Between blocks, the steel knife was cleaned with absolute ethanol.

Paraffin-blocks were cut in a microtome in 10 µm sections and 2 cuts from each block were used for DNA extraction. Slides were left for 5 minutes at 70ºC to increase tissue adherence to the glass surface and then placed at 37ºC until use.

Glass slides were placed in supports and washed 3 times with Ottix (Diapath, Martinengo, Italy), 10 minutes each.

Slides were next washed with absolute, 90% and 70% alcohol, 10 minutes each. After this, slides were washed with distilled water.

Eppendorf tubes were previously prepared with the identification number of each FFPE block and 250 µL PB buffer and 20 µL proteinase K (Ultraprep Tissue DNA kit, AHN Biotechnologie, Nordhausen, Germany) were added to each tube. The samples were scraped from the glass slides with the help of a pipette tip and placed in the corresponding

eppendorf. These were incubated overnight in a thermomixer, at 55ºC, at 300 rpm, to facilitate tissue digestion.

9.2.2 Extraction

The following day, 250 µL of AB buffer was added to each tube and these were vortexed for 30 seconds or until the pellet was resuspended.

The solution in each tube was transferred into a new eppendorf with a spin column (±700 µL) and samples were centrifuged for 1 minute and 40 seconds, at 14500 rpm. The flow-through was then discarded and 400 µL of WB buffer was added to each tube, which was then centrifuged again for 1 minute and 40 seconds, at 14500 rpm.

Flow-through was discarded and spin columns were washed, twice, with 400 µL of 70% alcohol. After the addition of 70% alcohol to the eppendorf tubes, these were centrifuged for 3 minutes and 30 seconds, at 14500 rpm.

At this point, flow-through was discarded and the columns were carefully transferred into 1.5 mL new eppendorf tubes, previously identified.

Then, 40µL of EB buffer pre-heated at 70ºC was added to the center of each column and incubated at room temperature for 2 minutes. Finally, solutions were centrifuged for 1 minute and 40 seconds, at 14500 rpm.

Columns were discarded and eppendorf tubes carefully closed.

9.2.3 DNA extraction from peripheral blood

Genomic DNA was isolated from peripheral blood leukocytes, using a modification from the original “salting out” method (184).

The first step consists of isolating mononuclear cells, through centrifugation of samples at 2000 rpm, for 20 minutes. This results in a cell distribution across the tube: on the bottom, a cellular phase, formed by erythrocytes and a buffy coat, composed of leukocytes; and on top a liquid phase, which contains the plasma. Plasma and the buffy coat were retrieved into a Falcon tube (50 mL), to which RCLB (Red Cell Lysis Buffer) was added until the final volume of 50 mL. Solution was homogenized by inversion and incubated for 10 minutes at room temperature. Next, centrifugation at 2000 rpm, for 10 minutes at 4ºC, was performed. Supernatant was rejected and the pellet was washed repeatedly with RCLB and centrifuged until all erythrocytes were lysed and the pellet turned white. Next, 3.5 mL of TE-2 (Tris-EDTA) buffer was added to the pellet, plus 200 µL of SDS 10% (Sodium Dodecyl Sulfate) and 10 µL of Proteinase K.

After soft agitation, samples were incubated at 42ºC for 12 hours, allowing full cell digestion. Following this step, samples were transferred into a conical tube of 15 mL, to which 1 mL of NaCl 6M was added. This buffer leads to the precipitation of proteins and release of DNA. The solution was then vortexed and placed in a magnetic agitator for 10 minutes. Next step was centrifugation at 3000 rpm, for 30 minutes, at 23ºC. This step allowed the separation of the protein component, which aggregates at the bottom of the eppendorf. Supernatant was transferred into a 15 mL Falcon and DNA precipitation was induced by adding 20 mL of absolute ethanol at -20ºC. Ethanol is responsible for the dehydration of the DNA molecule, and after repetitive inversions of the Falcon tube the DNA precipitate was visualized. This precipitate was washed twice with 5mL of 70% ethanol, at -20ºC, and resuspended in TE buffer in a 1.5 mL eppendorf. Finally, solution was left in an agitator for 12 hours and stored at -20ºC.

9.2.4 DNA quantification

Genomic DNA in the samples, extracted from paraffin blocks or peripheral blood, was quantified using NanoDrop spectrophotometer. DNA concentration and the ratios of absorbance at 280nm and 260nm ($A_{260/280}$) and 260nm and 230nm ($A_{260/230}$) were analyzed. The $A_{260/280}$ value gives information regarding DNA contamination of proteins and the $A_{260/230}$ values may indicate other contaminants, like phenols or salts.

The DNA was stored at -20ºC until PCR was performed.

9.2.5 Polymerase Chain Reaction (PCR)

This technique, first introduced by Mullins in 1986 (185) allows the enzymatic *de novo* synthesis of a specific DNA sequence. Through repetitive cycles of denaturation, annealing of specific oligonucleotide primers and polymerase extension, the DNA sequence limited by the 2 primers is doubled in each cycle, mimicking the *in vivo* process of DNA replication (186).

PCR Reactions were performed using the Qiagen Multiplex PCR kit (Valencia, CA, USA) and the conditions for amplification are described below:

Table 6: Description of the Multiplex PCR Components used for amplification of the C282Y and H63D variants of HFE.

Component	Volume/reaction	Final concentration
2× Multiplex PCR Mastermix	25 µL	1×
Q-solution, 5×	5 µL	0.5×
HFE C282Y/H63D Forward primer	100 µM	10 µM
HFE C282Y/H63D Reverse primer	100 µM	10 µM
Template DNA	Variable	≤1 µg DNA
Bi-distilled Water (Braun)	Variable	

For the detection of the C282Y polymorphism the following primers were used: 5'-CAA GTG CCT CCT TTG GTG AAG GTG ACA CAT-3' as the forward primer and 5'-CTC AGG CAC TCC TCT CAA CC-3' as the reverse primer (primers from Metabion, Steinkirchen, Germany). These primers amplify a fragment with 343 bp.

For the HFE H63D polymorphism, the following forward and reverse primers' sequences were used: 5'-ACA TGG TTA AGG CCT GTT GC-3' and 5'-GCC ACA TCT GGC TTA AAA TT-3' (primers from Metabion, Steinkirchen, Germany). These primers amplify a fragment with 294 bp.

Primers for detection of polymorphisms in the HFE gene were chosen according to Feder work (99).

Everytime PCR was performed, a negative control, consisting of mix without DNA template, was included.

The PCR program used for C282Y and H63D amplification was the following: an initial activation step at 95ºC, for 10 minutes, was performed to activate the HotStarTaq DNA polymerase; after this, 36 cycles, consisting of denaturation at 94ºC, for 30 seconds, annealing for 90s, at 58ºC, and extension for 90s, at 72ºC were performed. At last, reaction was extended at 72ºC, for 10 minutes.

9.2.6 Electrophoresis

Electrophoresis is based on the principle that applying an electric field will force the negative molecules, such as DNA, to migrate into the positive pole, through an agarose or polyacrylamide matrix. This separates molecules by size, because smaller molecules move faster and migrate further through the gel (187).

This technique was performed after PCR, in order to verify if amplification occurred.

First, agarose gel at 1.5% was prepared, mixing 4.5 g of agarose (GeneOn, Germany) with 300 mL of 1X TAE in an erlenmeyer flask. Then it was placed in a microwave, for 4 minutes, at full power. After this, 25µL of ethidium bromide (Invitrogen, Thermo Fisher Scientific, Massachusetts, USA) was added and the erlenmeyer flask was carefully stirred. When the agarose solution cooled down, it was poured slowly over a gel mold with the well combs in place. It was left at room temperature for 20-30 minutes, until completely solidified.

. When the agarose gel was totally solidified it was placed in the electrophoresis unit, agarose gel was covered with 1X TAE and the combs were removed.

Then, 5 µL of the amplicon were added to 2 µL of loading buffer and the resulting solution was loaded to the wells of the gel. A 100 bp molecular weight ladder was placed in the first lane of the gel and the samples were loaded into the following wells. The gel was run for 1 hour, at 150 V.

The electrophoresis gel was visualized under ultraviolet light. Visualization of the fragments with the respective lengths, described above, indicates that amplification was successful and further techniques could be performed.

9.2.7 PCR-RFLP

Restriction Fragment Length Polymorphism (RFLP) is one of the most used techniques to detect polymorphisms, especially those characterized by a single nucleotide variant. This technique consists of the amplification of a specific sequence containing the variant by PCR, followed by enzymatic restriction, which produces fragments with different lengths. Enzymes used are endonucleases that recognize and cut small specific DNA sequences (188). This technique takes advantage of the fact that single nucleotide polymorphisms (SNPs) are often responsible for the creation or abolishment of a restriction enzyme recognition site (189). The product of the enzymatic restriction is placed in an agarose or polyacrylamide gel and an electric field is applied. The fragments are separated by length, as described above.

To detect the presence or absence of the polymorphisms, PCR-RFLP technique was performed, using restriction enzymes and an agarose gel at 3%. The proceedings for the production of the agarose gel were the same as previously described, except that 9g of agarose was used, instead of 4,5g.

PCR tubes with the amplicons and the respective restriction mixes were placed at 37ºC in a heated chamber, overnight.

9.2.7.1 C282Y polymorphism in the HFE gene

In order to analyze the presence of this variant in the HFE gene, 1µL of RsaI enzyme (10U/µL) was added to 1µL of enzyme buffer (both from Sigma-Aldrich, St. Louis, USA).

To identify the C282Y polymorphism, the type II endonuclease RsaI was used. This enzyme recognizes the restriction site GT'AC and the mutation creates a new restriction site, which is recognized by the enzyme (190).

If the individual is homozygous dominant (CC), RsaI recognizes 1 restriction site and 2 fragments are observed with 203 and 140 bp length. If the individual harbors the SNPs in the 2 alleles (YY), homozygous recessive, the endonuclease recognizes 2 restrictions sites, producing 3 fragments with 203, 111 and 29 bp. If the individual is heterozygous (CY), the endonuclease produces the same fragments produced in homozygous dominant and recessive individuals: 203, 140, 111 and 29 bp.

9.2.7.2 H63D polymorphism in the HFE gene

For the H63D polymorphism, 0.5µL of MboI enzyme (10U/µL) and 2µL of enzyme buffer was added to each sample (both from Metabion, Germany)

MboI, which is a type II restriction enzyme, identifies and -GATC sequence and cleaves the amplified region in 3 different sites.

If the individual is homozygous dominant (HH), the enzyme localizes 2 cut sites in the sequence, producing 3 fragments with the following lengths: 138, 99 and 57 bp. In turn, if the individual is homozygous recessive (DD) one restriction site in abolished, producing 2 different lengths fragments: 237 and 57 bp. In the presence of the variant in one allele, meaning that the individual is heterozygous for the H63D polymorphism (HD), endonuclease MboI produces the same fragments produced in homozygous dominant and recessive individuals: 237, 138, 99 and 57 bp.

10. Statistical analysis

Data from breast samples were analyzed in 2 different manners: by lesion and by case.

10.1 Analysis by lesion

When performing this type of analysis, the diagnosis attributed to the TMA spot, regardless of the final diagnosis of the sample was considered. This means that from a case diagnosed as DCIS, normal and *in situ* regions were selected and evaluated separately; from a sample diagnosed as IDC, we selected normal, *in situ* and invasive regions. So, for each case, more than one different histological diagnosis was taken into account. Average values of each quantitative parameter, for different diagnosis, within the same case, were calculated. This allowed us to study different histological stages within the same case.

10.2 Analysis by case

A different approach was the analysis considering the final diagnosis of each lesion, as classified by the pathologist. For this, we calculated the average value from each parameter, obtaining only one entry for each lesion.

10.3 Statistical tests

Distribution and normality of data was first assessed by the Kolmogorov-Smirnov test, appropriate for analysis with more than 50 samples.

Pearson's Chi-Square was used to evaluate associations between categorical variables. To evaluate statistical differences between independent variables, in which one is categorical and the other is continuous, Mann-Whitney or Kruskal-Wallis tests were performed. The first one was used to determine statistical significance when 2 data sets were compared and Kruskal-Wallis test to compare between 3 set of data. The Dunn-Bonferroni post hoc method was performed following a significant Kruskal-Wallis test to determine the statistical significant between 2 specific groups. Spearman's rank correlation test was applied to evaluate the relationships between continuous variables.

Data was analyzed with IBM SPSS Statistics Versions 20.0 (SPSS Inc., IBM, Chicago, IL, USA) and statistical significance was accepted at $p<0.05$.

RESULTS

1. DESCRIPTIVE STATISTICS

Apart from the normal liver and lymph node tissues inserted as controls, TMA blocks contained 452 spots from breast samples, of which 155 disappeared during alignment, sectioning or were lost during immunohistochemistry procedures.

For statistical purposes, the same lesions from the same case were grouped and the mean value of each parameter analyzed was taken into account. In total, 141 samples were obtained to analyze by lesion, as described in table 7.

Moreover, in the analysis by case, cores from the same donor tissue diagnosed with the same histological type were grouped and their mean score calculated. If the representative lesion was not extracted from the donor paraffin block or the representative core was lost during procedures previously described, the case was excluded from the analysis. Out of the 120 samples included in this study, 83 cases were considered, corresponding to 21 samples obtained from reduction mammoplasty, 27 of ductal carcinoma *in situ* and 35 of invasive ductal carcinomas (cf. Supplementary material, Table 8).

Table 7: Tissue sample and core frequencies.

Diagnosis		Number of samples
Tissue sample	**Lesion**	
Normal sample (n=21)	Normal	21
DCIS (n=27)	Normal in DCIS	17
	Pure DCIS	27
IDC (n=35)	Normal in IDC	28
	DCIS in IDC	13
	Pure IDC	35

Variables tested for the normality were iron deposition in epithelial and stromal inflammatory cells, epithelial CCL2 expression, expression of ferroportin 1 in lymphocytes and macrophages, total macrophage infiltration and infiltration of CCL2-positive macrophages.

The resulting p-value was inferior to 0.05 in all variables, so distribution was considered not normal and non-parametric tests were performed (cf. Supplementary material, Table 9).

2. DAB-ENHANCED PERLS' STAINING

The presence of hemosiderin deposits was assessed in epithelial and stromal inflammatory cells by the DAB-enhanced Perls' staining method. The degradation of H_2O_2 by potassium ferrocyanide, together with the addition of DAB, results in the formation of a dark-brown coloration due to the polymerization of the chromogen. In epithelial and stromal cells, hemosiderin was found in the cytoplasm of these cells, as seen is figure 5.

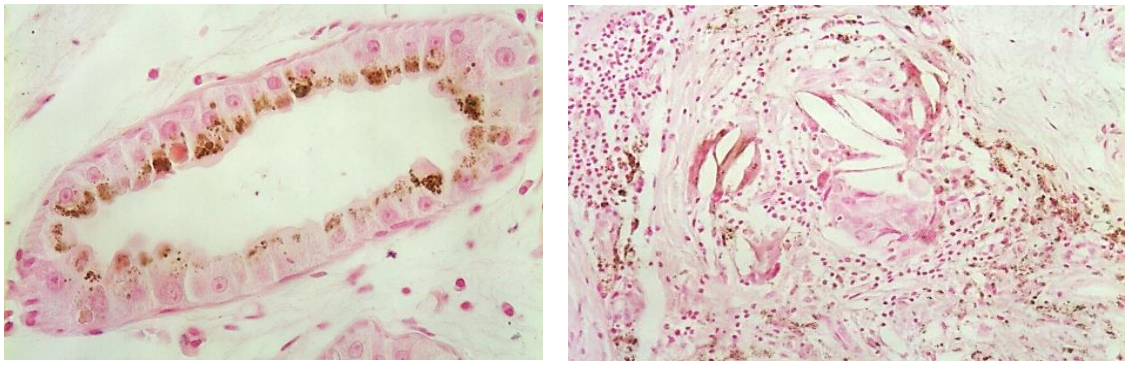

Figure 5: DAB-enhanced Perls' staining of breast tumors, in epithelial (left) and stromal inflammatory cells (right). Original magnification of 400X (left) and 200X (right).

Iron deposition on epithelial and stromal inflammatory cells was assessed on 81 and 70 samples, respectively.

In order to assess the percentage of cases presenting iron deposition in epithelial and stromal inflammatory cells, contingency tables were created in SPSS program and the values extracted from the corresponding tables. Graphs presented on figure 6 and 7 were designed from the values obtained.

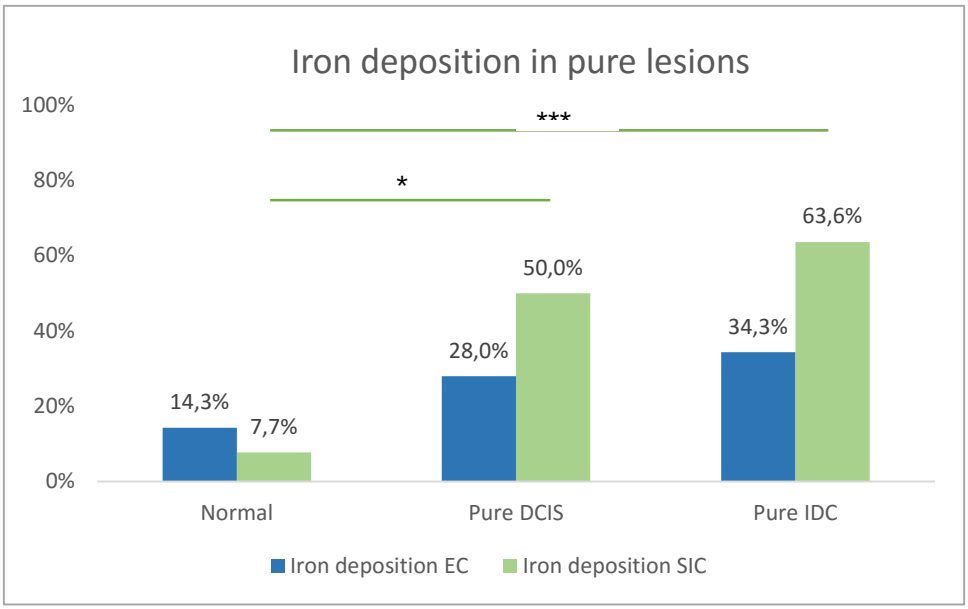

Figure 6: Iron deposition in epithelial (blue) and in stromal inflammatory cells (green) in pure lesions. Chi-square test for iron deposition in stromal inflammatory cells: between normal and pure DCIS p=0.011; between normal and pure IDC p=0.001 (*p< 0.05, **p< 0.01, ***p< 0.001). Abbreviations: EC, epithelial cells; SIC, stromal inflammatory cells; DCIS, ductal carcinoma *in situ*; IDC, invasive ductal carcinoma.

The presence of hemosiderin deposits in epithelial and stromal inflammatory cells was more evident in carcinomas than in normal tissue, as illustrated in figure 6.

Taking only pure lesions into consideration, 3 out of 21 normal lesions presented hemosiderin deposits in epithelial cells (14.3%). There is an increase in iron deposition in carcinomas: 7 out of 25 *in situ* lesions (28.0%) and 12 out of 35 of invasive lesions (34.3%) had hemosiderin deposits in the cytoplasm of tumor cells (cf. Supplementary material, Table 10).

Of the normal samples studied, 1 sample out of 13 (7.7%) presented hemosiderin deposits in stromal inflammatory cells. When looking at malignant lesions, 12 out of 24 pure DCIS lesions (50%) and 21 out of 33 pure IDC lesions (63.6%) presented iron deposition in macrophages and/or lymphocytes (cf. Supplementary material, Table 1w31).

Chi-square test was performed in order to assess differences between sub-groups of lesions. Statistically significant differences were found in iron deposition in stromal inflammatory cells, between sub-groups of lesions (p=0.003) (cf. Supplementary material, Tables 12 and 13). Chi-square test demonstrated that differences in the percentage of samples presenting iron deposition in stromal inflammatory cells are statistically significant when comparing normal tissue to pure DCIS lesions (p=0.011) (cf. Supplementary material, Table 14) and to pure IDC lesions (p=0.001) (cf. Supplementary material, Table 15 and 16).

Remarkably, iron accumulation was already observed in the histologically “normal” tissue adjacent to carcinomas, as illustrated in Figure 7.

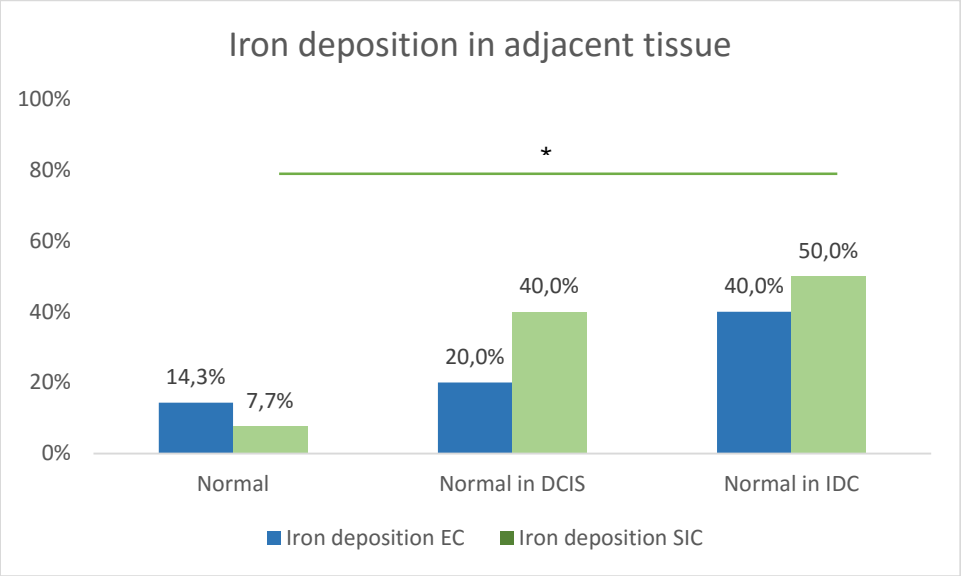

Figure 7: Iron deposition in epithelial (blue) and in stromal inflammatory cells (green) in histologically “normal” adjacent tissue. Chi-square test for iron deposition in stromal inflammatory cells: p=0.037; between normal and normal adjacent to IDC lesions p=0.011 (*p< 0.05, **p< 0.01, ***p< 0.001). Abbreviations: EC, epithelial cells; SIC, stromal inflammatory cells; DCIS, ductal carcinoma *in situ*; IDC, invasive ductal carcinoma.

Of the *in situ* cases, when the histologically “normal” tissue adjacent to the lesion was considered, 3 out of 15 samples analyzed presented hemosiderin deposits in epithelial cells (20%) and 6 out of 15 samples in stromal inflammatory cells (40%). When histologically “normal” regions from samples classified as IDC were studied, 10 out of 25 samples (40%) and 12 out of 24 samples (50%) presented iron deposition in epithelial and stromal inflammatory cells, respectively (cf. Supplementary material, Tables 17 and 18).

The presence of hemosiderin deposits in epithelial and in stromal inflammatory cells was more evident in histologically normal tissue adjacent to carcinomas than in control normal tissue, as illustrated in figure 7.

Chi-square test was performed. Statistically significant differences were found for iron deposition in stromal inflammatory cells, between sub-groups of lesions (p=0.037) (cf. Supplementary material, Tables 19 and 20). Differences in the percentage of samples presenting iron deposition in stromal inflammatory cells were statistically significant when comparing normal tissue to normal tissue adjacent to IDC lesions (p=0.011) (cf. Supplementary material, Tables 21, 22 and 23).

3.1 CCL2 expression

CCL2 immunostaining was detected on the cytoplasm of epithelial ductal cells and in some rare cases, in the nucleus. In the stromal compartment, monocytes, macrophages, neutrophils and fibroblasts also presented CCL2 expression in the cytoplasm. In figure 8, representative images of CCL2 staining in epithelial cells in normal, *in situ* and invasive lesions are presented.

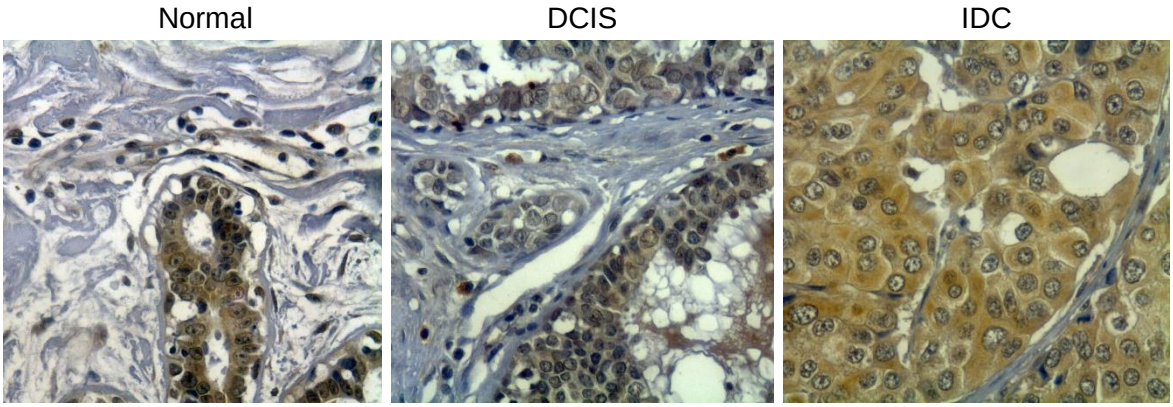

Figure 8: Representative images of epithelial CCL2 immunostaining in normal, DCIS (ductal carcinoma *in situ*) and IDC (invasive ductal carcinoma) cases. Original magnification 400X.

3.1.1 CCL2 expression in epithelial cells

CCL2 staining in epithelial cells was assessed in 80 samples, out of the 83 considered in this study. All normal samples were available for the evaluation of CCL2 epithelial expression (n=21). Looking at carcinoma lesions, CCL2 expression was analyzed in 92.6% of *in situ* lesions (n=25) and 97.1% of invasive lesions (n=34).

Considering that the expression of CCL2 in epithelial cells does not follow a normal distribution, non-parametric tests were performed and the median value of expression and interquartile range, between brackets, were presented. Results are demonstrated in figure 9, showing median values and error bars consisting of more or less 95% CI (confidence interval).

In normal samples, median value of CCL2 staining was 4.00 (0.00-5.00). The median CCL2 expression in pure DCIS lesions was 4.80 (4.00-5.50) and 5.00 (4.00-7.50) in pure IDC lesions.

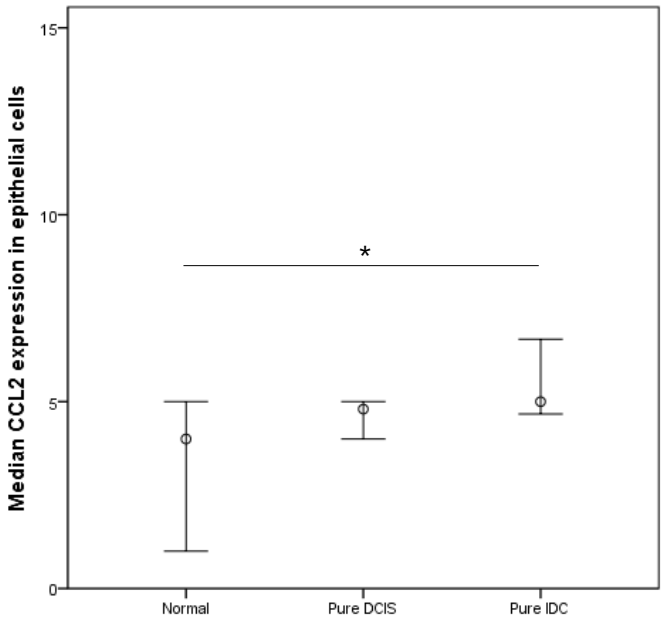

Figure 9: Median CCL2 expression in normal, pure ductal carcinoma *in situ* (DCIS) and invasive ductal carcinoma (IDC) lesions. Dunn-Bonferroni test: between normal and pure IDC p=0.017 (*p< 0.05, **p< 0.01, ***p< 0.001, versus precedent group). Error bars: 95% CI. Abbreviations: DCIS, ductal carcinoma *in situ*; IDC, invasive ductal carcinoma.

Expression of CCL2 in epithelial cells was positively associated with malignancy (n=80; p=0.007; r= 0.299), as assessed by the Spearman's rank correlation test (cf. Supplementary material, Table 24).

Kruskal-Wallis test was applied and revealed statistical differences between sub-groups of lesions regarding epithelial CCL2 expression (p=0.022). Dunn-Bonferroni correction showed that statistical significance was only reached when comparing normal to pure IDC lesions (p=0.017) (cf. Supplementary material, Tables 25 and 26).

CCL2 expression in epithelial cells was also analyzed in the histologically "normal" tissue adjacent to carcinoma lesions and results are illustrated in figure 10. Increased expression of CCL2 was already evident in the histologically "normal" tissue. The median CCL2 expression in "normal" tissue adjacent to DCIS lesions (n=16) was 5.00 (4.25-5.00) and 5.00 (3.735-5.50) in normal tissue adjacent to IDC lesions (n=27).

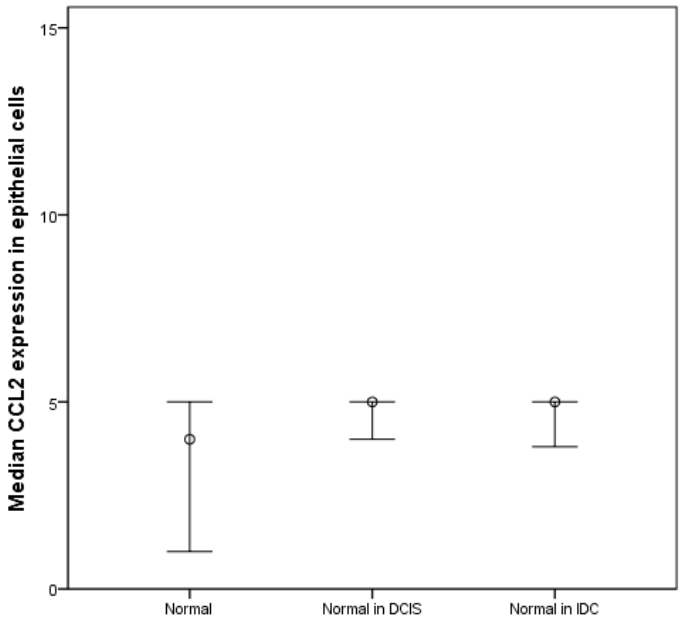

Figure 10: Median epithelial CCL2 expression in histologically normal tissue, adjacent to carcinoma lesions. Error bars: 95% CI. Abbreviations: DCIS, ductal carcinoma *in situ*; IDC, invasive ductal carcinoma.

Kruskal-Wallis test revealed no statistical differences in epithelial CCL2 expression between these sub-groups of lesions (p=0.067) (cf. Supplementary material, Table 27).

3.1.2 CCL2 expression in macrophages

CCL2 expression was also studied in cells from the monocytic lineage and was assessed on 74 samples, consisting of 19 normal cases, 23 pure DCIS and 32 invasive ductal carcinomas. Expression of this chemokine was mainly observed on the cytoplasm of macrophages. Although other cells presented CCL2 expression, such as neutrophils and fibroblasts, only monocytic cells were considered.

In figure 11, images of immunohistochemistry for CD68 and CCL2, in the same tissue section, are presented.

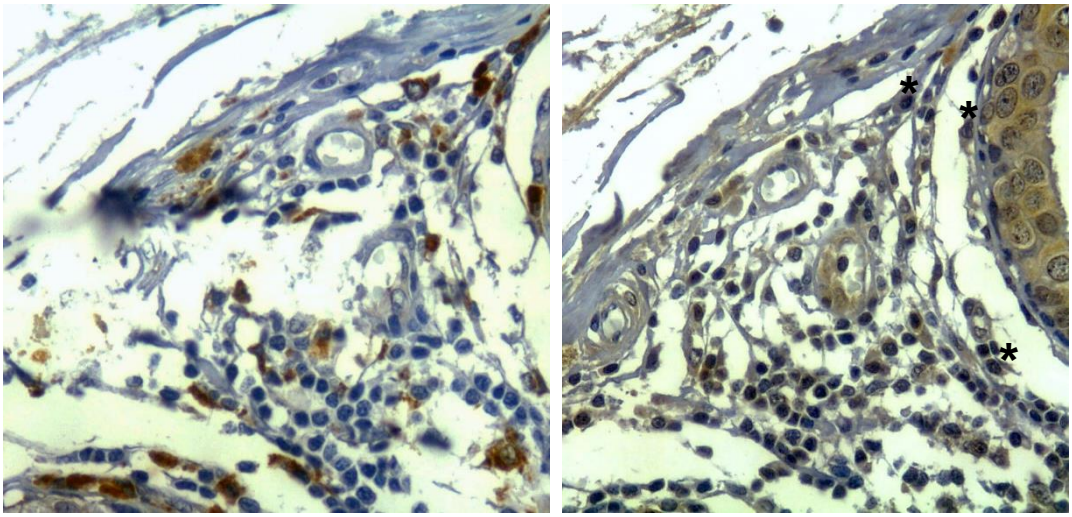

Figure 11: Section of a DCIS (ductal carcinoma *in* situ) lesion, immunostained for CD68 (on the left) and CCL2 (on the right). A few examples of CCL2-positive macrophages are shown and marked with an *. Original magnification 400X.

The median count for CCL2-positive macrophages in normal spots was 3.00; in pure ductal *in situ* lesions the median value was of 16.00 (7.00-25.50) and 8.00 (2.50-36.50) in ductal invasive cases, as demonstrated in figure 12.

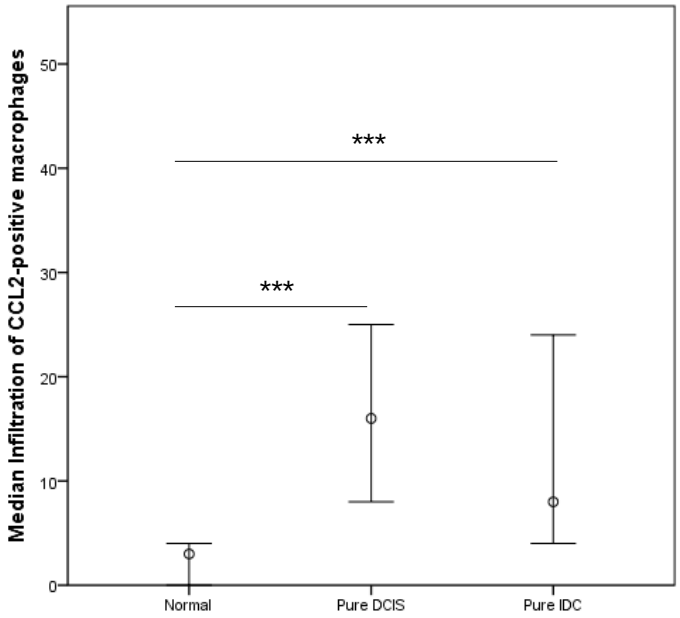

Figure 12: Infiltration of CCL2-positive macrophages in Pure Lesions. Dunn-Bonferroni test: between normal and pure DCIS p<0.001; between normal and pure IDC p=0.001 (*p< 0.05, **p< 0.01, ***p< 0.001, versus precedent group). Error bars: 95% CI. Abbreviations: DCIS, ductal carcinoma *in situ*; IDC, invasive ductal carcinoma.

As assessed by the Spearman's rank correlation coefficient, infiltration of CCL2-positive macrophages was positively associated with malignancy (n=74; p=0.003; r = 0.335) (cf. Supplementary material, Table 28).

Kruskal-Wallis test was applied to compare differences between sub-groups of lesions, regarding the infiltration of macrophages expressing CCL2. The test revealed statistically significant differences ($p<0.001$). The Dunn-Bonferroni test revealed that differences were statistically significant when comparing normal samples to pure DCIS ($p<0.001$). The same occurs when comparing normal to pure IDC samples ($p=0.001$) (cf. Supplementary material, Tables 29 and 30).

Infiltration of CCL2-positive macrophages was also assessed in the histologically "normal" tissue adjacent to carcinoma lesions and results are present in figure 13. In "normal" tissue adjacent to DCIS lesions (n=12) the median count of CCL2-positive macrophages was 7.00 (3.00-14.00) and in the "normal" tissue adjacent to invasive lesions (n=24), the median value of the count of CCL2-positive macrophages was of 3.00 (1.50-8.00).

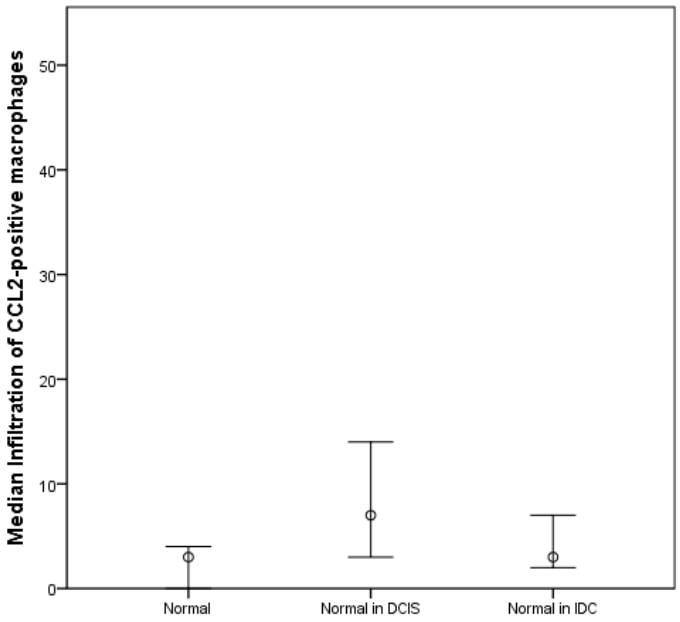

Figure 13: Infiltration of CCL2-positive macrophages in normal adjacent tissue. Error bars: 95% CI. Abbreviations: DCIS, ductal carcinoma *in situ*; IDC, invasive ductal carcinoma.

Kruskal-Wallis test revealed no statistical differences in the infiltration of CCL2-positive macrophages between these sub-groups of lesions ($p=0.069$) (cf. Supplementary material, Table 31).

3.3 CD68 expression

CD68 immunohistochemistry was performed in order to facilitate macrophage counting and assess total macrophage infiltration. As explained previously, identification of macrophages was complemented by analysis of cell and nuclear morphology.

CD68 expression was detected mainly on the membrane of macrophages, but some diffusion into the cytoplasm was also observed.

In figure 14, representative images of CD68 staining in normal, *in situ* and invasive lesions are presented.

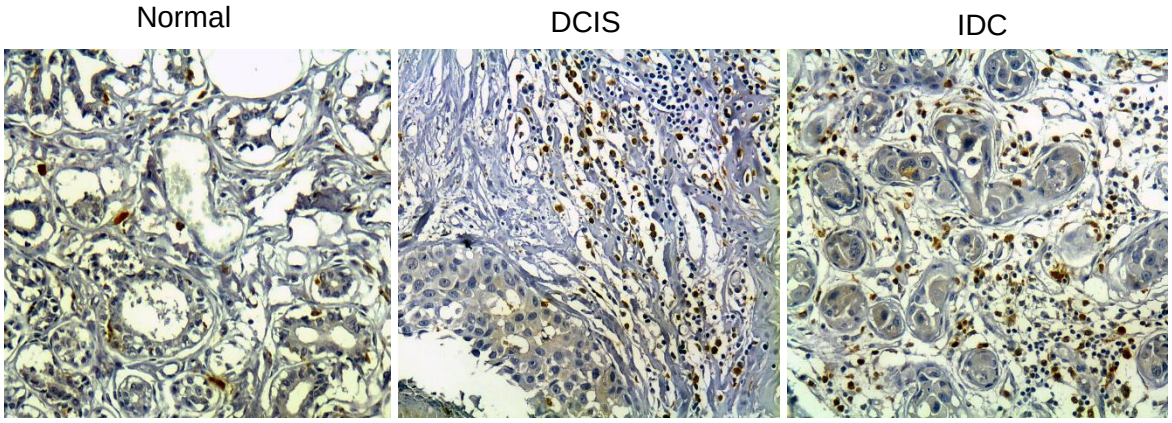

Figure 14: Representative images of CD68 immunostaining in normal, DCIS (ductal carcinoma *in situ*) and IDC (invasive ductal carcinoma) cases. Original magnification 200X.

Infiltration of CD68-positive cells was assessed on 75 samples: 18 normal samples, 23 *in situ* and 34 invasive cases. Macrophage infiltration was more evident in carcinoma than in normal mastectomy samples.

The median count of macrophages in normal tissues was 18.50 (10.00-47.00). In carcinoma lesions, the median value was of 74.00 (61.00-106.50) in *in situ* cases and of 109.00 (91.00-189.00) in invasive lesions, as illustrated in figure 15.

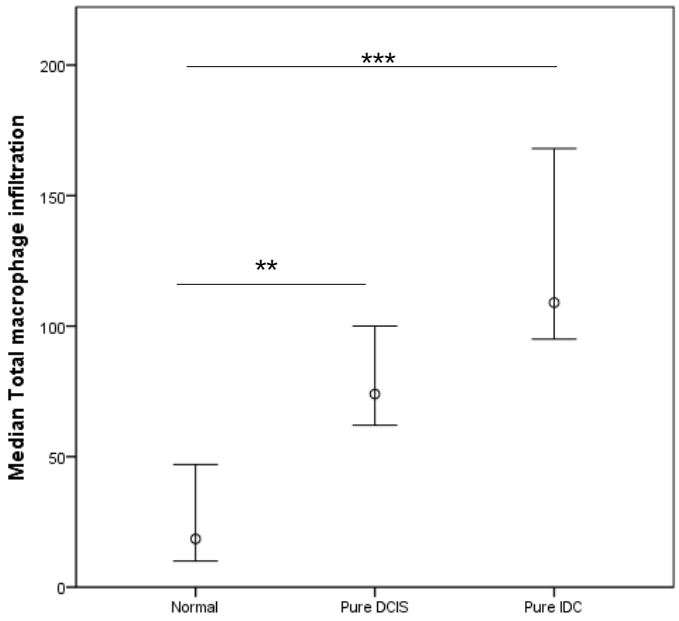

Figure 15: Total macrophage infiltration in pure lesions. Dunn-Bonferroni test: between normal and pure DCIS p=0.003 and normal and pure IDC p<0.001 (*p< 0.05, **p< 0.01, ***p< 0.001, versus precedent group). Error bars: 95% CI. Abbreviations: DCIS, ductal carcinoma *in situ*; IDC, invasive ductal carcinoma.

According to the Spearman's rank test, the number of macrophages in the tissues was positively associated with malignancy (n=75; p<0.001; r= 0.630) (cf. Supplementary material, Table 32).

Kruskal-Wallis test was performed and differences between sub-groups of pure lesions were statistically significant (p<0.001). Dunn-Bonferroni test revealed statistically significant differences when comparing normal to pure DCIS (p=0.003) and normal comparing to pure IDC (p<0.001) (cf. Supplementary material, Tables 33 and 34).

Total macrophage infiltration was also assessed in the "normal" tissue adjacent to neoplastic lesion. A total of 13 normal in DCIS and 26 normal in IDC samples were analyzed.

In the histologically "normal" tissue adjacent to DCIS lesions, the median count of macrophages was of 46.00 (33.00-49.00) and 36.00 (17.00-95.00) in "normal" tissue adjacent to invasive samples, as illustrated in figure 16.

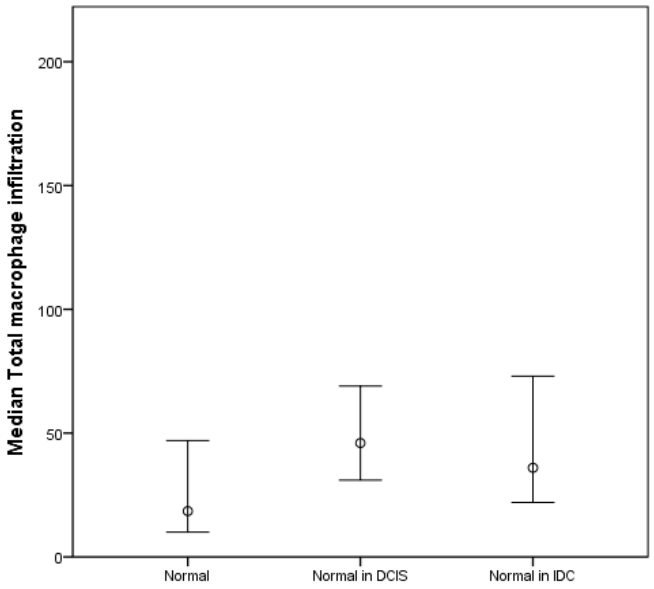

Figure 16: Total macrophage infiltration in normal tissue adjacent to carcinoma lesions. Error bars: 95% CI. Abbreviations: DCIS, ductal carcinoma *in situ*; IDC, invasive ductal carcinoma.

Kruskal-Wallis test revealed no statistically significant differences in the total macrophage infiltration between these sub-groups of lesions (p=0.099) (cf. Supplementary material, Table 35).

3.4 Ferroportin 1 expression

Data regarding ferroportin 1 expression was obtained from the PhD thesis where this work is included (Marques *et al*., unpublished data). Our research group demonstrated previously that stromal inflammatory cells present alterations regarding ferroportin 1 expression. (data not shown). In the context of this study, it was our goal to analyze if these alterations were due to the deposition of iron in the breast tissue.

In figure 17, a representative image of ferroportin 1 staining in an *in situ* sample is presented. Membrane and cytoplasmic staining in lymphocytes and macrophages was clearly evident in cases with this diagnosis.

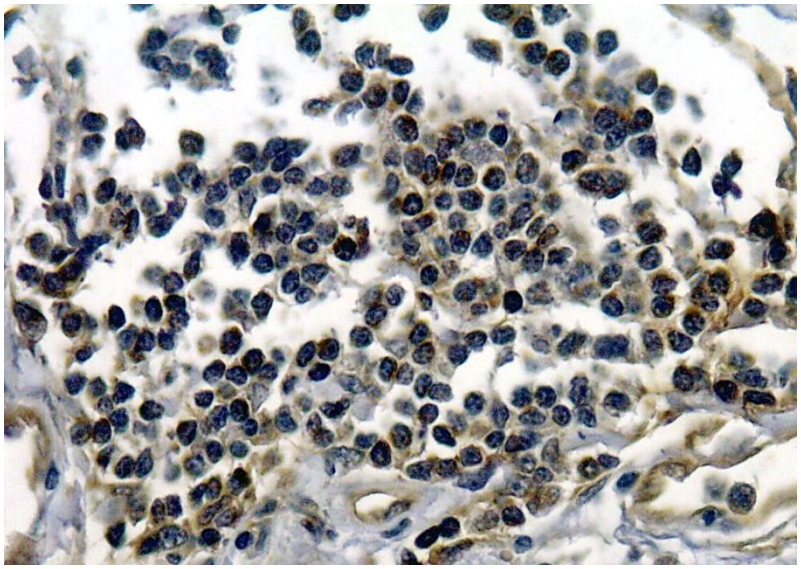

Figure 17: Section of a DCIS (ductal carcinoma *in situ*) lesion, immunostained for ferroportin 1. Stromal inflammatory cells present an evident immunostaining, particularly in the cytoplasm. Original magnification 400X.

3.4.1 Ferroportin 1 expression in macrophages

Ferroportin 1 expression in macrophages was assessed on 54 samples: 3 normal samples, 21 pure DCIS and 30 pure IDC.

In normal samples the median expression of ferroportin 1 in macrophages was 1.00 (1.50-1.00). In pure DCIS lesions the median expression was of 10.00 (8.00-10.00) and 6.00 (4.00-8.00) in invasive lesions, as illustrated in figure 18.

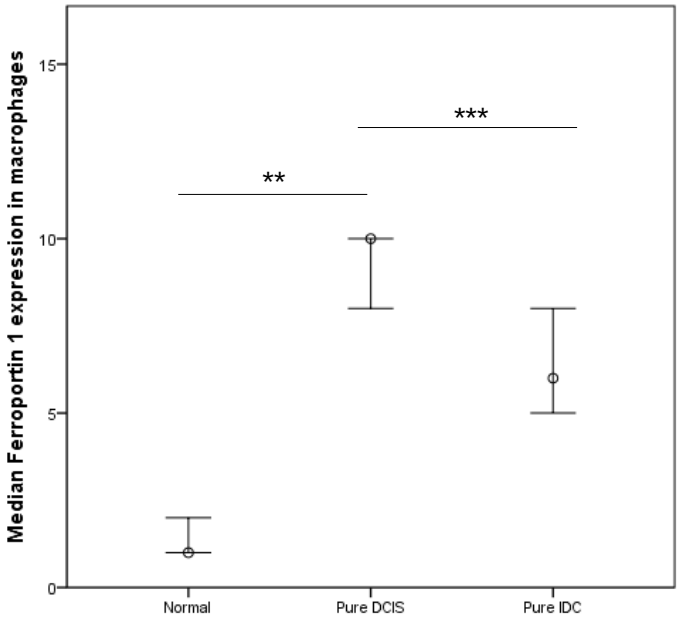

Figure 18: Ferroportin 1 expression in macrophages, in pure lesions. Dunn-Bonferroni test: between normal and pure DCIS p=0.001; pure DCIS and pure IDC p<0.001 (*p< 0.05, **p< 0.01, ***p< 0.001, versus precedent group). Error bars: 95% CI. Abbreviations: DCIS, ductal carcinoma *in situ*; IDC, invasive ductal carcinoma.

Kruskal-Wallis test was performed and statistically significant differences were found between sub-groups of pure lesions (p<0.001). According to the Dunn-Bonferroni correction, differences in ferroportin 1 expression in macrophages were statistically significant when comparing normal samples to pure DCIS (p=0.001) and pure DCIS to pure IDC (p<0.001).

Expression of ferroportin 1 in macrophages was also assessed in histologically "normal" tissue adjacent to carcinoma lesions.

Histologically "normal" tissue surrounding *in situ* lesions (n=4) presented a mean expression for ferroportin 1 of 12.50 (10.00-15.00) and 10.00 (6.00-10.00) in "normal" tissue next to invasive lesions (n=12), as demonstrated in figure 19.

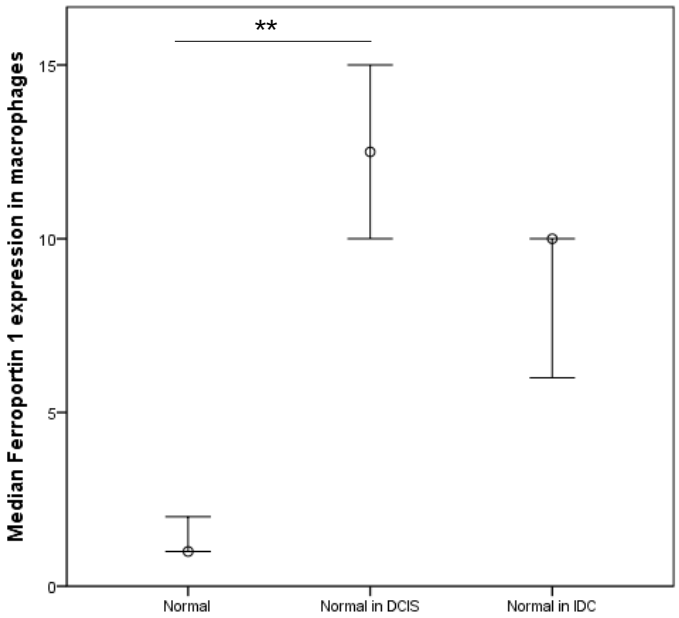

Figure 19: Ferroportin 1 expression in macrophages, in histologically "normal" tissue adjacent to carcinoma lesions. Dunn-Bonferroni test: between normal and "normal" tissue adjacent to DCIS lesions p=0.007 (*p< 0.05, **p< 0.01, ***p< 0.001, versus precedent group). Error bars: 95% CI. Abbreviations: DCIS, ductal carcinoma *in situ*; IDC, invasive ductal carcinoma.

Kruskal-Wallis test revealed statistically significant differences between sub-groups of lesions, regarding ferroportin 1 expression in macrophages (p=0.009). According to the Dunn-Bonferroni test, differences between sub-groups of lesions were only statistically significant when comparing normal tissue to "normal" tissue adjacent to DCIS lesions (p=0.007).

3.4.2 Ferroportin 1 expression in lymphocytes

Ferroportin 1 expression in lymphocytes was assessed on 54 samples: 3 normal samples, 21 pure DCIS and 30 pure IDC.

In normal samples, the median expression of ferroportin 1 in lymphocytes was 1.50 (1.00-3.50). In *in situ* lesions, median value obtained was 5.00 (3.00-7.33) and 5.50 (4.00-10.00) in invasive lesions, as demonstrated in figure 20.

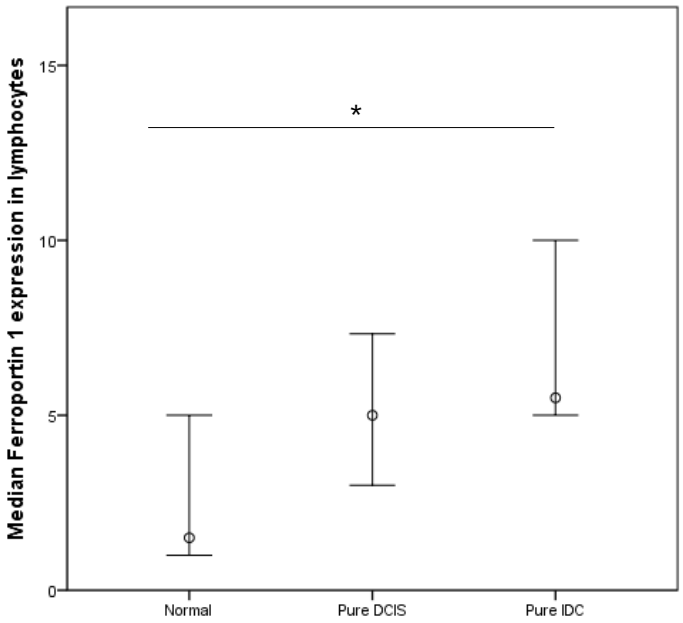

Figure 20: Ferroportin 1 expression in lymphocytes, in pure lesions. Dunn-Bonferroni test: between normal pure IDC p=0.016 (*p< 0.05, **p< 0.01, ***p< 0.001, versus precedent group). Error bars: 95% CI. Abbreviations: DCIS, ductal carcinoma *in situ*; IDC, invasive ductal carcinoma.

Kruskal-Wallis test was applied and revealed statistically significant differences between sub-groups of lesions (p=0.011). Differences between normal samples and pure IDC were statistically significant (p=0.016).

Expression of ferroportin 1 in lymphocytes was also assessed in the histologically “normal” tissue adjacent to carcinoma lesions. Median expression of “normal” in DCIS samples was of 4.00 (4.00-9.50; n=3) and 7.00 (4.50-10.00; n=12) in “normal” tissue surrounding invasive lesions, as illustrated in figure 21.

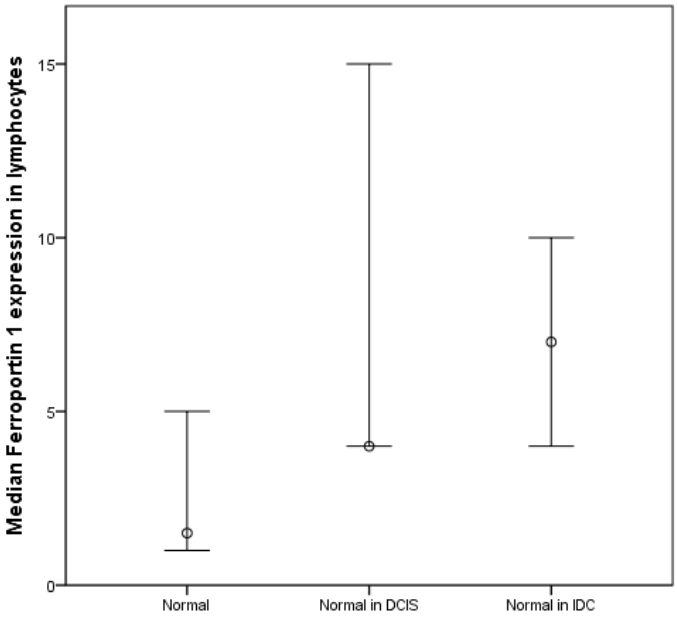

Figure 21: Ferroportin 1 expression in lymphocytes, in histologically “normal” tissue adjacent to carcinoma lesions. Error bars: 95% CI. Abbreviations: DCIS, ductal carcinoma *in situ*; IDC, invasive ductal carcinoma.

Kruskal-Wallis test was performed and no statistically significant differences were found between sub-groups of lesions, regarding ferroportin 1 expression in lymphocytes (p=0.079).

4.1 CCL2 expression and macrophage infiltration

To analyze correlations between CCL2 staining in epithelial cells, total macrophage infiltration and infiltration of CCL2-positive macrophages, Spearman's correlation tests were performed. All analysis were performed considering representative cases only (n=83).

Epithelial CCL2 expression was not associated with total macrophage infiltration (n=75; p=0.609) (cf. Supplementary material, Table 36), but was positively associated with infiltration of CCL2-positive macrophages (n=73; p=0.022; r=0.267) (cf. Supplementary material, Table 37).

Moreover, infiltration of CCL2-positive macrophages was positively correlated with total macrophage infiltration (n=73; p<0.001; r=0.488) (cf. Supplementary material, Table 38). Linear correlation and respective r-squared values are presented in figure 22.

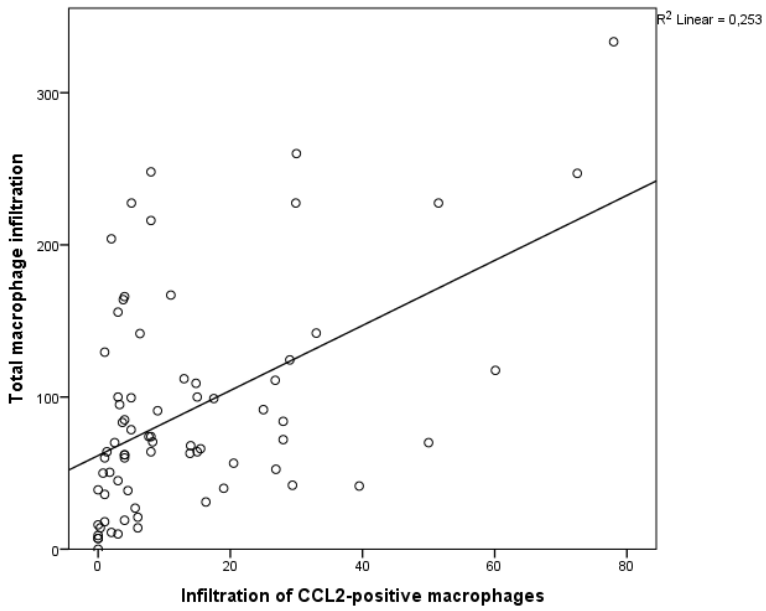

Figure 22: Correlation graph between infiltration of CCL2-positive macrophages and total macrophage infiltration. Linear r-squared value=0.253.

4.2 Epithelial CCL2 expression and iron deposition

Next, possible correlations between expression of CCL2 in epithelial cells and iron deposition were assessed.

Samples presenting iron deposits in epithelial cells show similar median CCL2 immunostaining to samples without iron deposits, as illustrated in figure 23. Epithelial CCL2 expression was not associated with iron deposition in epithelial cells (n=79; p=0.892) (cf. Supplementary material, Table 39).

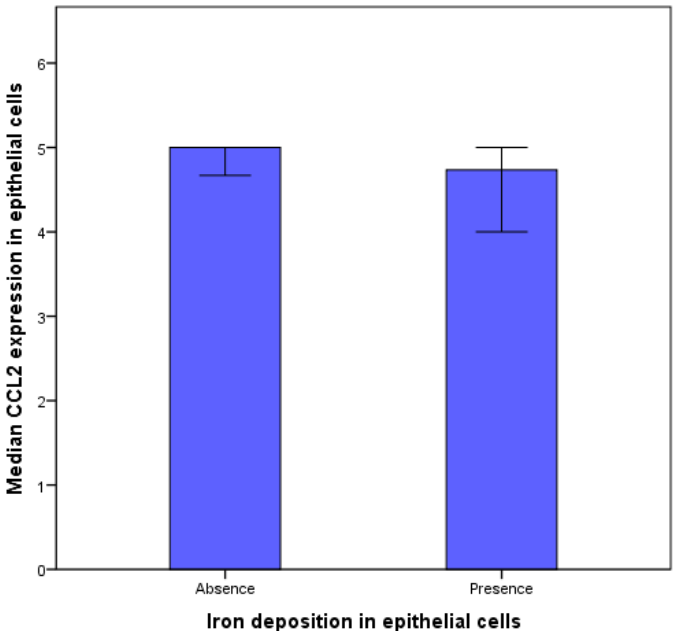

Figure 23: Median CCL2 expression in epithelial cells according to tissue iron deposition status in epithelial cells (p>0.05). Error bars: 95% CI.

Epithelial CCL2 expression was, however, positively associated with iron deposition in stromal inflammatory cells (n=69; p=0.001) (cf. Supplementary material, Table 40). In the presence of hemosiderin deposits in lymphocytes and macrophages, median CCL2 expression in epithelial cells was of 4.80 (3.00-5.00); in the absence of iron deposition in stromal inflammatory cells, epithelial CCL2 expression was of 5.00 (4.00-6.67), as illustrated in figure 24.

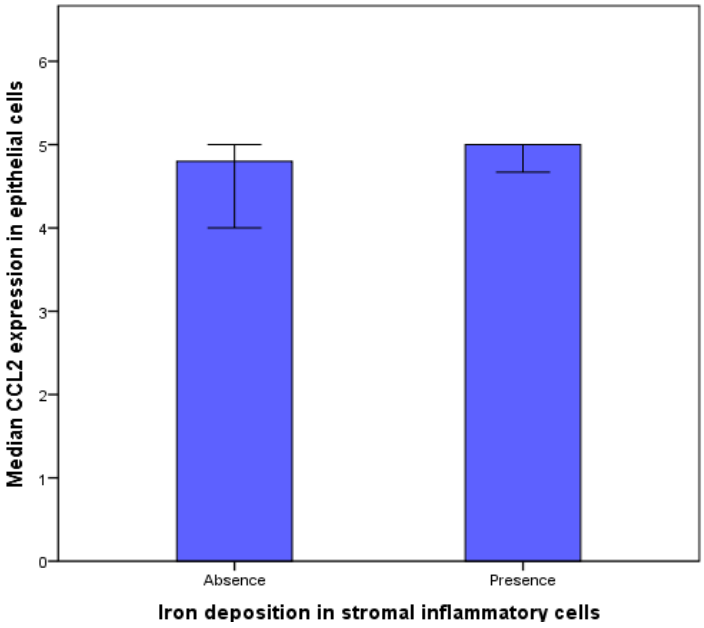

Figure 24: Median CCL2 expression in epithelial cells according to tissue iron deposition status in stromal inflammatory cells. Error bars: 95% CI.

4.3 Epithelial CCL2 expression and ferroportin 1 expression

We assessed if ferroportin 1 expression in lymphocytes and macrophages was somehow correlated with epithelial CCL2 expression. Of note, FPN 1 expression in lymphocytes was not associated with iron deposition in either epithelial cells (n=56; p=0.302) (cf. Supplementary material, Table 41) or in stromal inflammatory cells (n=55; p=0.408) (cf. Supplementary material, Table 42) and FPN 1 expression in macrophages was also not associated with iron deposition in epithelial cells (n=56; p=0.645) (cf. Supplementary material, Table 43) or in stromal inflammatory cells (n=54; p=0.334) (cf. Supplementary material, Table 44).

As illustrated in figure 25, CCL2 expression in epithelial cells was positively associated with FPN 1 expression in lymphocytes (n=55; p=0.001; r= 0.428). It was not correlated with FPN 1 expression in macrophages (n=54; p=0.842).

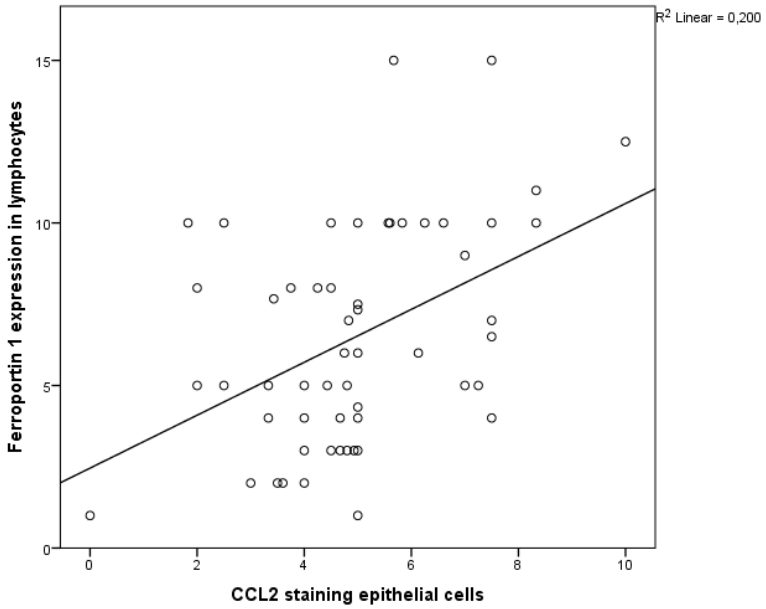

Figure 25: Correlation between CCL2 expression in epithelial cells and ferroportin 1 expression in lymphocytes (p=0.001). Linear r-squared value=0.200.

5.1 C282Y variant

From the 83 samples included in this study, 7 could not be amplified by PCR due to DNA degradation. PCR-RFLP technique was performed on 76 samples, consisting of 67 samples classified as CC and 9 samples classified as CY. No homozygous recessive individuals were found in this study.

In order to assess the percentage of cases genotyped as CC or CY, contingency tables were created and the values extracted from the corresponding tables. Graph presented on figure 26 was designed from the values obtained.

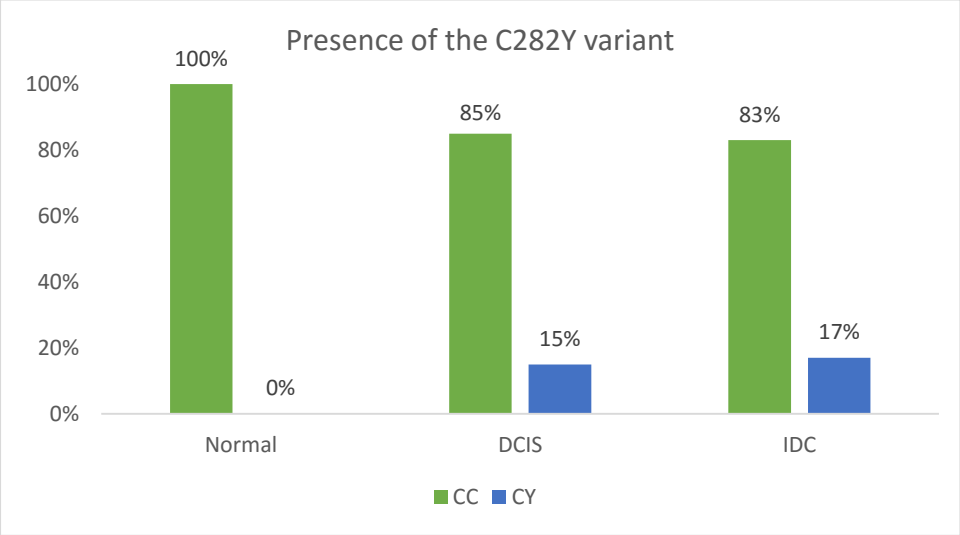

Figure 26: Percentage of samples genotyped as CC or CY by samples diagnosis.

Genotyping for the C282Y variant was possible in all normal samples (n=21) and all were classified as homozygous dominant. Of the DCIS samples, 3 out of 20 (15%) were classified as CY, heterozygous; of the IDC samples 17% were also heterozygous.

Chi-square test was performed in order to assess differences in the proportion of C282Y variants between sub-groups of lesions. No statistically significant differences were found between the presence of the C282Y variant and sample diagnosis (p=0.138) (cf. Supplementary material, Table 45).

The frequency of individuals with the C282Y variants was similar to the frequency found in the general population. However, considering its relative low frequency we did not performed further statistical tests with this variant.

5.2 H63D variant

From the 83 samples included in this study for the detection of the H63D variant, 18 samples could not be amplified due to DNA degradation. A total of 36 cases were classified as homozygous dominant, 27 as heterozygous and 2 as homozygous recessive.

As performed for the C282Y variant, contingency tables were created and the values extracted from the corresponding tables. Graph presented on figure 27 was designed from the values obtained.

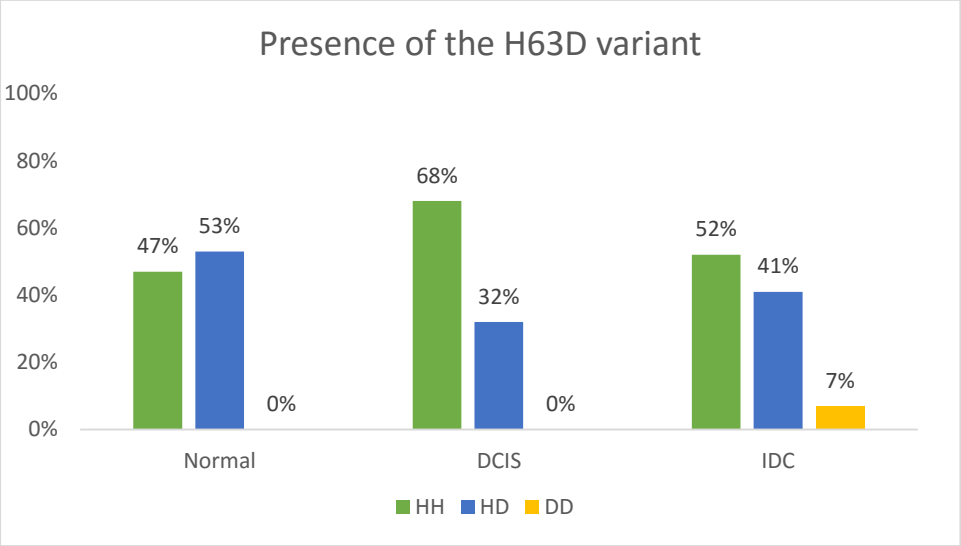

Figure 27: Percentage of samples genotyped as HH, HD or DD by samples diagnosis.

Out of the 19 normal samples, 9 (47%) were classified as homozygous dominant and 10 (53%) as heterozygous. Considering *in situ* samples, 13 out of 19 (68%) were classified as homozygous dominant and 32% as heterozygous. From the invasive samples, 52% (14 out of 27) were homozygous dominant, 41% (22 out of 27) were heterozygous and 7% (2 out of 27) were homozygous recessive.

Chi-square test was performed in order to assess differences in the distribution of the variables analyzed. No statistically significant differences were found between the presence of the H63D variant and sample diagnosis (p=0.380).

Considering only this polymorphism, heterozygous and homozygous recessive individuals were grouped and Chi-square test was performed taken 2 sub-groups into account. No statistically significant association were found between the presence of the H63D variant and sample diagnosis (p=0.866) (cf. Supplementary material, Table 46).

5.2.1 H63D variant and tissue iron status

Given the role of HFE in regulating iron homeostasis (98), the influence of the H63D variant in tissue iron status was next evaluated.

Percentage of cases, from each genotype, presenting or not iron deposition in epithelial and stromal inflammatory cells, were extracted from contingency tables.

Chi-square test was performed to assess if differences in the distribution were statistically significant. No statistically significant differences were found in iron deposition in epithelial or stromal inflammatory cells, between H63D genotypes (p=0.288 and p=0.166, respectively) (cf. Supplementary material, Tables 47 and 48).

5.2.2 H63D variant and CCL2 expression

To detect differences in the median expression of CCL2 between genotypes, Mann-Whitney's test was performed, taking 2 sub-groups into consideration: homozygous dominant (HH) and another sub-group composed by heterozygous and homozygous recessive (HD+DD) individuals. This test was performed on 62 samples: 35 homozygous dominant (HH) and 27 heterozygous and homozygous recessive. As illustrated in figure 28, regarding CCL2 epithelial expression, no statistically differences were found between homozygous dominant and heterozygous or homozygous recessive individuals for the H63D allelles (p=0.545) (cf. Supplementary material, Table 49).

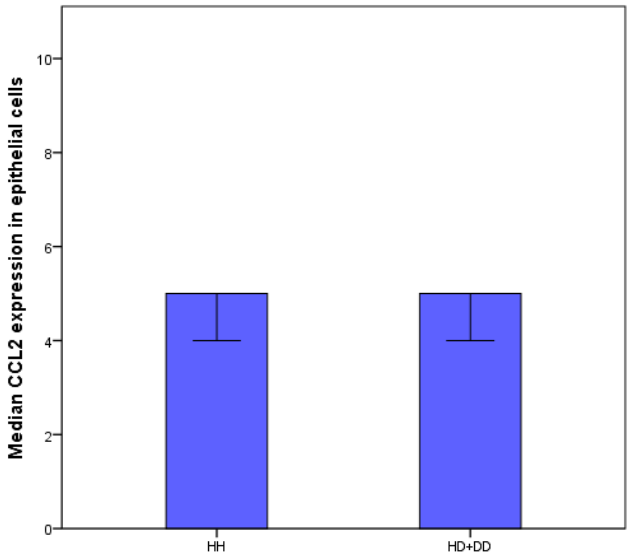

Figure 28: Median CCL2 expression in epithelial cells according to the genotype in epithelial cells. Mann Whitney's U test: p-value>0.05. Error bars: 95% CI.

6.1 Pathological and clinical parameters

Pathological and clinical features were obtained from interin pathological reports. The following parameters were considered for this study:

- Tumor size;
- Estrogen receptor (ER);
- Progesterone receptor (PR);
- Human epidermal growth factor 2 (HER-2);
- Hormonal receptor status;
- Molecular subtype, which is a system of breast cancer classification , based on gene expression profiles (191). Four molecular subtypes are typically considered:
    - Luminal A: characterized by positivity of the ER and/or the PR; HER-2 negativity
    - Luminal B: characterized by positivity of the ER and/or the PR; HER-2 positivity.
    - HER-2 amplification: characterized by ER and PR negativity; HER-2 positivity;
    - Basal-like/Triple-negative: negativity of the ER, PR and HER-2.
- Lymph Node involvement;
- Leukocyte count, including total number of neutrophils, lymphocytes, monocytes, eosinophils and basophils per µL.

6.2 Epithelial CCL2 expression

The only statistically significant clinical correlation of epithelial CCL2 expression was found with ER-negative status (n=25; p=0.021) (cf. Supplementary material, Table 50). A total of 25 DCIS samples were considered, 7 of which were ER-negative and 18 were ER-positive. CCL2 expression was significantly higher in epithelial cells of ER-negative DCIS cases, as illustrated in figure 29.

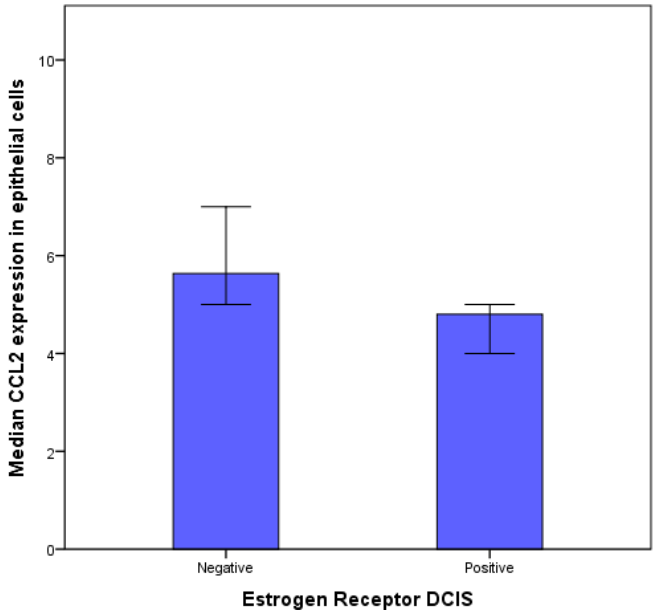

Figure 29: Median CCL2 expression in epithelial cells in samples ER-negative and ER-positive. Mann-whitney's U test: p=0.021. Error bars: 95% CI. Abbreviations: DCIS, Ductal carcinoma *in situ*; ER, estrogen receptor.

In invasive samples, CCL2 expression in epithelial cells was not associated with the estrogen receptor status (n=32; p=0.836) (cf. Supplementary material, Table 51).

Although borderline, epithelial CCL2 expression, was also positively associated with the total peripheral blood monocyte count at the time of diagnosis (n=55; p=0.050) (cf. Supplementary material, Table 52).

No significant associations were found between epithelial CCL2 expression and the other clinical features, namely: tumor size (n=57; p=0.332), progesterone receptor status (in 25 DCIS cases p=0.282 and in 32 IDC cases p=0.263), HER-2 status (n=55; p=0.575), molecular subtype (n=55; p=0.215) and lymph node involvement (n=33; p=0.817) (cf. Supplementary material, Table 53-56).

6.3 Infiltration of CCL2-positive macrophages

There were no significant associations between the infiltration of CCL2-positive macrophages and any of the clinico-pathological features considered for this study.

6.4 Total macrophage infiltration

There were no significant associations between total macrophage infiltration and any of clinico-pathological features considered for this study.

DISCUSSION

Efforts to understand the biology of breast cancer have generally focused on the study of alterations displayed by epithelial cells, but accumulating evidences suggest that cells in the tumor microenvironment also undergo alterations in response to stimuli sent by epithelial cells and consequently contribute to tumor progression (192). Moreover, data from different scientific fields of research suggest that in current cancer biology, it should be virtually impossible to address the importance of the tumor microenvironment without considering the role of iron (193).

The first goal of this thesis was to characterize normal control tissues, from aesthetic reduction mammoplasty samples and breast cancer samples, using the DAB-enhanced Perls' staining technique. A higher percentage of breast cancer samples displayed hemosiderin deposits in epithelial tumor cells, comparing with normal samples. Remarkably, this pattern of iron deposition was evident not only in the established malignant lesions, but also in the hypothetically "normal" tissue adjacent to the representative breast lesion.

Neoplastic cells have high requirements for iron, due to their incessant proliferation. This results in iron deregulation favoring higher intracellular iron concentrations [9]. Alterations in the expression of iron-related proteins in the breast cancer context have been extensively studied. Increased expression of the transferrin receptor 1 (TfR1) in the surface of neoplastic cells is the most obvious argument for the importance of iron in tumor progression (194). As first demonstrated by Pinnix and colleagues, the deregulation of the ferroportin/hepcidin axis may be central in breast tumor progression (113). Moreover, Chen and colleagues, validating a previous work by Zhang and co-workers (195), recently reported that the ferroportin 1 reduction in epithelial cells was associated with increased concentration of ferritin, the central iron storage protein. Increased intracellular iron levels observed, reflected by the concentration of the ferritin light chain, suggest that actively proliferating neoplastic cells have a constant supply of iron, necessary for metabolic reactions (196).

In the study here presented, established lesions (pure DCIS and pure IDC) display iron deposition in the epithelial compartment, characteristic of actively proliferating tumor cells. Moreover, histologically "normal" tissue adjacent to these lesions also present hemosiderin deposits. These results led us to hypothesize that the histologically "normal" tissue adjacent to carcinomas already presents alterations that predispose the microenvironment to acquire more iron for metabolic processes. So iron deregulation may be previous to the establishment of the pure lesions and is already present in non-malignant lesions, such as hyperplasias, facilitating epithelial cell proliferation, dysplasia and the potential accumulation of mutations (27).

Iron deposition was not limited to epithelial cells. Increased iron deposition was also observed in lymphocytes and/or macrophages, especially in carcinoma samples.

Macrophages are known to be specialized cells in handling iron at the systemic level (197) and erythrophagocytosis is a representative example. This process is performed by splenic and hepatic macrophages, which engulf senescent and damaged erythrocytes, in order to recycle iron for the production of hemoglobin in new red blood cells (197). In response to heme released from erythrophagocytosis of senescent red blood cells, ferroportin 1 expression in macrophages is upregulated (198). In situations of local increase of blood flow, such as angiogenesis, macrophages mimic this process by delivering iron to facilitate tumor growth (193). Lymphocytes are also capable of uptaking non-transferrin-bound iron, as demonstrated by a recent study by Pinto and colleagues (199), where they provided evidence supporting the hypothesis that circulating immune cells may have a surveillance role in controlling potential iron toxicity (193).

Phenotypic characterization of macrophages, focusing on the expression of iron-associated proteins, has become a point of interest. This is because iron may shape macrophage polarization, but the polarization of macrophages can also have important effects on iron metabolism (133). Inflammatory or M1 macrophages are characterized by iron retention, due to increased induction of ferritin secretion and downregulation of ferroportin 1 expression. On the other hand, M2 macrophages act as iron-deficient and present lower intracellular iron levels than M1 macrophages. In Corna's work, these macrophages were characterized by higher TfR1 and FPN 1 expression and suppression of ferritin (200).

Description of the populations of macrophages present in the tumor microenvironment is beyond the scope of this work, but it was reported that these cells mainly have a M2-like phenotype (131). Unpublished work performed by our group reported that, although the tumor microenvironment consists of cells with both activation phenotypes, M2-like macrophages are predominant. Recalcati and colleagues reported that M2 macrophages are capable of exporting iron *in vitro.* In the same study, in which a tumor cell line was grown in the conditioned media of M2 macrophages, the authors concluded that tumor-associated macrophages may also exacerbate the neoplastic disease by supplying iron to actively proliferating tumor cells (133). As also reported in the work here presented, increased ferroportin 1 expression in lymphocytes and macrophages, particularly in the transition to the *in situ* state may reinforce the iron exporting phenotype suggested for stromal inflammatory cells.

Results from our study suggest that circulating macrophages and lymphocytes, loaded with iron, migrate into the tumor site. Locally, due to an increase in ferroportin 1 expression, these stromal inflammatory cells release iron, important for the proliferation of neoplastic cells. As in epithelial cells, iron deposition in stromal inflammatory cells is already visible in the histologically “normal” tissue adjacent to carcinomas.

Chemokines are best known for their ability to induce the migration of cells and significantly contribute to cancer progression and metastasis (201). Taken this into consideration, expression of CCL2 in epithelial and stromal inflammatory cells was analyzed by immunohistochemistry. CCL2 has been described an as important chemokine in breast cancer context (156). Results from several authors demonstrate that CCL2 has little or no effect on carcinoma cell proliferation or survival (170, 202), but promotes angiogenesis and the release of a wide array of proangiogenic factors and enzymes, such as metalloproteinases (203, 204).

In this study, an increased expression of CCL2 in epithelial and stromal inflammatory cells was observed with increased malignancy. This correlation was detected not only in established breast cancer lesions, but also in the hypothetically “normal” tissue adjacent to these lesions.

Mantovani was the first to report that tumor-derived chemokines could be responsible for the attraction of monocytes to the tumor nest, where they could enhance tumor progression, by supplying growth and angiogenic factors (125). In our study, although there was no significant association between tumor CCL2 expression and total macrophage infiltration, there was a significant association with the infiltration of CCL2-positive macrophages.

The evidence of a significant association between epithelial CCL2 expression and the infiltration of CCL2-positive macrophages consolidates the idea of a paracrine signaling pathway. Several authors demonstrated the existence of this pathway, in which tumor cells produce CCL2, responsible for the egress of CCR2-positive monocytes from the bone marrow into the tumor area (205). Moreover, tissue macrophages also secrete CCL2, recruiting more macrophages, as demonstrated by Fujimoto and colleagues (165), forming a paracrine signaling pathway. Furthermore, the infiltration of CCL2-positive macrophages was positively associated with the total macrophage infiltration. These results suggest that, as proposed by Fujimoto and colleagues, CCL2 produced by macrophages, attracted by CCL2 produced by tumor cells, is accountable for the attraction of macrophages from the bone marrow into the breast tumor milieu (165).

Epithelial CCL2 expression was already evident in the histologically “normal” tissue adjacent to carcinomas. One can hypothesize that histologically “normal” tissue already presents deregulation, which may be responsible for the secretion of this chemokine. Through the paracrine signaling pathway previously suggested, epithelial expression of CCL2 may result in infiltration of CCL2-positive macrophages, which are also increased in pre-malignant tissue, facilitating malignant progression.

In this study, a gradual increase in the amount of infiltrating macrophages, CD68-positive cells, from normal breast to ductal carcinoma *in situ* and invasive ductal carcinoma was evident. This increase in total macrophage infiltration was already visible in the hypothetically “normal” tissue adjacent to carcinoma lesions. As reported by several authors, there is a positive correlation between the number of tumor-associated macrophages and malignancy (138), and monocytes are often already increased at a very early stage of tumor development (206), as observed in the work here reported. This observation may be explained by the paracrine signaling pathway and by the fact that in the histologically “normal” tissue adjacent to carcinomas there is already an increase in the infiltration of CCL2-positive macrophages.

Influence of iron status in CCL2 expression was already demonstrated by Mitchell and colleagues (173). In other studies, not related to neoplastic disease, alterations in iron levels, by supplementation or administration of iron chelators, also influenced CCL2 protein levels (207-210). Considering all the studies and the role of macrophages in iron homeostasis and that these cells are attracted into the tumor microenvironment by CCL2, we hypothesized if CCL2 could, in part, be associated with iron deregulation, in breast cancer context.

Herein, the presence of hemosiderin deposits in stromal inflammatory cells was positively associated with increased CCL2 expression in epithelial cells. This significant association may suggest iron as a putative driving force to enhance CCL2 expression in the breast tumor environment, as previously described by Mitchell and colleagues in the neuroinflammatory context (173). The evident increase in iron deposition in the histologically “normal” tissue adjacent to carcinomas could explain the visible increase in CCL2 expression in these same stages. Alternatively, CCL2 expression could be the driving force to increase iron deposition. Our results suggest that iron loaded leukocytes may be attracted to pre-malignant sites by CCL2. At the tumor site, macrophages and lymphocytes

release iron, by upregulating the expression of ferroportin 1, which results in increased CCL2 expression and infiltration of more CCL2-positive macrophages.

Lawless and colleagues performed a study in which the presence of the HFE H63D variant was associated with the increase in CCL2 serum levels (172). In a study performed by Mitchell and co-workers, using a neuroblastoma cell line, the presence of the H63D variant was also associated with increased CCL2 expression (173). These studies led us to analyze if the HFE variants could influence CCL2 expression in breast cancer context. In our study no statistically significant association with HFE variant alleles was found. The lack of association between any of the HFE variants and CCL2 expression can be explained by the small number of heterozygous and homozygous recessive individuals in this study. Also, we cannot ignore different methodologies used in these studies: in the study by Mitchell *in vitro* experiments were performed, and Lawless used peripheral blood samples. One can hypothesize that locally, HFE variants do not play an important role in regulating CCL2 expression.

Delaby and colleagues demonstrated that ferroportin 1 expression in macrophages and lymphocytes was mainly regulated by iron levels, putatively by the IRP-IRE system (198). In our study the expression of ferroportin 1 in lymphocytes and macrophages was not significantly associated with iron deposition, suggesting the existence of another possible player involved in the setting of an iron exporting phenotype in stromal inflammatory cells.

Considering these results, we hypothesized that CCL2 could be associated with ferroportin 1 expression. We found that the expression of this iron exporter in lymphocytes, but not in macrophages, was significantly correlated with CCL2 expression in epithelial cells. This result suggests a novel putative role for this chemokine as a modulator of the iron export phenotype in stromal cells.

When circulating leukocytes arrive at the tumor site, the expression of CCL2 by epithelial cells may be a key factor in upregulating the expression of ferroportin 1 in lymphocytes. Although no correlation was found with the expression of this exporter in macrophages, reports have demonstrated that M2 macrophages, the most frequent in the tumor microenvironment, have an iron-exporting phenotype (133). Also, other players may attract macrophages into the tumor site and promote the “iron-export phenotype”. Induction of HO-1 expression in M2-macrophages seems to play a role in the iron release-prone phenotype of these cells. Heme in the new vessels can be a cause for the upregulation of HO-1 and the establishment of the iron-exporting phenotype (133).

In this study, CCL2 expression was associated with ER-negative status, one of the classical biomarkers of breast cancer negative prognosis. As reported by Chavey and colleagues (211), CCL2 expression was increased in ER-negative tumors. Opposite to reported by Svensson and colleagues (212), we observed that estrogen-receptor negative samples showed higher levels of CCL2 expression. Different methodologies performed may explained opposite results. In our study, tumor CCL2 expression was analyzed, whereas in Svensson's work extracellular CCL2 levels were considered. Moreover, for our study pre- and postmenopausal women were selected, while in the study previously reported only post-menopausal women were studied.

CONCLUSIONS

This study provides new data regarding the role of iron in breast cancer. Moreover, this deregulation is not limited to epithelial cells, because stromal inflammatory cells also show increased hemosiderin deposition, associated with increased malignancy. Striking increase in ferroportin 1 (FPN 1) expression in these cells, especially in the transition to the pre-invasive stage (DCIS), suggests that macrophages and lymphocytes may contribute to breast tumor progression, by supplying iron for actively proliferating breast tumor cells.

Herein, new considerations regarding the role of CCL2 in breast tumor promotion are described. Associations between epithelial CCL2 expression and infiltration of CCL2-positive macrophages, together with the association between infiltration of CCL2-positive macrophages and total macrophage infiltration suggest a putative paracrine signaling pathway. Considering the role of macrophages in breast tumor, we hypothesize that CCL2 and this paracrine signaling pathway plays a detrimental part in breast tumor progression, by facilitating extravasation and metastasis.

Analyzing the results obtained in this work, we propose the following mechanism, illustrated in figure 30: circulating macrophages and lymphocytes, described as actively iron storing cells, are attracted into the tumor site by CCL2 produced by neoplastic cells. When macrophages and lymphocytes arrive at the tumor milieu, FPN 1 expression is upregulated, at least partially by the expression of CCL2, and iron is supplied for non-malignant cells. Iron is then responsible for the proliferation of transformed malignant cells and the increase in epithelial CCL2 expression, which may trigger the paracrine signaling pathway. CCL2 secreted by epithelial cells is responsible for the attraction of more CCR2-positive macrophages, which secrete CCL2 and consequently attract circulating monocytes, through a stromal cell amplifying system. This results in increased macrophage infiltration and increased supply of iron for actively proliferating neoplastic cells.

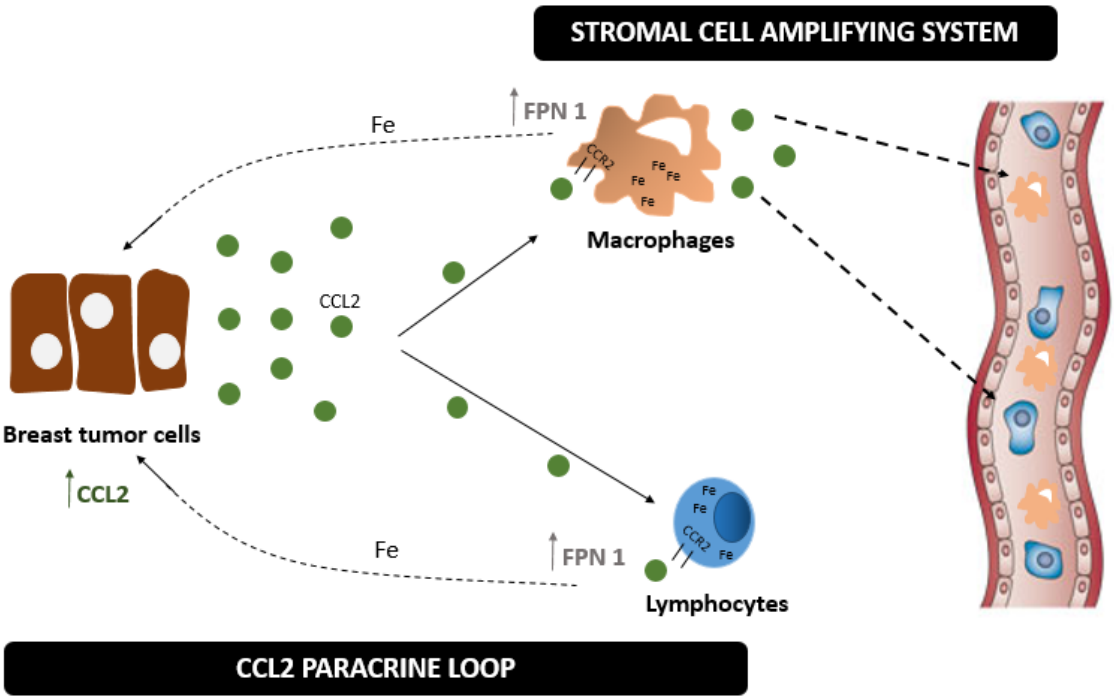

Figure 30: Proposed mechanism for the CCL2-induced pathway: CCL2 (green circles), produced by breast tumor cells, attract circulating CCR2-positive cells, such as macrophages and lymphocytes, which are iron-loaded. When these stromal inflammatory cells arrive to the tumor microenvironment, FPN 1 expression is upregulated, partially by the expression of CCL2, and iron (Fe) is supplied for proliferating epithelial cells. Iron supplied by macrophages and lymphocytes leads to increased proliferation and CCL2 secretion by tumor cells, triggering the paracrine signalling pathway, between tumor and immune cells. Macrophages are also accountable for the production of CCL2, resulting in increased leukocyte infiltration and increased iron supply for proliferating neoplastic cells.

In conclusion, this work reports that stromal inflammatory cells, as demonstrated by increased FPN 1 expression and hemosiderin deposition, play a role in supplying iron to actively proliferating tumor cells. Moreover CCL2, whose expression may be putatively enhanced by increased iron deposition in stromal inflammatory cells, contributes not only to increase macrophage infiltration into the tumor microenvironment, but also may play a role in regulating tumor iron nutrition and progression.

BIBLIOGRAPHY

1. Inman JL, Robertson C, Mott JD, Bissell MJ. 2015. Mammary gland development: cell fate specification, stem cells and the microenvironment. *Development* 142: 1028-42
2. Harris JR, Lippman, M.E., Morrow, M. and Osborne, C. 2014. Diseases of the Breast. *PA: Lippincott Williams & Wilkins (5th Edition)*
3. Riordan J, Wambach, K. 2009. Breastfeeding And Human Lactation. *Jones & Bartlett Learning (4th Edition)*
4. Rosen PP. 2014. Rosen's Breast Pathology. *PA: Lippincott Williams & Wilkins, 4th Edition*
5. Sgroi DC. 2010. Preinvasive breast cancer. *Annu Rev Pathol* 5: 193-221
6. Figueroa JD, Pfeiffer RM, Patel DA, Linville L, Brinton LA, Gierach GL, Yang XR, Papathomas D, Visscher D, Mies C, Degnim AC, Anderson WF, Hewitt S, Khodr ZG, Clare SE, Storniolo AM, Sherman ME. 2014. Terminal duct lobular unit involution of the normal breast: implications for breast cancer etiology. *J Natl Cancer Inst* 106
7. Gray H, Carter, H.V. 2008. Gray's Anatomy. *Churchill Livingstone (40th Edition)*
8. DeSantis CE, Lin CC, Mariotto AB, Siegel RL, Stein KD, Kramer JL, Alteri R, Robbins AS, Jemal A. 2014. Cancer Treatment and Survivorship Statistics, 2014. *Ca-a Cancer Journal for Clinicians* 64: 252-71
9. Jemal A, Bray F, Center MM, Ferlay J, Ward E, Forman D. 2011. Global Cancer Statistics. *Ca-a Cancer Journal for Clinicians* 61: 69-90
10. WHO. 2008. The Global Burden of Disease: 2004 Update. *Geneva: World Health Organization; 2008.*
11. Ferlay J, Steliarova-Foucher E, Lortet-Tieulent J, Rosso S, Coebergh JWW, Comber H, Forman D, Bray F. 2013. Cancer incidence and mortality patterns in Europe: Estimates for 40 countries in 2012. *European Journal of Cancer* 49: 1374-403
12. Ferlay J SI, Ervik M, Dikshit R, Eser S, Mathers C, Rebelo M, Parkin DM, Forman D, Bray, F. GLOBOCAN 2012 v1.0. 2013. Cancer Incidence and Mortality Worldwide: IARC CancerBase No. 11 [Internet]. *Lyon, France: International Agency for Research on Cancer. Available from: http://globocan.iarc.fr, accessed on 23/june/1991.*
13. http://globocan.iarc.fr/Pages/fact_sheets_population.aspx *(accessed on 05/11/2014)*
14. Burstein HJ, Polyak K, Wong JS, Lester SC, Kaelin CM. 2004. Ductal carcinoma in situ of the breast. *N Engl J Med* 350: 1430-41
15. Wellings SR, Jensen HM. 1973. On the origin and progression of ductal carcinoma in the human breast. *J Natl Cancer Inst* 50: 1111-8
16. Lakhani SR, Ellis, I.O., Schnitt, S.J., et al. 2012. World Health Organization classification of tumours the breast. 4th ed. *Lyons, France: International Agency for Research on Cancer*
17. Dupont WD, Page DL. 1985. Risk-Factors for Breast-Cancer in Women with Proliferative Breast Disease. *New England Journal of Medicine* 312: 146-51
18. Tavassoli FD, P. . 2003. World Health Organization Classification of Tumours. Pathology and Genetics of Tumours of the Breast and Female Genital Organs. *IARC Press*
19. Ernster VL, Barclay J, Kerlikowske K, Grady D, Henderson C. 1996. Incidence of and treatment for ductal carcinoma in situ of the breast. *JAMA* 275: 913-8
20. Espina V, Liotta LA. 2011. What is the malignant nature of human ductal carcinoma in situ? *Nat Rev Cancer* 11: 68-75
21. Sanders ME, Schuyler PA, Dupont WD, Page DL. 2005. The natural history of low-grade ductal carcinoma in situ of the breast in women treated by biopsy only revealed over 30 years of long-term follow-up. *Cancer* 103: 2481-4
22. Lester SC, Bose S, Chen YY, Connolly JL, de Baca ME, Fitzgibbons PL, Hayes DF, Kleer C, O'Malley FP, Page DL, Smith BL, Weaver DL, Winer E, Pathologists CA. 2009. Protocol for the Examination of Specimens From Patients With Ductal Carcinoma In Situ of the Breast. *Archives of Pathology & Laboratory Medicine* 133: 15-25
23. Lerwill MF. 2004. Current practical applications of diagnostic immunohistochemistry in breast pathology. *Am J Surg Pathol* 28: 1076-91

24. Lampejo OT, Barnes DM, Smith P, Millis RR. 1994. Evaluation of infiltrating ductal carcinomas with a DCIS component: correlation of the histologic type of the in situ component with grade of the infiltrating component. *Semin Diagn Pathol* 11: 215-22
25. Ma XJ, Salunga R, Tuggle JT, Gaudet J, Enright E, McQuary P, Payette T, Pistone M, Stecker K, Zhang BM, Zhou YX, Varnholt H, Smith B, Gadd M, Chatfield E, Kessler J, Baer TM, Erlander MG, Sgroi DC. 2003. Gene expression profiles of human breast cancer progression. *Proc Natl Acad Sci U S A* 100: 5974-9
26. Le NTV, Richardson DR. 2002. The role of iron in cell cycle progression and the proliferation of neoplastic cells. *Biochimica Et Biophysica Acta-Reviews on Cancer* 1603: 31-46
27. Torti SV, Torti FM. 2013. Iron and cancer: more ore to be mined. *Nat Rev Cancer* 13: 342-55
28. Thelander L, Reichard P. 1979. Reduction of Ribonucleotides. *Annual Review of Biochemistry* 48: 133-58
29. Ajioka RS, Phillips JD, Kushner JP. 2006. Biosynthesis of heme in mammals. *Biochim Biophys Acta* 1763: 723-36
30. Kulp KS, Green SL, Vulliet PR. 1996. Iron deprivation inhibits cyclin-dependent kinase activity and decreases cyclin D CDK4 protein levels in asynchronous MDA-MB-453 human breast cancer cells. *Experimental Cell Research* 229: 60-8
31. Shen J, Sheng XP, Chang ZN, Wu Q, Wang S, Xuan ZL, Li D, Wu YL, Shang YJ, Kong XT, Yu L, Li L, Ruan KC, Hu HY, Huang Y, Hui LJ, Xie D, Wang FD, Hu RG. 2014. Iron Metabolism Regulates p53 Signaling through Direct Heme-p53 Interaction and Modulation of p53 Localization, Stability, and Function. *Cell Reports* 7: 180-93
32. Eklund H, Uhlin U, Farnegardh M, Logan DT, Nordlund P. 2001. Structure and function of the radical enzyme ribonucleotide reductase. *Progress in Biophysics & Molecular Biology* 77: 177-268
33. Sanvisens N, Bano MC, Huang MX, Puig S. 2011. Regulation of Ribonucleotide Reductase in Response to Iron Deficiency. *Molecular Cell* 44: 759-69
34. Lederman HM, Cohen A, Lee JWW, Freedman MH, Gelfand EW. 1984. Deferoxamine - a Reversible S-Phase Inhibitor of Human-Lymphocyte Proliferation. *Blood* 64: 748-53
35. Nyholm S, Mann GJ, Johansson AG, Bergeron RJ, Graslund A, Thelander L. 1993. Role of ribonucleotide reductase in inhibition of mammalian cell growth by potent iron chelators. *J Biol Chem* 268: 26200-5
36. Cooper CE, Lynagh GR, Hoyes KP, Hider RC, Cammack R, Porter JB. 1996. The relationship of intracellular iron chelation to the inhibition and regeneration of human ribonucleotide reductase. *J Biol Chem* 271: 20291-9
37. Eriksson S, Graslund A, Skog S, Thelander L, Tribukait B. 1984. Cell cycle-dependent regulation of mammalian ribonucleotide reductase. The S phase-correlated increase in subunit M2 is regulated by de novo protein synthesis. *J Biol Chem* 259: 11695-700
38. Gao J, Richardson DR. 2001. The potential of iron chelators of the pyridoxal isonicotinoyl hydrazone class as effective antiproliferative agents, IV: The mechanisms involved in inhibiting cell-cycle progression. *Blood* 98: 842-50
39. Donnellan R, Chetty R. 1998. Cyclin D1 and human neoplasia. *Journal of Clinical Pathology-Molecular Pathology* 51: 1-7
40. Nurtjahja-Tjendraputra E, Fu D, Phang JM, Richardson DR. 2007. Iron chelation regulates cyclin D1 expression via the proteasome: a link to iron deficiency-mediated growth suppression. *Blood* 109: 4045-54
41. White JC, Beaven GH. 1954. A Review of the Varieties of Human Haemoglobin in Health and Disease. *Journal of Clinical Pathology* 7: 175-200
42. Hsia CC. 1998. Respiratory function of hemoglobin. *N Engl J Med* 338: 239-47
43. Provan D. 1999. Mechanisms and management of iron deficiency anaemia. *Br J Haematol* 105 Suppl 1: 19-26

44. Andrews PA. 2000. Disorders of iron metabolism. *New England Journal of Medicine* 342: 1293-
45. Anderson CP, Shen M, Eisenstein RS, Leibold EA. 2012. Mammalian iron metabolism and its control by iron regulatory proteins. *Biochim Biophys Acta* 1823: 1468-83
46. McCance RA, Widdowson EM. 1938. The absorption and excretion of iron following oral and intravenous administration. *Journal of Physiology-London* 94: 148-54
47. Beard JL, Dawson H, Pinero DJ. 1996. Iron metabolism: A comprehensive review. *Nutrition Reviews* 54: 295-317
48. Andrews NC, Schmidt PJ. 2007. Iron homeostasis. *Annual Review of Physiology* 69: 69-85
49. Tenhunen R, Grasbeck R, Kouvonen I, Lundberg M. 1980. An Intestinal Receptor for Heme - Its Partial Characterization. *International Journal of Biochemistry* 12: 713-6
50. Riedel HD, Remus AJ, Fitscher BA, Stremmel W. 1995. Characterization and Partial-Purification of a Ferrireductase from Human Duodenal Microvillus Membranes. *Biochemical Journal* 309: 745-8
51. Donovan A, Lima CA, Pinkus JL, Pinkus GS, Zon LI, Robine S, Andrews NC. 2005. The iron exporter ferroportin/Slc40a1 is essential for iron homeostasis. *Cell Metabolism* 1: 191-200
52. Vulpe CD, Kuo YM, Murphy TL, Cowley L, Askwith C, Libina N, Gitschier J, Anderson GJ. 1999. Hephaestin, a ceruloplasmin homologue implicated in intestinal iron transport, is defective in the sla mouse. *Nature Genetics* 21: 195-9
53. Bogniard RP, Whipple GH. 1932. V. The Iron Content of Blood Free Tissues and Viscera : Variations Due to Diet, Anemia and Hemoglobin Injections. *J Exp Med* 55: 653-65
54. Sherwood RA, Pippard MJ, Peters TJ. 1998. Iron homeostasis and the assessment of iron status. *Annals of Clinical Biochemistry* 35: 693-708
55. Munoz M, Villar I, Garcia-Erce JA. 2009. An update on iron physiology. *World Journal of Gastroenterology* 15: 4617-26
56. Flowers CA, Kuizon M, Beard JL, Skikne BS, Covell AM, Cook JD. 1986. A Serum Ferritin Assay for Prevalence Studies of Iron-Deficiency. *American Journal of Hematology* 23: 141-51
57. Berlin NI, Waldmann TA, Weissman SM. 1959. Life Span of Red Blood Cell. *Physiological Reviews* 39: 577-616
58. De Domenico I, Ward DM, Kaplan J. 2008. Regulation of iron acquisition and storage: consequences for iron-linked disorders. *Nature Reviews Molecular Cell Biology* 9: 72-81
59. Ganz T. 2003. Hepcidin, a key regulator of iron metabolism and mediator of anemia of inflammation. *Blood* 102: 783-8
60. Ganz T, Nemeth E. 2011. Hepcidin and Disorders of Iron Metabolism. *Annual Review of Medicine, Vol 62, 2011* 62: 347-60
61. Kautz L, Jung G, Valore EV, Rivella S, Nemeth E, Ganz T. 2014. Identification of erythroferrone as an erythroid regulator of iron metabolism. *Nat Genet* 46: 678-84
62. Nemeth E, Tuttle MS, Powelson J, Vaughn MB, Donovan A, Ward DM, Ganz T, Kaplan J. 2004. Hepcidin regulates cellular iron efflux by binding to ferroportin and inducing its internalization. *Science* 306: 2090-3
63. Hentze MW, Muckenthaler MU, Galy B, Camaschella C. 2010. Two to tango: regulation of Mammalian iron metabolism. *Cell* 142: 24-38
64. Meguro R, Asano Y, Odagiri S, Li C, Iwatsuki H, Shoumura K. 2007. Nonheme-iron histochemistry for light and electron microscopy: a historical, theoretical and technical review. *Arch Histol Cytol* 70: 1-19
65. Richardson DR, Ponka P. 1997. The molecular mechanisms of the metabolism and transport of iron in normal and neoplastic cells. *Biochim Biophys Acta* 1331: 1-40
66. Hentze MW, Kuhn LC. 1996. Molecular control of vertebrate iron metabolism: mRNA-based regulatory circuits operated by iron, nitric oxide, and oxidative stress. *Proc Natl Acad Sci U S A* 93: 8175-82
67. Torti SV, Torti FM. 2011. Ironing out cancer. *Cancer Res* 71: 1511-4

68. Trowbridge IS, Lopez F. 1982. Monoclonal-Antibody to Transferrin Receptor Blocks Transferrin Binding and Inhibits Human-Tumor Cell-Growth Invitro. *Proceedings of the National Academy of Sciences of the United States of America-Biological Sciences* 79: 1175-9
69. Larrick JW, Cresswell P. 1979. Modulation of Cell-Surface Iron Transferrin Receptors by Cellular Density and State of Activation. *Journal of Supramolecular Structure* 11: 579-86
70. Taetle R, Honeysett JM. 1987. Effects of monoclonal anti-transferrin receptor antibodies on in vitro growth of human solid tumor cells. *Cancer Res* 47: 2040-4
71. Andrews NC. 2005. Understanding heme transport. *N Engl J Med* 353: 2508-9
72. Trinder D, Morgan E, Baker E. 1986. The mechanisms of iron uptake by fetal rat hepatocytes in culture. *Hepatology* 6: 852-8
73. Richardson DR, Baker E. 1990. The uptake of iron and transferrin by the human malignant melanoma cell. *Biochim Biophys Acta* 1053: 1-12
74. Richardson DR, Neumannova V, Nagy E, Ponka P. 1995. The effect of redox-related species of nitrogen monoxide on transferrin and iron uptake and cellular proliferation of erythroleukemia (K562) cells. *Blood* 86: 3211-9
75. Trinder D, Zak O, Aisen P. 1996. Transferrin receptor-independent uptake of differic transferrin by human hepatoma cells with antisense inhibition of receptor expression. *Hepatology* 23: 1512-20
76. Marcus DM, Zinberg N. 1975. Measurement of Serum Ferritin by Radioimmunoassay - Results in Normal Individuals and Patients with Breast-Cancer. *Journal of the National Cancer Institute* 55: 791-5
77. Kew MC, Torrance JD, Derman D, Simon M, Macnab GM, Charlton RW, Bothwell TH. 1978. Serum and Tumor Ferritins in Primary Liver Cancer. *Gut* 19: 294-9
78. Hann HWL, Levy HM, Evans AE. 1980. Serum Ferritin as a Guide to Therapy in Neuro-Blastoma. *Cancer Research* 40: 1411-3
79. Vaughn CB, Weinstein R, Bond B, Rice R, Vaughn RW, Mckendrick A, Ayad G, Rockwell MA, Rocchio R. 1987. Ferritin Content in Human Cancerous and Noncancerous Colonic Tissue. *Cancer Investigation* 5: 7-10
80. Iancu TC. 1989. Iron and Neoplasia - Ferritin and Hemosiderin in Tumor-Cells. *Ultrastructural Pathology* 13: 573-84
81. Harrison PM, Arosio P. 1996. The ferritins: molecular properties, iron storage function and cellular regulation. *Biochim Biophys Acta* 1275: 161-203
82. Broxmeyer HE, Bognacki J, Dorner MH, Desousa M. 1981. Identification of Leukemia-Associated Inhibitory Activity as Acidic Isoferritins - a Regulatory Role for Acidic Isoferritins in the Production of Granulocytes and Macrophages. *Journal of Experimental Medicine* 153: 1426-44
83. Broxmeyer HE, Cooper S, Levi S, Arosio P. 1991. Mutated recombinant human heavy-chain ferritins and myelosuppression in vitro and in vivo: a link between ferritin ferroxidase activity and biological function. *Proc Natl Acad Sci U S A* 88: 770-4
84. Kwok JC, Richardson DR. 2002. The iron metabolism of neoplastic cells: alterations that facilitate proliferation? *Crit Rev Oncol Hematol* 42: 65-78
85. Tsuji Y, Kwak E, Saika T, Torti SV, Torti FM. 1993. Preferential repression of the H subunit of ferritin by adenovirus E1A in NIH-3T3 mouse fibroblasts. *J Biol Chem* 268: 7270-5
86. Wu KJ, Polack A, Dalla-Favera R. 1999. Coordinated regulation of iron-controlling genes, H-ferritin and IRP2, by c-MYC. *Science* 283: 676-9
87. Neilands JB. 1995. Siderophores - Structure and Function of Microbial Iron Transport Compounds. *Journal of Biological Chemistry* 270: 26723-6
88. Leng XH, Ding T, Lin H, Wang Y, Hu LM, Hu JH, Feig B, Zhang W, Pusztai L, Symmans WF, Wu Y, Arlinghaus RB. 2009. Inhibition of Lipocalin 2 Impairs Breast Tumorigenesis and Metastasis. *Cancer Research* 69: 8579-84

89. Berger T, Cheung CC, Elia AJ, Mak TW. 2010. Disruption of the Lcn2 gene in mice suppresses primary mammary tumor formation but does not decrease lung metastasis. *Proceedings of the National Academy of Sciences of the United States of America* 107: 2995-3000
90. Tesfay L, Clausen KA, Kim JW, Hegde P, Wang X, Miller LD, Deng Z, Blanchette N, Arvedson T, Miranti CK, Babitt JL, Lin HY, Peehl DM, Torti FM, Torti SV. 2015. Hepcidin Regulation in Prostate and Its Disruption in Prostate Cancer. *Cancer Res*
91. Huang X. 2003. Iron overload and its association with cancer risk in humans: evidence for iron as a carcinogenic metal. *Mutation Research-Fundamental and Molecular Mechanisms of Mutagenesis* 533: 153-71
92. Weinberg ED. 1992. Roles of iron in neoplasia. Promotion, prevention, and therapy. *Biol Trace Elem Res* 34: 123-40
93. Stevens RG, Graubard BI, Micozzi MS, Neriishi K, Blumberg BS. 1994. Moderate Elevation of Body Iron Level and Increased Risk of Cancer Occurrence and Death. *International Journal of Cancer* 56: 364-9
94. Mainous AG, Gill JM, Everett CJ. 2005. Transferrin saturation, dietary iron intake, and risk of cancer. *Annals of Family Medicine* 3: 131-7
95. Cade J, Thomas E, Vail A. 1998. Case-control study of breast cancer in south east England: nutritional factors. *Journal of Epidemiology and Community Health* 52: 105-10
96. Kabat GC, Miller AB, Jain M, Rohan TE. 2007. Dietary iron and heme iron intake and risk of breast cancer: A prospective cohort study. *Cancer Epidemiology Biomarkers & Prevention* 16: 1306-8
97. Torti SV, Torti FM. 2013. Cellular iron metabolism in prognosis and therapy of breast cancer. *Crit Rev Oncog* 18: 435-48
98. Fleming RE, Sly WS. 2002. Mechanisms of iron accumulation in hereditary hemochromatosis. *Annual Review of Physiology* 64: 663-80
99. Feder JN, Gnirke A, Thomas W, Tsuchihashi Z, Ruddy DA, Basava A, Dormishian F, Domingo R, Ellis MC, Fullan A, Hinton LM, Jones NL, Kimmel BE, Kronmal GS, Lauer P, Lee VK, Loeb DB, Mapa FA, McClelland E, Meyer NC, Mintier GA, Moeller N, Moore T, Morikang E, Prass CE, Quintana L, Starnes SM, Schatzman RC, Brunke KJ, Drayna DT, Risch NJ, Bacon BR, Wolff RK. 1996. A novel MHC class I-like gene is mutated in patients with hereditary haemochromatosis. *Nature Genetics* 13: 399-408
100. Olynyk JK. 1999. A population-based study of the clinical expression of the hemochromatosis gene (vol 341, pg 718, 1999). *New England Journal of Medicine* 341: 1708-
101. Feder JN, Penny DM, Irrinki A, Lee VK, Lebron JA, Watson N, Tsuchihashi Z, Sigal E, Bjorkman PJ, Schatzman RC. 1998. The hemochromatosis gene product complexes with the transferrin receptor and lowers its affinity for ligand binding. *Proc Natl Acad Sci U S A* 95: 1472-7
102. Feder JN, Tsuchihashi Z, Irrinki A, Lee VK, Mapa FA, Morikang E, Prass CE, Starnes SM, Wolff RK, Parkkila S, Sly WS, Schatzman RC. 1997. The hemochromatosis founder mutation in HLA-H disrupts beta2-microglobulin interaction and cell surface expression. *J Biol Chem* 272: 14025-8
103. de Valk B, Addicks MA, Gosriwatana I, Lu S, Hider RC, Marx JJ. 2000. Non-transferrin-bound iron is present in serum of hereditary haemochromatosis heterozygotes. *Eur J Clin Invest* 30: 248-51
104. Kallianpur AR, Hall LD, Yadav M, Christman BW, Dittus RS, Haines JL, Parl FF, Summar ML. 2004. Increased prevalence of the HFE C282Y hemochromatosis allele in women with breast cancer. *Cancer Epidemiology Biomarkers & Prevention* 13: 205-12
105. Osborne NJ, Gurrin LC, Allen KJ, Constantine CC, Delatycki MB, McLaren CE, Gertig DM, Anderson GJ, Southey MC, Olynyk JK, Powell LW, Hopper JL, Giles GG, English DR. 2010. HFE C282Y Homozygotes Are at Increased Risk of Breast and Colorectal Cancer. *Hepatology* 51: 1311-8

106. Beckman LE, Van Landeghem GF, Sikstrom C, Wahlin A, Markevarn B, Hallmans G, Lenner P, Athlin L, Stenling R, Beckman L. 1999. Interaction between haemochromatosis and transferrin receptor genes in different neoplastic disorders. *Carcinogenesis* 20: 1231-3
107. Hunt JR, Zeng HW. 2004. Iron absorption by heterozygous carriers of the HFE C282Y mutation associated with hemochromatosis. *American Journal of Clinical Nutrition* 80: 924-31
108. Hrabinski D, Hertz JL, Tantillo C, Berger V, Sherman AR. 1995. Iron repletion attenuates the protective effects of iron deficiency in DMBA-induced mammary tumors in rats. *Nutr Cancer* 24: 133-42
109. Vandewalle B, Hornez L, Revillion F, Lefebvre J. 1989. Secretion of Transferrin by Human-Breast Cancer-Cells. *Biochemical and Biophysical Research Communications* 163: 149-54
110. Weinstein RE, Bond BH, Silberberg BK, Vaughn CB, Subbaiah P, Pieper DR. 1989. Tissue ferritin concentration and prognosis in carcinoma of the breast. *Breast Cancer Res Treat* 14: 349-53
111. Guner G, Kirkali G, Yenisey C, Tore IR. 1992. Cytosol and Serum Ferritin in Breast-Carcinoma. *Cancer Letters* 67: 103-12
112. Rossiello R, Carriero MV, Giordano GG. 1984. Distribution of ferritin, transferrin and lactoferrin in breast carcinoma tissue. *J Clin Pathol* 37: 51-5
113. Pinnix ZK, Miller LD, Wang W, D'Agostino R, Jr., Kute T, Willingham MC, Hatcher H, Tesfay L, Sui G, Di X, Torti SV, Torti FM. 2010. Ferroportin and iron regulation in breast cancer progression and prognosis. *Sci Transl Med* 2: 43ra56
114. Miller LD, Coffman LG, Chou JW, Black MA, Bergh J, D'Agostino R, Jr., Torti SV, Torti FM. 2011. An iron regulatory gene signature predicts outcome in breast cancer. *Cancer Res* 71: 6728-37
115. Pietras K, Ostman A. 2010. Hallmarks of cancer: interactions with the tumor stroma. *Exp Cell Res* 316: 1324-31
116. Vargas AC, Reed AEM, Waddell N, Lane A, Reid LE, Smart CE, Cocciardi S, da Silva L, Song S, Chenevix-Trench G, Simpson PT, Lakhani SR. 2012. Gene expression profiling of tumour epithelial and stromal compartments during breast cancer progression. *Breast Cancer Research and Treatment* 135: 153-65
117. Ruffell B, Au A, Rugo HS, Esserman LJ, Hwang ES, Coussens LM. 2012. Leukocyte composition of human breast cancer. *Proc Natl Acad Sci U S A* 109: 2796-801
118. Swartz MA, Iida N, Roberts EW, Sangaletti S, Wong MH, Yull FE, Coussens LM, DeClerck YA. 2012. Tumor Microenvironment Complexity: Emerging Roles in Cancer Therapy. *Cancer Research* 72: 2473-80
119. Nicolson GL. 1991. Quantitative variations in gene expression: possible role in cellular diversification and tumor progression. *J Cell Biochem* 46: 277-83
120. Ma XJ, Dahiya S, Richardson E, Erlander M, Sgroi DC. 2009. Gene expression profiling of the tumor microenvironment during breast cancer progression. *Breast Cancer Research* 11
121. Condeelis J, Pollard JW. 2006. Macrophages: Obligate partners for tumor cell migration, invasion, and metastasis. *Cell* 124: 263-6
122. Pollard JW. 2008. Macrophages define the invasive microenvironment in breast cancer. *Journal of Leukocyte Biology* 84: 623-30
123. Pollard JW. 2004. Tumour-educated macrophages promote tumour progression and metastasis. *Nature Reviews Cancer* 4: 71-8
124. Ueno T, Toi M, Saji H, Muta M, Bando H, Kuroi K, Koike M, Inadera H, Matsushima K. 2000. Significance of macrophage chemoattractant protein-1 in macrophage recruitment, angiogenesis, and survival in human breast cancer. *Clinical Cancer Research* 6: 3282-9
125. Mantovani A, Bottazzi B, Colotta F, Sozzani S, Ruco L. 1992. The Origin and Function of Tumor-Associated Macrophages. *Immunology Today* 13: 265-70
126. Murray PJ, Wynn TA. 2011. Protective and pathogenic functions of macrophage subsets. *Nat Rev Immunol* 11: 723-37

127. Geissmann F, Manz MG, Jung S, Sieweke MH, Merad M, Ley K. 2010. Development of Monocytes, Macrophages, and Dendritic Cells. *Science* 327: 656-61
128. Ginhoux F, Jung S. 2014. Monocytes and macrophages: developmental pathways and tissue homeostasis. *Nature Reviews Immunology* 14: 392-404
129. van Furth R, Cohn ZA. 1968. The origin and kinetics of mononuclear phagocytes. *J Exp Med* 128: 415-35
130. Laoui D, Movahedi K, Van Overmeire E, Van den Bossche J, Schouppe E, Mommer C, Nikolaou A, Morias Y, De Baetselier P, Van Ginderachter JA. 2011. Tumor-associated macrophages in breast cancer: distinct subsets, distinct functions. *Int J Dev Biol* 55: 861-7
131. Mantovani A, Sozzani S, Locati M, Allavena P, Sica A. 2002. Macrophage polarization: tumor-associated macrophages as a paradigm for polarized M2 mononuclear phagocytes. *Trends in Immunology* 23: 549-55
132. Biswas SK, Mantovani A. 2010. Macrophage plasticity and interaction with lymphocyte subsets: cancer as a paradigm. *Nat Immunol* 11: 889-96
133. Recalcati S, Locati M, Marini A, Santambrogio P, Zaninotto F, De Pizzol M, Zammataro L, Girelli D, Cairo G. 2010. Differential regulation of iron homeostasis during human macrophage polarized activation. *Eur J Immunol* 40: 824-35
134. Gammella E, Buratti P, Cairo G, Recalcati S. 2014. Macrophages: central regulators of iron balance. *Metallomics* 6: 1336-45
135. Tang. 2013. Tumor-associated macrophages as potencial diagnostic and prognostic biomarkers in breast cancer. *Cancer Letters* 332: 3-10
136. Lin EY, Nguyen AV, Russell RG, Pollard JW. 2001. Colony-stimulating factor 1 promotes progression of mammary tumors to malignancy. *J Exp Med* 193: 727-40
137. Aharinejad S, Abraham D, Paulus P, Abri H, Hofmann M, Grossschmidt K, Schafer R, Stanley ER, Hofbauer R. 2002. Colony-stimulating factor-1 antisense treatment suppresses growth of human tumor xenografts in mice. *Cancer Res* 62: 5317-24
138. Medrek C, Ponten F, Jirstrom K, Leandersson K. 2012. The presence of tumor associated macrophages in tumor stroma as a prognostic marker for breast cancer patients. *BMC Cancer* 12: 306
139. Coussens LM, Werb Z. 2002. Inflammation and cancer. *Nature* 420: 860-7
140. Hagemann T, Robinson SC, Schulz M, Trumper L, Balkwill FR, Binder C. 2004. Enhanced invasiveness of breast cancer cell lines upon co-cultivation with macrophages is due to TNF-alpha dependent up-regulation of matrix metalloproteases. *Carcinogenesis* 25: 1543-9
141. Sapi E, Kacinski BM. 1999. The role of CSF-1 in normal and neoplastic breast physiology. *Proc Soc Exp Biol Med* 220: 1-8
142. Goswami S, Sahai E, Wyckoff JB, Cammer M, Cox D, Pixley FJ, Stanley ER, Segall JE, Condeelis JS. 2005. Macrophages promote the invasion of breast carcinoma cells via a colony-stimulating factor-1/epidermal growth factor paracrine loop. *Cancer Res* 65: 5278-83
143. de Castro G, Puglisi F, de Azambuja E, El Saghir NS, Awada A. 2006. Angiogenesis and cancer: A cross-talk between basic science and clinical trials (the "do ut des" paradigm). *Critical Reviews in Oncology Hematology* 59: 40-50
144. Bingle L, Brown NJ, Lewis CE. 2002. The role of tumour-associated macrophages in tumour progression: implications for new anticancer therapies. *J Pathol* 196: 254-65
145. Leek RD, Harris AL. 2002. Tumor-associated macrophages in breast cancer. *J Mammary Gland Biol Neoplasia* 7: 177-89
146. Benizri E, Ginouves A, Berra E. 2008. The magic of the hypoxia-signaling cascade. *Cellular and Molecular Life Sciences* 65: 1133-49
147. Harris AL. 2002. Hypoxia - A key regulatory factor in tumour growth. *Nature Reviews Cancer* 2: 38-47
148. Carmeliet P. 2005. VEGF as a key mediator of angiogenesis in cancer. *Oncology* 69 Suppl 3: 4-10

149. Clauss M, Gerlach M, Gerlach H, Brett J, Wang F, Familletti PC, Pan YC, Olander JV, Connolly DT, Stern D. 1990. Vascular permeability factor: a tumor-derived polypeptide that induces endothelial cell and monocyte procoagulant activity, and promotes monocyte migration. *J Exp Med* 172: 1535-45
150. Leek RD, Harris AL, Lewis CE. 1994. Cytokine networks in solid human tumors: regulation of angiogenesis. *J Leukoc Biol* 56: 423-35
151. Hoeben A, Landuyt B, Highley MS, Wildiers H, Van Oosterom AT, De Bruijn EA. 2004. Vascular endothelial growth factor and angiogenesis. *Pharmacol Rev* 56: 549-80
152. Boudreau A, van't Veer LJ, Bissell MJ. 2012. An "elite hacker": breast tumors exploit the normal microenvironment program to instruct their progression and biological diversity. *Cell Adh Migr* 6: 236-48
153. Laing KJ, Secombes CJ. 2004. Chemokines. *Developmental and Comparative Immunology* 28: 443-60
154. Homey B, Muller A, Zlotnik A. 2002. Chemokines: agents for the immunotherapy of cancer? *Nat Rev Immunol* 2: 175-84
155. Bacon K, Baggiolini M, Broxmeyer H, Horuk R, Lindley I, Mantovani A, Matsushima K, Murphy P, Nomiyama H, Oppenheim J, Rot A, Schall T, Tsang M, Thorpe R, Van Damme J, Wadhwa M, Yoshie O, Zlotnik A, Zoon K, No IWSC. 2003. Chemokine/chemokine receptor nomenclature. *Cytokine* 21: 48-9
156. Soria G, Ben-Baruch A. 2008. The inflammatory chemokines CCL2 and CCL5 in breast cancer. *Cancer Lett* 267: 271-85
157. Carr MW, Roth SJ, Luther E, Rose SS, Springer TA. 1994. Monocyte Chemoattractant Protein-1 Acts as a T-Lymphocyte Chemoattractant. *Proceedings of the National Academy of Sciences of the United States of America* 91: 3652-6
158. Allavena P, Bianchi G, Zhou D, Vandamme J, Jilek P, Sozzani S, Mantovani A. 1994. Induction of Natural-Killer-Cell Migration by Monocyte Chemotactic Protein-1, Protein-2 and Protein-3. *European Journal of Immunology* 24: 3233-6
159. Hembruff SL, Jokar I, Yang L, Cheng N. 2010. Loss of transforming growth factor-beta signaling in mammary fibroblasts enhances CCL2 secretion to promote mammary tumor progression through macrophage-dependent and -independent mechanisms. *Neoplasia* 12: 425-33
160. Qian BZ, Li J, Zhang H, Kitamura T, Zhang J, Campion LR, Kaiser EA, Snyder LA, Pollard JW. 2011. CCL2 recruits inflammatory monocytes to facilitate breast-tumour metastasis. *Nature* 475: 222-5
161. Deshmane SL, Kremlev S, Amini S, Sawaya BE. 2009. Monocyte chemoattractant protein-1 (MCP-1): an overview. *J Interferon Cytokine Res* 29: 313-26
162. Izhak L, Wildbaum G, Jung S, Stein A, Shaked Y, Karin N. 2012. Dissecting the autocrine and paracrine roles of the CCR2-CCL2 axis in tumor survival and angiogenesis. *PLoS One* 7: e28305
163. Valkovic T, Lucin K, Krstulja M, Dobi-Babic R, Jonjic N. 1998. Expression of monocyte chemotactic protein-1 in human invasive ductal breast cancer. *Pathology Research and Practice* 194: 335-40
164. Valkovic T, Dobrila F, Melato M, Sasso F, Rizzardi C, Jonjic N. 2002. Correlation between vascular endothelial growth factor, angiogenesis, and tumor-associated macrophages in invasive ductal breast carcinoma. *Virchows Arch* 440: 583-8
165. Fujimoto H, Sangai T, Ishii G, Ikehara A, Nagashima T, Miyazaki M, Ochiai A. 2009. Stromal MCP-1 in mammary tumors induces tumor-associated macrophage infiltration and contributes to tumor progression. *Int J Cancer* 125: 1276-84
166. Charo IF, Ransohoff RM. 2006. The many roles of chemokines and chemokine receptors in inflammation. *N Engl J Med* 354: 610-21
167. Li M, Knight DA, L AS, Smyth MJ, Stewart TJ. 2013. A role for CCL2 in both tumor progression and immunosurveillance. *Oncoimmunology* 2: e25474

168. Conti I, Rollins BJ. 2004. CCL2 (monocyte chemoattractant protein-1) and cancer. *Semin Cancer Biol* 14: 149-54
169. Loberg RD, Ying C, Craig M, Yan L, Snyder LA, Pienta KJ. 2007. CCL2 as an important mediator of prostate cancer growth in vivo through the regulation of macrophage infiltration. *Neoplasia* 9: 556-62
170. Bonapace L, Coissieux MM, Wyckoff J, Mertz KD, Varga Z, Junt T, Bentires-Alj M. 2014. Cessation of CCL2 inhibition accelerates breast cancer metastasis by promoting angiogenesis. *Nature*
171. Mleczko-Sanecka K, Mingang, Z., Sandro, A., Maja, V.S. 2014. The chemokine CCL2 is a novel modifier of tissue iron levels and a predictor of disease severity in Hereditary Hemochromatosis. *European Iron Club Meeting 2014 Abstract Book, Verona*
172. Lawless MW, White M, Mankan AK, O'Dwyer MJ, Norris S. 2007. Elevated MCP-1 serum levels are associated with the H63D mutation and not the C282Y mutation in hereditary hemochromatosis. *Tissue Antigens* 70: 294-300
173. Mitchell RM, Lee SY, Randazzo WT, Simmons Z, Connor JR. 2009. Influence of HFE variants and cellular iron on monocyte chemoattractant protein-1. *J Neuroinflammation* 6: 6
174. Moch H, Kononen J, Kallioniemi OP, Sauter G. 2001. Tissue microarrays: What will they bring to molecular and anatomic pathology? *Advances in Anatomic Pathology* 8: 14-20
175. Voduc D, Kenney C, Nielsen TO. 2008. Tissue Microarrays in clinical oncology. *Seminars in Radiation Oncology* 18: 89-97
176. Giltnane JM, Rimm DL. 2005. Technology Insight: identification of biomarkers with tissue microarray technology. *Nature Clinical Practice Urology* 2: A104-A11
177. Munro HN, Linder MC. 1978. Ferritin - Structure, Biosynthesis, and Role in Iron-Metabolism. *Physiological Reviews* 58: 317-96
178. Roschzttardtz H, Conejero G, Curie C, Mari S. 2009. Identification of the Endodermal Vacuole as the Iron Storage Compartment in the Arabidopsis Embryo. *Plant Physiology* 151: 1329-38
179. van Duijn S, Nabuurs RJ, van Duinen SG, Natte R. 2013. Comparison of histological techniques to visualize iron in paraffin-embedded brain tissue of patients with Alzheimer's disease. *J Histochem Cytochem* 61: 785-92
180. Maddox PH, Jenkins D. 1987. 3-Aminopropyltriethoxysilane (APES): a new advance in section adhesion. *J Clin Pathol* 40: 1256-7
181. Holness CL, Simmons DL. 1993. Molecular-Cloning of Cd68, a Human Macrophage Marker Related to Lysosomal Glycoproteins. *Blood* 81: 1607-13
182. Saito N, Pulford KAF, Bretongorius J, Masse JM, Mason DY, Cramer EM. 1991. Ultrastructural-Localization of the Cd68 Macrophage-Associated Antigen in Human Blood Neutrophils and Monocytes. *American Journal of Pathology* 139: 1053-9
183. Gottfried E, Kunz-Schughart LA, Weber A, Rehli M, Peuker A, Muller A, Kastenberger M, Brockhoff G, Andreesen R, Kreutz M. 2008. Expression of CD68 in non-myeloid cell types. *Scandinavian Journal of Immunology* 67: 453-63
184. Miller SA, Dykes DD, Polesky HF. 1988. A simple salting out procedure for extracting DNA from human nucleated cells. *Nucleic Acids Res* 16: 1215
185. Mullis K, Faloona F, Scharf S, Saiki R, Horn G, Erlich H. 1986. Specific enzymatic amplification of DNA in vitro: the polymerase chain reaction. *Cold Spring Harb Symp Quant Biol* 51 Pt 1: 263-73
186. Kubista M, Andrade JM, Bengtsson M, Forootan A, Jonak J, Lind K, Sindelka R, Sjoback R, Sjogreen B, Strombom L, Stahlberg A, Zoric N. 2006. The real-time polymerase chain reaction. *Mol Aspects Med* 27: 95-125
187. Aaij C, Borst P. 1972. The gel electrophoresis of DNA. *Biochim Biophys Acta* 269: 192-200
188. Mamotte CD. 2006. Genotyping of single nucleotide substitutions. *Clin Biochem Rev* 27: 63-75

189. Narayanan S. 1991. Applications of restriction fragment length polymorphism. *Ann Clin Lab Sci* 21: 291-6
190. Lynn SP, Cohen LK, Kaplan S, Gardner JF. 1980. Rsai - a New Sequence-Specific Endonuclease Activity from Rhodopseudomonas-Sphaeroides. *Journal of Bacteriology* 142: 380-3
191. Schnitt SJ. 2010. Classification and prognosis of invasive breast cancer: from morphology to molecular taxonomy. *Mod Pathol* 23 Suppl 2: S60-4
192. Junttila MR, de Sauvage FJ. 2013. Influence of tumour micro-environment heterogeneity on therapeutic response. *Nature* 501: 346-54
193. de Sousa M. 2011. An outsider's perspective-ecotaxis revisited: an integrative review of cancer environment, iron and immune system cells. *Integrative Biology* 3: 343-9
194. Faulk WP, Hsi BL, Stevens PJ. 1980. Transferrin and Transferrin Receptors in Carcinoma of the Breast. *Lancet* 2: 390-2
195. Zhang S, Chen Y, Guo W, Yuan L, Zhang D, Xu Y, Nemeth E, Ganz T, Liu S. 2014. Disordered hepcidin-ferroportin signaling promotes breast cancer growth. *Cell Signal* 26: 2539-50
196. Chen Y, Zhang SP, Wang XY, Guo WL, Wang L, Zhang DQ, Yuan L, Zhang ZH, Xu Y, Liu SJ. 2015. Disordered signaling governing ferroportin transcription favors breast cancer growth. *Cellular Signalling* 27: 168-76
197. Ganz T. 2012. Macrophages and Systemic Iron Homeostasis. *Journal of Innate Immunity* 4: 446-53
198. Delaby C, Pilard N, Hetet G, Driss F, Grandchamp B, Beaumont C, Canonne-Hergaux F. 2005. A physiological model to study iron recycling in macrophages. *Experimental Cell Research* 310: 43-53
199. Pinto JP, Arezes J, Dias V, Oliveira S, Viera I, Costa M, Vos M, Carlsson A, Rikers Y, Rangel M, Porto G. 2014. Physiological implications of NTBI uptake by T lymphocytes. *Frontiers in Pharmacology* 5
200. Corna G, Campana L, Pignatti E, Castiglioni A, Tagliafico E, Bosurgi L, Campanella A, Brunelli S, Manfredi AA, Apostoli P, Silvestri L, Camaschella C, Rovere-Querini P. 2010. Polarization dictates iron handling by inflammatory and alternatively activated macrophages. *Haematologica* 95: 1814-22
201. Allavena P, Germano G, Marchesi F, Mantovani A. 2011. Chemokines in cancer related inflammation. *Exp Cell Res* 317: 664-73
202. Fang WB, Jokar I, Zou A, Lambert D, Dendukuri P, Cheng N. 2012. CCL2/CCR2 chemokine signaling coordinates survival and motility of breast cancer cells through Smad3 protein- and p42/44 mitogen-activated protein kinase (MAPK)-dependent mechanisms. *J Biol Chem* 287: 36593-608
203. Salcedo R, Ponce ML, Young HA, Wasserman K, Ward JM, Kleinman HK, Oppenheim JJ, Murphy WJ. 2000. Human endothelial cells express CCR2 and respond to MCP-1: direct role of MCP-1 in angiogenesis and tumor progression. *Blood* 96: 34-40
204. Kitamura T, Qian BZ, Soong D, Cassetta L, Noy R, Sugano G, Kato Y, Li J, Pollard JW. 2015. CCL2-induced chemokine cascade promotes breast cancer metastasis by enhancing retention of metastasis-associated macrophages. *J Exp Med*
205. Sierra-Filardi E, Nieto C, Dominguez-Soto A, Barroso R, Sanchez-Mateos P, Puig-Kroger A, Lopez-Bravo M, Joven J, Ardavin C, Rodriguez-Fernandez JL, Sanchez-Torres C, Mellado M, Corbi AL. 2014. CCL2 shapes macrophage polarization by GM-CSF and M-CSF: identification of CCL2/CCR2-dependent gene expression profile. *J Immunol* 192: 3858-67
206. Mantovani A, Schioppa T, Porta C, Allavena P, Sica A. 2006. Role of tumor-associated macrophages in tumor progression and invasion. *Cancer Metastasis Rev* 25: 315-22
207. Johnson ACM, Becker K, Zager RA. 2010. Parenteral iron formulations differentially affect MCP-1, HO-1, and NGAL gene expression and renal responses to injury. *American Journal of Physiology-Renal Physiology* 299: F426-F35

208. Valenti L, Dongiovanni P, Motta BM, Swinkels DW, Bonara P, Rametta R, Burdick L, Frugoni C, Fracanzani AL, Fargion S. 2011. Serum Hepcidin and Macrophage Iron Correlate With MCP-1 Release and Vascular Damage in Patients With Metabolic Syndrome Alterations. *Arteriosclerosis Thrombosis and Vascular Biology* 31: 683-90
209. Zager RA. 2005. Parenteral iron treatment induces MCP-1 accumulation in plasma, normal kidneys, and in experimental nephropathy. *Kidney International* 68: 1533-42
210. Zhang WJ, Wei H, Frei B. 2010. The iron chelator, desferrioxamine, reduces inflammation and atherosclerotic lesion development in experimental mice. *Experimental Biology and Medicine* 235: 633-41
211. Chavey C, Bibeau F, Gourgou-Bourgade S, Burlinchon S, Boissiere F, Laune D, Roques S, Lazennec G. 2007. Oestrogen receptor negative breast cancers exhibit high cytokine content. *Breast Cancer Res* 9: R15
212. Svensson S, Abrahamsson A, Vazquez Rodriguez G, Olsson AK, Jensen L, Cao Y, Dabrosin C. 2015. CCL2 and CCL5 are novel therapeutic targets for estrogen-dependent breast cancer. *Clin Cancer Res*

SUPPLEMENTARY MATERIAL

1.1 Tissue sample and core frequencies

Table 8: Frequencies and percentages of lesions considered in this study.

Lesion Diagnosis

		Frequency	Percent	Valid Percent	Cumulative Percent
Valid	Normal	21	14,9	14,9	14,9
	Normal in DCIS	17	12,1	12,1	27,0
	Normal in IDC	28	19,9	19,9	46,8
	Pure DCIS	27	19,1	19,1	66,0
	DCIS in IDC	13	9,2	9,2	75,2
	Pure IDC	35	24,8	24,8	100,0
	Total	141	100,0	100,0	

Table 9: Table demonstrating the p-value obtained from the Kolmogorov-Smirnov test, performed in order to assess the distribution and normality of data.

Tests of Normality

	Kolmogorov-Smirnov[a]			Shapiro-Wilk		
	Statistic	df	Sig.	Statistic	df	Sig.
CCL2 expression in epithelial cells	,296	59	,000	,866	59	,000
Iron deposition in epithelial cells	,414	59	,000	,606	59	,000
Iron deposition in stromal inflammatory cells	,379	59	,000	,628	59	,000
Ferroportin 1 expression in lymphocytes	,149	59	,002	,932	59	,003
Ferroportin 1 expression in macrophages	,151	59	,002	,955	59	,029
Total macrophage infiltration	,163	59	,000	,835	59	,000
Infiltration of CCL2-positive macrophages	,241	59	,000	,641	59	,000

a. Lilliefors Significance Correction

2.1 Iron deposition in pure lesions

Table 10: Contingency table demonstrating the frequencies and percentages of normal, pure DCIS and pure IDC samples presenting iron deposition in epithelial cells.

Crosstab

			Iron deposition in epithelial cells		Total
			Absence	Presence	
Diagnosis	Normal	Count	18	3	21
		% within Diagnosis	85,7%	14,3%	100,0%
		% within Iron deposition in epithelial cells	30,5%	13,6%	25,9%
		% of Total	22,2%	3,7%	25,9%
	Pure DCIS	Count	18	7	25
		% within Diagnosis	72,0%	28,0%	100,0%
		% within Iron deposition in epithelial cells	30,5%	31,8%	30,9%
		% of Total	22,2%	8,6%	30,9%
	Pure IDC	Count	23	12	35
		% within Diagnosis	65,7%	34,3%	100,0%
		% within Iron deposition in epithelial cells	39,0%	54,5%	43,2%
		% of Total	28,4%	14,8%	43,2%
Total		Count	59	22	81
		% within Diagnosis	72,8%	27,2%	100,0%
		% within Iron deposition in epithelial cells	100,0%	100,0%	100,0%
		% of Total	72,8%	27,2%	100,0%

Table 11: Contingency table demonstrating the frequency and percentage of normal, pure DCIS and pure IDC samples with iron deposition in stromal inflammatory cells.

Crosstab

			Iron deposition in stromal inflammatory cells		Total
			Absence	Presence	
Diagnosis	Normal	Count	12	1	13
		% within Diagnosis	92,3%	7,7%	100,0%
		% within Iron deposition in stromal inflammatory cells	33,3%	2,9%	18,6%
		% of Total	17,1%	1,4%	18,6%
	Pure DCIS	Count	12	12	24
		% within Diagnosis	50,0%	50,0%	100,0%
		% within Iron deposition in stromal inflammatory cells	33,3%	35,3%	34,3%
		% of Total	17,1%	17,1%	34,3%
	Pure IDC	Count	12	21	33
		% within Diagnosis	36,4%	63,6%	100,0%
		% within Iron deposition in stromal inflammatory cells	33,3%	61,8%	47,1%
		% of Total	17,1%	30,0%	47,1%
Total		Count	36	34	70
		% within Diagnosis	51,4%	48,6%	100,0%
		% within Iron deposition in stromal inflammatory cells	100,0%	100,0%	100,0%
		% of Total	51,4%	48,6%	100,0%

Table 12: Pearson's Chi-square test: differences in iron deposition in epithelial cells between sub-groups of lesions.

Chi-Square Tests

	Value	df	Asymp. Sig. (2-sided)
Pearson Chi-Square	2,667[a]	2	,264
Likelihood Ratio	2,869	2	,238
Linear-by-Linear Association	2,608	1	,106
N of Valid Cases	81		

a. 0 cells (0,0%) have expected count less than 5. The minimum expected count is 5,70.

Table 13: Pearson's Chi-square test: differences in iron deposition in stromal inflammatory cells between sub-groups of lesions.

Chi-Square Tests

	Value	df	Asymp. Sig. (2-sided)
Pearson Chi-Square	11,715[a]	2	,003
Likelihood Ratio	13,400	2	,001
Linear-by-Linear Association	11,083	1	,001
N of Valid Cases	70		

a. 0 cells (0,0%) have expected count less than 5. The minimum expected count is 6,31.

Table 14: Pearson's Chi-square test: differences in iron deposition in stromal inflammatory cells between normal and pure DCIS lesions.

Chi-Square Tests

	Value	df	Asymp. Sig. (2-sided)	Exact Sig. (2-sided)	Exact Sig. (1-sided)
Pearson Chi-Square	6,623[a]	1	,010		
Continuity Correction[b]	4,896	1	,027		
Likelihood Ratio	7,651	1	,006		
Fisher's Exact Test				,013	,011
Linear-by-Linear Association	6,444	1	,011		
N of Valid Cases	37				

a. 1 cells (25,0%) have expected count less than 5. The minimum expected count is 4,57.

Table 15: Pearson's Chi-square test: differences in iron deposition in stromal inflammatory cells between normal and pure IDC lesions.

Chi-Square Tests

	Value	df	Asymp. Sig. (2-sided)	Exact Sig. (2-sided)	Exact Sig. (1-sided)
Pearson Chi-Square	11,697[a]	1	,001		
Continuity Correction[b]	9,563	1	,002		
Likelihood Ratio	13,370	1	,000		
Fisher's Exact Test				,001	,001
Linear-by-Linear Association	11,443	1	,001		
N of Valid Cases	46				

a. 0 cells (0,0%) have expected count less than 5. The minimum expected count is 6,22.

b. Computed only for a 2x2 table

Table 16: Pearson's Chi-square test: differences in iron deposition in stromal inflammatory cells between pure DCIS and pure IDC lesions.

Chi-Square Tests

	Value	df	Asymp. Sig. (2-sided)	Exact Sig. (2-sided)	Exact Sig. (1-sided)
Pearson Chi-Square	1,060[a]	1	,303		
Continuity Correction[b]	,574	1	,449		
Likelihood Ratio	1,059	1	,303		
Fisher's Exact Test				,416	,224
Linear-by-Linear Association	1,041	1	,308		
N of Valid Cases	57				

a. 0 cells (0,0%) have expected count less than 5. The minimum expected count is 10,11.

b. Computed only for a 2x2 table

2.2 Iron deposition in adjacent tissue

Table 17: Contingency table demonstrating the frequency and percentage of normal samples and samples constituted by histologically “normal” tissue adjacent to DCIS or IDC presenting iron deposition in epithelial cells.

Crosstab

			Iron deposition in epithelial cells		Total
			Absence	Presence	
Lesion Diagnosis	Normal	Count	18	3	21
		% within Lesion Diagnosis	85,7%	14,3%	100,0%
		% within Iron deposition in epithelial cells	40,0%	18,8%	34,4%
		% of Total	29,5%	4,9%	34,4%
	Normal in DCIS	Count	12	3	15
		% within Lesion Diagnosis	80,0%	20,0%	100,0%
		% within Iron deposition in epithelial cells	26,7%	18,8%	24,6%
		% of Total	19,7%	4,9%	24,6%
	Normal in IDC	Count	15	10	25
		% within Lesion Diagnosis	60,0%	40,0%	100,0%
		% within Iron deposition in epithelial cells	33,3%	62,5%	41,0%
		% of Total	24,6%	16,4%	41,0%
Total		Count	45	16	61
		% within Lesion Diagnosis	73,8%	26,2%	100,0%
		% within Iron deposition in epithelial cells	100,0%	100,0%	100,0%
		% of Total	73,8%	26,2%	100,0%

Table 18: Contingency table demonstrating the frequency and percentage of normal samples and samples constituted by histologically “normal” tissue adjacent to DCIS or IDC presenting iron deposition in stromal inflammatory cells.

Crosstab

			Iron deposition in stromal inflammatory cells		Total
			Absence	Presence	
Lesion Diagnosis	Normal	Count	12	1	13
		% within Lesion Diagnosis	92,3%	7,7%	100,0%
		% within Iron deposition in stromal inflammatory cells	36,4%	5,3%	25,0%
		% of Total	23,1%	1,9%	25,0%
	Normal in DCIS	Count	9	6	15
		% within Lesion Diagnosis	60,0%	40,0%	100,0%
		% within Iron deposition in stromal inflammatory cells	27,3%	31,6%	28,8%
		% of Total	17,3%	11,5%	28,8%
	Normal in IDC	Count	12	12	24
		% within Lesion Diagnosis	50,0%	50,0%	100,0%
		% within Iron deposition in stromal inflammatory cells	36,4%	63,2%	46,2%
		% of Total	23,1%	23,1%	46,2%
Total		Count	33	19	52
		% within Lesion Diagnosis	63,5%	36,5%	100,0%
		% within Iron deposition in stromal inflammatory cells	100,0%	100,0%	100,0%
		% of Total	63,5%	36,5%	100,0%

Table 19: Pearson's Chi-square test: differences in iron deposition in epithelial cells between sub-groups of lesions.

Chi-Square Tests

	Value	df	Asymp. Sig. (2-sided)
Pearson Chi-Square	4,299[a]	2	,117
Likelihood Ratio	4,317	2	,116
Linear-by-Linear Association	3,936	1	,047
N of Valid Cases	61		

a. 1 cells (16,7%) have expected count less than 5. The minimum expected count is 3,93.

Table 20: Pearson's Chi-square test: differences in iron deposition in stromal inflammatory cells between sub-groups of lesions.

Chi-Square Tests

	Value	df	Asymp. Sig. (2-sided)
Pearson Chi-Square	6,618[a]	2	,037
Likelihood Ratio	7,759	2	,021
Linear-by-Linear Association	5,945	1	,015
N of Valid Cases	52		

a. 1 cells (16,7%) have expected count less than 5. The minimum expected count is 4,75.

Table 21: Pearson's Chi-square test: differences in iron deposition in stromal inflammatory cells between normal and "normal" tissue adjacent to DCIS lesions.

Chi-Square Tests

	Value	df	Asymp. Sig. (2-sided)	Exact Sig. (2-sided)	Exact Sig. (1-sided)
Pearson Chi-Square	,206[a]	1	,650		
Continuity Correction[b]	,000	1	1,000		
Likelihood Ratio	,203	1	,652		
Fisher's Exact Test				,677	,493
Linear-by-Linear Association	,200	1	,655		
N of Valid Cases	36				

a. 2 cells (50,0%) have expected count less than 5. The minimum expected count is 2,50.

b. Computed only for a 2x2 table

Table 22: Pearson's Chi-square test: differences in iron deposition in stromal inflammatory cells between normal and "normal" tissue adjacent to IDC lesions.

Chi-Square Tests

	Value	df	Asymp. Sig. (2-sided)	Exact Sig. (2-sided)	Exact Sig. (1-sided)
Pearson Chi-Square	6,623[a]	1	,010		
Continuity Correction[b]	4,896	1	,027		
Likelihood Ratio	7,651	1	,006		
Fisher's Exact Test				,013	,011
Linear-by-Linear Association	6,444	1	,011		
N of Valid Cases	37				

a. 1 cells (25,0%) have expected count less than 5. The minimum expected count is 4,57.

b. Computed only for a 2x2 table

Table 23: Pearson's Chi-square test: differences in iron deposition in stromal inflammatory cells between "normal" tissue adjacent to DCIS lesions and normal tissue adjacent to IDC lesions.

Chi-Square Tests

	Value	df	Asymp. Sig. (2-sided)	Exact Sig. (2-sided)	Exact Sig. (1-sided)
Pearson Chi-Square	,371[a]	1	,542		
Continuity Correction[b]	,078	1	,780		
Likelihood Ratio	,373	1	,541		
Fisher's Exact Test				,742	,391
Linear-by-Linear Association	,362	1	,547		
N of Valid Cases	39				

a. 0 cells (0,0%) have expected count less than 5. The minimum expected count is 6,92.

b. Computed only for a 2x2 table

3.1 Epithelial CCL2 expression

Table 24: Spearman's rank correlation test: Epithelial CCL2 expression.

Correlations

			CCL2 expression in epithelial cells	Diagnosis
Spearman's rho	CCL2 expression in epithelial cells	Correlation Coefficient	1,000	,299**
		Sig. (2-tailed)	.	,007
		N	80	80
	Diagnosis	Correlation Coefficient	,299**	1,000
		Sig. (2-tailed)	,007	.
		N	80	83

**. Correlation is significant at the 0.01 level (2-tailed).

Table 25: Kruskal-Wallis test: differences in epithelial CCL2 expression between sub-groups of pure lesions.

Ranks

	Diagnosis	N	Mean Rank
CCL2 expression in epithelial cells	Normal	21	29,17
	Pure DCIS	25	41,40
	Pure IDC	34	46,84
	Total	80	

Test Statistics[a,b]

	CCL2 expression in epithelial cells
Chi-Square	7,678
df	2
Asymp. Sig.	,022

a. Kruskal Wallis Test

b. Grouping Variable: Diagnosis

Table 26: Dunn-Bonferroni test: differences in epithelial CCL2 expression between sub-groups of pure lesions.

Sample1-Sample2	Test Statistic	Std. Error	Std. Test Statistic	Sig.	Adj.Sig.
Normal-Pure DCIS	-12,233	6,826	-1,792	,073	,219
Normal-Pure IDC	-17,672	6,400	-2,761	,006	,017
Pure DCIS-Pure IDC	-5,438	6,076	-,895	,371	1,000

Each row tests the null hypothesis that the Sample 1 and Sample 2 distributions are the same.
Asymptotic significances (2-sided tests) are displayed. The significance level is ,05.

Table 27: Kruskal-Wallis test: differences in epithelial CCL2 expression between normal tissue from reduction mammoplasties and histologically "normal" tissue adjacent to carcinomas.

Ranks

	Diagnosis	N	Mean Rank
CCL2 expression in epithelial cells	Normal	21	25,02
	Normal in DCIS	16	35,06
	Normal in IDC	27	36,80
	Total	64	

Test Statistics[a,b]

	CCL2 expression in epithelial cells
Chi-Square	5,393
df	2
Asymp. Sig.	,067

a. Kruskal Wallis Test

b. Grouping Variable: Diagnosis

3.2 CCL2 expression in macrophages

Table 28: Spearman's rank correlation test: infiltration of CCL2-positive macrophages.

Correlations

			Infiltration of CCL2-positive macrophages	Diagnosis
Spearman's rho	Infiltration of CCL2-positive macrophages	Correlation Coefficient	1,000	,335**
		Sig. (2-tailed)	.	,004
		N	74	74
	Diagnosis	Correlation Coefficient	,335**	1,000
		Sig. (2-tailed)	,004	.
		N	74	83

**. Correlation is significant at the 0.01 level (2-tailed).

Table 29: Kruskal-Wallis test: differences in the infiltration of CCL2-positive macrophages between pure sub-groups of lesions.

Ranks

	Diagnosis	N	Mean Rank
Infiltration of CCL2-positive macrophages	Normal	19	18,89
	Pure DCIS	23	47,96
	Pure IDC	32	41,03
	Total	74	

Test Statistics[a,b]

	Infiltration of CCL2-positive macrophages
Chi-Square	20,618
df	2
Asymp. Sig.	,000

a. Kruskal Wallis Test

b. Grouping Variable: Diagnosis

Table 30: Dunn-Bonferroni test: differences in the infiltration of CCL2-positive macrophages between sub-groups of pure lesions.

Sample1-Sample2	Test Statistic	Std. Error	Std. Test Statistic	Sig.	Adj.Sig.
Normal-Pure IDC	-22,137	6,214	-3,562	,000	,001
Normal-Pure DCIS	-29,062	6,651	-4,369	,000	,000
Pure IDC-Pure DCIS	6,925	5,865	1,181	,238	,713

Each row tests the null hypothesis that the Sample 1 and Sample 2 distributions are the same.
Asymptotic significances (2-sided tests) are displayed. The significance level is ,05.

Table 31: Kruskal-Wallis test: differences in the infiltration of CCL2-positive macrophages between normal tissue from reduction mammoplasties and histologically "normal" tissue adjacent to carcinomas.

Ranks

	Diagnosis	N	Mean Rank
Infiltration of CCL2-positive macrophages	Normal	19	22,79
	Normal in DCIS	12	36,33
	Normal in IDC	24	27,96
	Total	55	

Test Statistics[a,b]

	Infiltration of CCL2-positive macrophages
Chi-Square	5,342
df	2
Asymp. Sig.	,069

a. Kruskal Wallis Test

b. Grouping Variable: Diagnosis

3.3 CD68 expression

Table 32: Spearman's rank correlation test: total macrophage infiltration.

Correlations

			Diagnosis	Total macrophage infiltration
Spearman's rho	Diagnosis	Correlation Coefficient	1,000	,630**
		Sig. (2-tailed)	.	,000
		N	83	75
	Total macrophage infiltration	Correlation Coefficient	,630**	1,000
		Sig. (2-tailed)	,000	.
		N	75	75

**. Correlation is significant at the 0.01 level (2-tailed).

Table 33: Kruskal-Wallis test: differences in total macrophage infiltration between sub-groups of pure lesions.

Ranks

	Diagnosis	N	Mean Rank
Total macrophage infiltration	Normal	18	14,89
	Pure DCIS	23	37,70
	Pure IDC	34	50,44
	Total	75	

Test Statistics[a,b]

	Total macrophage infiltration
Chi-Square	31,333
df	2
Asymp. Sig.	,000

a. Kruskal Wallis Test

b. Grouping Variable: Diagnosis

Table 34: Dunn-Bonferroni test: differences in the total macrophage infiltration between sub-groups of pure lesions.

Sample1-Sample2	Test Statistic	Std. Error	Std. Test Statistic	Sig.	Adj.Sig.
Normal-Pure DCIS	-22,807	6,858	-3,326	,001	,003
Normal-Pure IDC	-35,552	6,352	-5,597	,000	,000
Pure DCIS-Pure IDC	-12,746	5,883	-2,166	,030	,091

Each row tests the null hypothesis that the Sample 1 and Sample 2 distributions are the same.
Asymptotic significances (2-sided tests) are displayed. The significance level is ,05.

Table 35: Kruskal-Wallis test: differences in the total macrophage infiltration between normal tissue from reduction mammoplasties and histologically "normal" tissue adjacent to carcinomas.

Ranks

	Diagnosis	N	Mean Rank
Total macrophage infiltration	Normal	18	22,17
	Normal in DCIS	13	33,65
	Normal in IDC	26	31,40
	Total	57	

Test Statistics[a,b]

	Total macrophage infiltration
Chi-Square	4,619
df	2
Asymp. Sig.	,099

a. Kruskal Wallis Test

b. Grouping Variable: Diagnosis

Table 36: Spearman's rank correlation test: epithelial CCL2 expression and total macrophage infiltration.

Correlations

		CCL2 expression in epithelial cells	Total macrophage infiltration
Spearman's rho	CCL2 expression in epithelial cells	1,000	,060
		.	,609
		80	75

Table 37: Spearman's rank correlation test: epithelial CCL2 expression and infiltration of CCL2-positive macrophages.

Correlations

		CCL2 expression in epithelial cells	Infiltration of CCL2-positive macrophages
Spearman's rho	CCL2 expression in epithelial cells	1,000	,267
		.	,022
		80	73

Table 38: Spearman's rank correlation test: infiltration of CCL2-positive macrophages and total macrophage infiltration.

Correlations

		Infiltration of CCL2-positive macrophages	Total macrophage infiltration
Spearman's rho	Infiltration of CCL2-positive macrophages	1,000	,488
		.	,000
		75	73

Table 39: Mann-Whitney test: differences in epithelial CCL2 expression, regarding the presence of hemosiderin deposition in epithelial cells.

Test Statistics[a]

	CCL2 expression in epithelial cells
Mann-Whitney U	721,500
Wilcoxon W	1946,500
Z	-,137
Asymp. Sig. (2-tailed)	,891

a. Grouping Variable: Iron deposition in epithelial cells

Table 40: Mann-Whitney test: differences in epithelial CCL2 expression, regarding the presence of hemosiderin deposition in stromal inflammatory cells.

Test Statistics[a]

	CCL2 expression in epithelial cells
Mann-Whitney U	323,500
Wilcoxon W	788,500
Z	-3,177
Asymp. Sig. (2-tailed)	,001

a. Grouping Variable: Iron deposition in stromal inflammatory cells

Table 41: Mann-Whitney test: differences in ferroportin 1 expression in lymphocytes, regarding the presence of hemosiderin deposition in epithelial cells.

Test Statistics[a]

	Ferroportin 1 expression in lymphocytes
Mann-Whitney U	321,500
Wilcoxon W	849,500
Z	-1,042
Asymp. Sig. (2-tailed)	,298

a. Grouping Variable: Iron deposition in epithelial cells

Table 42: Mann-Whitney test: differences in ferroportin 1 expression in lymphocytes, regarding the presence of hemosiderin deposition in stromal inflammatory cells.

Test Statistics[a]

	Ferroportin 1 expression in lymphocytes
Mann-Whitney U	302,500
Wilcoxon W	512,500
Z	-,837
Asymp. Sig. (2-tailed)	,403

a. Grouping Variable: Iron deposition in stromal inflammatory cells

Table 43: Mann-Whitney test: differences in ferroportin 1 expression in macrophages, regarding the presence of hemosiderin deposition in epithelial cells.

Test Statistics[a]

	Ferroportin 1 expression in macrophages
Mann-Whitney U	356,000
Wilcoxon W	884,000
Z	-,467
Asymp. Sig. (2-tailed)	,640

a. Grouping Variable: Iron deposition in epithelial cells

Table 44: Mann-Whitney test: differences in ferroportin 1 expression in macrophages, regarding the presence of hemosiderin deposition in stromal inflammatory cells.

Test Statistics[a]

	Ferroportin 1 expression in macrophages
Mann-Whitney U	286,000
Wilcoxon W	496,000
Z	-,975
Asymp. Sig. (2-tailed)	,329

a. Grouping Variable: Iron deposition in stromal inflammatory cells

Table 45: Pearson's Chi-square test: differences in the distribution of the C282Y variants between sub-groups of lesions.

Chi-Square Tests

	Value	df	Asymp. Sig. (2-sided)
Pearson Chi-Square	3,954[a]	2	,138
Likelihood Ratio	6,314	2	,043
Linear-by-Linear Association	3,336	1	,068
N of Valid Cases	76		

a. 3 cells (50,0%) have expected count less than 5. The minimum expected count is 2,37.

Table 46: Pearson's Chi-square test: analyzing differences in the distribution of the H63D variants between sub-groups of lesions.

Chi-Square Tests

	Value	df	Asymp. Sig. (2-sided)
Pearson Chi-Square	1,937[a]	2	,380
Likelihood Ratio	1,975	2	,372
Linear-by-Linear Association	,029	1	,866
N of Valid Cases	65		

a. 0 cells (0,0%) have expected count less than 5. The minimum expected count is 8,48.

Table 47: Pearson's Chi-square test: differences in the distribution of the H63D variants with the presence of iron deposition in epithelial cells.

Chi-Square Tests

	Value	df	Asymp. Sig. (2-sided)	Exact Sig. (2-sided)	Exact Sig. (1-sided)
Pearson Chi-Square	,664[a]	1	,415		
Continuity Correction[b]	,314	1	,575		
Likelihood Ratio	,668	1	,414		
Fisher's Exact Test				,455	,288
Linear-by-Linear Association	,654	1	,419		
N of Valid Cases	65				

a. 0 cells (0,0%) have expected count less than 5. The minimum expected count is 11,60.

b. Computed only for a 2x2 table

Table 48: Pearson's Chi-square test: differences in the distribution of the H63D variants with the presence of iron deposition in stromal inflammatory cells.

Chi-Square Tests

	Value	df	Asymp. Sig. (2-sided)	Exact Sig. (2-sided)	Exact Sig. (1-sided)
Pearson Chi-Square	1,542[a]	1	,214		
Continuity Correction[b]	,941	1	,332		
Likelihood Ratio	1,544	1	,214		
Fisher's Exact Test				,280	,166
Linear-by-Linear Association	1,514	1	,219		
N of Valid Cases	56				

a. 0 cells (0,0%) have expected count less than 5. The minimum expected count is 10,71.

b. Computed only for a 2x2 table

Table 49: Mann-Whitney test: differences in the median expression of CCL2 between H63D variants.

Test Statistics[a]

	CCL2 expression in epithelial cells
Mann-Whitney U	430,000
Wilcoxon W	808,000
Z	-,606
Asymp. Sig. (2-tailed)	,545

a. Grouping Variable: H63D_grouped

Table 50: Mann-Whitney test: differences in the median expression of CCL2 regarding the ER-status, in DCIS samples.

Test Statistics[a]

	CCL2 expression in epithelial cells
Mann-Whitney U	25,000
Wilcoxon W	196,000
Z	-2,305
Asymp. Sig. (2-tailed)	,021
Exact Sig. [2*(1-tailed Sig.)]	,021[b]

a. Grouping Variable: Estrogen Receptor DCIS

Table 51: Mann-Whitney test: differences in the median expression of CCL2 regarding the ER-status, in IDC samples.

Test Statistics[a]

	CCL2 expression in epithelial cells
Mann-Whitney U	60,500
Wilcoxon W	411,500
Z	-,848
Asymp. Sig. (2-tailed)	,397
Exact Sig. [2*(1-tailed Sig.)]	,408[b]

a. Grouping Variable: Estrogen Receptor IDC

b. Not corrected for ties.

Table 52: Spearman's rank correlation test: CCL2 expression and leukocyte count.

Correlations

		CCL2 expression in epithelial cells	Monocytes	Total leukocytes	Lymphocytes
Spearman's rho	CCL2 expression in epithelial cells	1,000	,266	,009	-,023
		.	,050	,950	,867
		80	55	55	55

Table 53: Mann-Whitney test: differences in the median expression of CCL2 regarding the PR-status, in DCIS samples.

Test Statistics[a]

	CCL2 expression in epithelial cells
Mann-Whitney U	57,000
Wilcoxon W	162,000
Z	-1,097
Asymp. Sig. (2-tailed)	,273
Exact Sig. [2*(1-tailed Sig.)]	,291[b]

a. Grouping Variable: Progesterone Receptor DCIS

b. Not corrected for ties.

Table 54: Mann-Whitney test: differences in the median expression of CCL2 regarding the PR-status, in IDC samples.

Test Statistics[a]

	CCL2 expression in epithelial cells
Mann-Whitney U	87,000
Wilcoxon W	318,000
Z	-1,134
Asymp. Sig. (2-tailed)	,257
Exact Sig. [2*(1-tailed Sig.)]	,271[b]

a. Grouping Variable: Progesterone Receptor IDC

Table 55: Mann-Whitney test: differences in the median expression of CCL2 regarding the HER-2 status.

Test Statistics[a]

	CCL2 expression in epithelial cells
Mann-Whitney U	310,000
Wilcoxon W	500,000
Z	-,568
Asymp. Sig. (2-tailed)	,570

a. Grouping Variable: HER-2 status

Table 56: Mann-Whitney test: differences in the median expression of CCL2 regarding lymph node involvement.

Test Statistics[a]

	CCL2 expression in epithelial cells
Mann-Whitney U	126,500
Wilcoxon W	316,500
Z	-,237
Asymp. Sig. (2-tailed)	,812
Exact Sig. [2*(1-tailed Sig.)]	,815[b]

. Grouping Variable: Lymph node involvement